Identification of Cell Biomechanical Signatures Using Three Dimensional Isotropic Microstructures

Mehdi Nikkhah

Dissertation submitted to the faculty of the Virginia Polytechnic Institute and State University in partial fulfillment of the requirements for the degree of

Doctor of Philosophy

In

Mechanical Engineering

Masoud Agah, Chair

Jeannine S. Strobl, Member

Roop L. Mahajan, Member

Padma Rajagopalan, Member

Marissa Nichole Rylander, Member

December 03, 2010

Blacksburg, Virginia

Keywords: MicroElectroMechanical Systems (MEMS), Isotropic, Silicon, Three Dimensional (3-D), Atomic Force Microscopy (AFM), Breast Cancer, HS68, MCF10A, MDA-MB-231, Suberoylanilide Hydroxamic Acid (SAHA)

Identification of Cell Biomechanical Signatures Using Three dimensional Isotropic Microstructures

By

Mehdi Nikkhah

ABSTRACT

Micro and nanofabrication technologies have been used extensively in many biomedical and biological applications. Integration of MEMS technology and biology (BioMEMS) enables precise control of the cellular microenvironments and offers high throughput systems. The focus of this research was to develop three dimensional (3-D) isotropic microstructures for comprehensive analysis on cell-substrate interactions. The aim was to investigate whether the normal and cancerous cells differentially respond to their underlying substrate and whether the differential response of the cells leads to a novel label-free technique to distinguish between normal and cancerous cells.

Three different generations of 3-D isotropic microstructures comprised of curved surfaces were developed using a single-mask, single-etch step process. Our experimental model included HS68 normal human fibroblasts, MCF10A normal human breast epithelial cells and MDA-MB-231 metastatic human breast cancer cells. Primary findings on the first generation of silicon substrates demonstrated a distinct adhesion and growth behavior in HS68 and MDA-MB-231 cells. MDA-MB-231 cells deformed while the fibroblasts stretched and elongated their cytoskeleton on the curved surfaces. Unlike fibroblasts, MDA-MB-231 cells mainly trapped and localized inside the deep microchambers. Detailed investigations on cytoskeletal organization, adhesion pattern and morphology of the cells on the second generation of the silicon substrates demonstrated that cytoskeletal prestress and microtubules organization in HS68 cells, cell-cell junction and cell-substrate adhesion strength in MCF10A cells, and deformability of MDA-MB-231 cells (obtained by using AFM technique) affect their behavior inside the etched cavities. Treatment of MDA-MB-231 cells with experimental breast cancer drug, SAHA, on the second generation of substrates, significantly altered the cells morphology, cytoarchitecture and adhesion pattern inside the 3-D microstructures. Third generation of silicon substrates was developed for comprehensive analysis on behavior of MDA-MB-231 and MCF10A cells in a co-culture system in response to SAHA drug. Formation of colonies of both cell types was evident

inside the cavities within a few hours after seeding the cells on the chips. SAHA selectively altered the morphology and cytoarchitecture in MDA-MB-231 cells. Most importantly, the majority of MDA-MB-231 cells stretched inside the etched cavities, while the adhesion pattern of MCF10A cells remained unaltered. In the last part of this dissertation, using AFM analysis, we showed that the growth medium composition has a pronounced effect on cell elasticity. Our findings demonstrated that the proposed isotropic silicon microstructures have potential applications in development of biosensor platforms for cell segregation as well as conducting fundamental biological studies.

To My Beloved Parents,

Farideh Mohajeri

and

Gholamhossein Nikkhah

Acknowledgements

Completion of a PhD dissertation is not possible without the support of numerous people. I am pleased to extend my deepest gratitude to many whose support enabled me over the past few years to successfully complete my research. PhD studies have shaped my thinking and my perspective on scientific problems, and have led me where I am in my scientific research and personal life.

I cherish my parents' everlasting and unconditional love and support. They were the first who instilled in me a strong work ethics. Their continued encouragements as well as their faith in my abilities have been a source of strength and inspiration during my graduate school years while I have been away from home. I also thank my sister Maryam and her family and my brother Mehrdad for their support.

My sincere acknowledgment goes to my advisor, Dr. Masoud Agah. I would like to thank him for his guidance, advice and support. His encouragements from the early days of working at VT MEMS lab enabled me to develop a thorough understanding of the subject and achieve a successful outcome at the end.

I would like to thank Dr. Jeannine S. Strobl, a major contributor to this work and a member of my PhD dissertation committee. Dr. Strobl's involvement and guidance in this project has been tremendous. She supervised and trained me to conduct cell biology experiments. Her kind donation of equipment to help establish VT MEMS Bio lab contributed greatly to this research.

My sincere thanks go to the members of my PhD dissertation committee, Dr. Padma Rajagopalan (Chemical Engineering), Dr. Roop L. Mahajan (Mechanical Engineering), and Dr. Marissa Nichole Rylander (Mechanical Engineering) for their providing valuable insights and feedbacks into my research. I especially would like to recognize Dr. Rajagopalan's contribution; I learned a lot through our conversations and meetings.

I am grateful to Dr. Eva M. Schmelz (Human Nutrition, Food and Exercise) and Dr. Raffaella De Vita (Engineering Science and Mechanics), who have been collaborating with our lab since 2009. Their suggestions and inputs certainly raised the bar and introduced high standards into my research.

I would like to seize this opportunity to thank Dr. Karen DePauw, Vice President and Dean for Graduate Education for her generosity, dedication, and commitment to the graduate community at Virginia Tech. Her continued encouragement allowed me to grow as a student leader and a successful team player.

I extend my deepest gratitude to the following people who afforded me immense help and technical assistance throughout my dissertation work: Mr. Don Leber (Manager, Micron Clean Room Facilities), Dr. Kristi DeCourcy (Manager, Fralin Life Science Institute Confocal Microscopy Laboratory), Ms. Kathy Lowe (Manager, Morphology Laboratory, Virginia College of Veterinary Medicine), Mr. John McIntosh and Mr. Stephen McCartney (ICTAS Nanoscale Characterization and Fabrication Laboratory), and Ms. Kate Schallhorn (Carl Zeiss Microimaging). I sincerely appreciate Dr. Maren Roman (Wood Science and Forest Products) for her providing us with the AFM equipment.

Special thanks are due to VT MEMS lab's graduate and undergraduate students, past and present, for their contribution to the progress of this project through their technical assistance: Mr. Kevin Gantz, Ms. Vaishnavi Srinivasaraghavan, Mr. Alperen Ketene, Mr. Bhanu Peddi, Mr. Adedamola Omotosho, and Mr. Rithirong Thandee. I also would like to thank my VT MEMS colleagues, Mr. Bassam Alfeeli and Mr. Shree Narayanan for their friendship and fruitful conversations during the years of working at VT MEMS lab and afterwards.

I am forever indebted to my dear friend, Najm al-Din (Najma) Yousefi, for his keen eyes in reading my essays. He has been a great teacher who showed me how to be a good writer. Najma and his wife, Mehri, are my family in Blacksburg.

I also would like to extend my thanks to my great friends, Amin Zareian and Alireza Farjoud, for their support and friendship during the past few years of our graduate studies at Virginia Tech and afterwards.

This dissertation is dedicated to my beloved parents: Farideh Mohajeri and Gholamhossein Nikkhah.

Mehdi Nikkhah
December 2010

Table of Contents

List of Figures

List of Tables

1 Chapter One: Introduction

1.1 A brief overview on cell components and structure

Cells are structural and functional units of living materials that share similar machinery for their basic functions. The cell can be categorized into two different types: eukaryotic and prokaryotic. Eukaryotic cells contain nucleus which carries the genetic material and other complex structures and organelles surrounded by a lipid bilayer membrane. Prokaryotes cells lack a membrane-bound nucleus and instead of having a chromosomal DNA, their genetic information is in a circular DNA structure called plasmid. Eukaryotic cells are much larger and much more complex than prokaryotic cells. Animal cells are typical of the eukaryotic cells [1]. Figure 1-1 shows a schematic drawing of a typical eukaryotic cell. The interior structure of these cells includes components such as a nucleus, mitochondria, endoplasmic reticulum, Golgi apparatus, and cytoskeleton. These components are suspended in the cell cytoplasm and are encapsulated within the cell membrane. The cell membrane maintains an electrical potential difference between the interior components of the cells and the extracellular environment and controls the flow of ions into and out of the cell through ion channels.

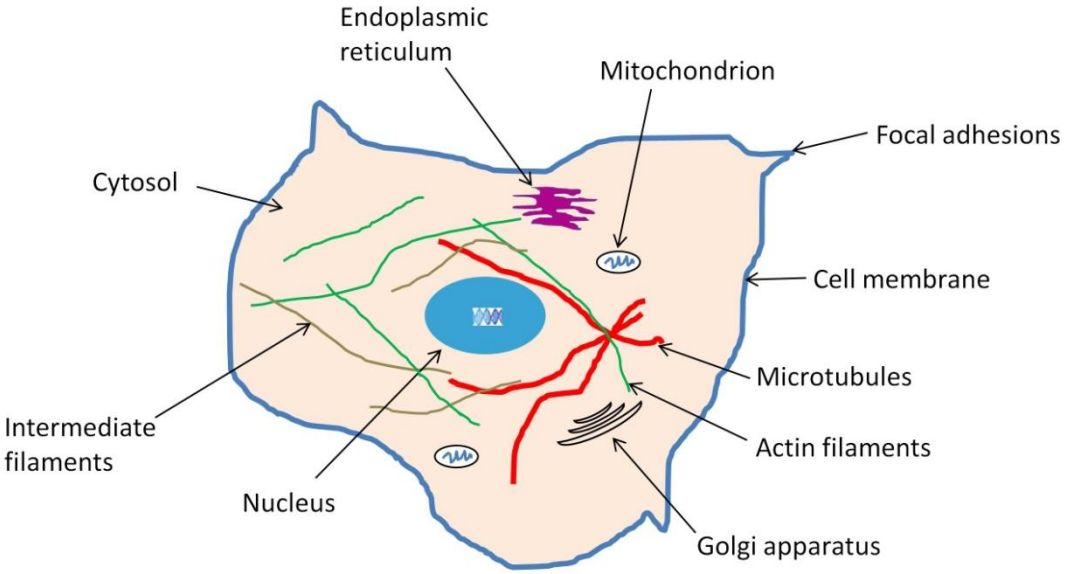

Figure 1-1 The content of a eukaryotic cell including Nucleus, Mitochondria, Endoplasmic reticulum, Golgi apparatus and Cytoskeleton.

Cell is a dynamic structure which can react to environmental variations and stimuli. One of the major components of a cell is the cytoskeleton. Cytoskeleton is a dynamic three dimensional and adaptable structure which contains a complex network of proteins. It is a primary determinant of the cell shape and its mechanical properties. It also plays a major role in other cellular processes such as cell migration and mitosis. The cytoskeleton is composed of three types of major fibers: microtubules, intermediate filaments, and actin filaments. The eukaryotic cells assemble a wide variety of structures using these three basic filaments [1]. Figure 1-2 shows the confocal images of the cytoskeletal structure of HS68 normal human fibroblast cells.

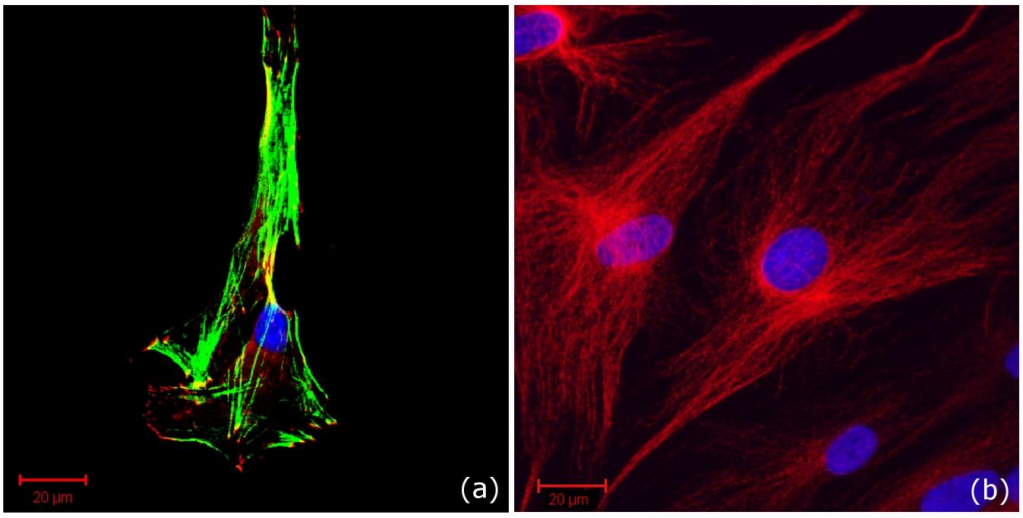

Figure 1-2 Cytoskeletal structure of the nucleus (blue), actin filaments (green), vinculin (red) (a) and microtubules (red) (b) of HS68 normal human fibroblast cells.

Actin filaments are formed by the polymerization of monomeric actin (G-actin) into linear and twisted strands of filamentous actin (F-actin). Monomeric actin includes 375 amino acids with molecular weight of 43 kDa. The diameter of F-actin filaments is 7-9 nm; actin filaments have a barbed end and pointed end establishing a structural polarity. Polymerization of actin occurs at the barbed (positive) end while depolymerization occurs at the pointed (negative) end. Actin constitutes a major part of the proteins in the cell (1-10 percent). Previous measurements of the mechanical properties of actin suggest that actin filaments are stiff with the Young's modulus of $1.3\text{-}2.5\times10^{9}$ Pa which is comparable to polystyrene with the Young's modulus of 3×10^{9} Pa. The persistence length of actin is 15 µm [1-4]. With the aid of various actin binding proteins (ABPs), F-actin fibers can be reorganized into stress fibers or three dimensional (3-D) lattice networks. The actin fibers can be organized differently depending on the eukaryotic cell type. Actin

filaments play a major role in the cell migration process. Stress fibers align in the direction of cell migration. Both G-actin and F-actin are highly concentrated in cell protrusions, including lamellipodia (broad, sheet-like extensions) and fillipodia (spike-like protrusions) during cell migration [1]. In addition actin filaments are major determinant of the cell overall elasticity [5-7].

Microtubules are the second major fibers involved with the cytoskeleton structure of cells. They are constructed from α- and β-tubulin and two 55 kDa polypeptides; they form a hollow rod with an outer diameter of 25 nm, inner diameter of 14 nm and a persistence length of 6000 μm [8]. Microtubules have a high flexural stiffness (2.6×10^{-23} Nm^2) and their Young's modulus is about 1.9×10^9 Pa [2]. Microtubules determine cell shape especially during mitosis and exhibit a more dynamic structure than actin exhibiting a half-life on the order of a few minutes [1].

Intermediate filaments constitute about 1% of the total protein in most cells. Their structure consists of a central α-helical domain with more than 300 amino acids. Their formation begins with the assembly of dimers into coiled coil structures followed by tetramers formation to form protofilaments. Eight protofilaments assemble to form a rope-like structure. Their diameter is 10 nm which falls between that of the actin filaments and microtubules. Their Young's modulus is 1×10^9 Pa [2] and have a persistence length of approximately 1μm [9]. Intermediate filaments either form a meshwork called a nuclear lamina just beneath the inner nuclear membrane or extend across the cytoplasm giving cells mechanical strength [1].

1.2 Microsystems for biological analysis

With the recent advances in various scientific fields, there has been a significant need for increasing experimental capabilities, flexibilities and the scale of information. In the field of biology, large amounts of data are required for protein identification and single cell analysis. Many experiments are performed manually or semi-automatically which limits the amount of information that can be gathered by scientists [10]. With respect to therapeutic strategies, there has been unprecedented challenge to expand the pool of molecular targets, novel compounds, and biological assays to foster new drug discoveries [11]. Scale and flexibility is the demand of pharmaceutical industries in a move towards cell-based assays with parallel processing

capabilities for different cell lines derived from various tissue origins [12]. Therefore, there is a significant motivation to design higher throughput systems in order to perform experiments that acquire large amount of data [13-18].

Using MicroElectroMechanical Systems (MEMS) technology is one of the promising ways to address the need for creating high throughput systems. MEMS devices can be fabricated using standard circuit technology and photolithographic techniques with features at the length scale in the range of millimeters to submicrometers. Integration of MEMS technology and biology (BioMEMS) not only offers high throughput systems but it also enables tightly control of the cellular microenvironment by varying cell-cell, cell-substrate, and cell-medium interactions [19]. Using this technology, it is possible to precisely regulate cell behavior *in vitro* rather than simply mimicking *in vivo* conditions. Figure 1-3 summarizes some of the major applications of BioMEMS. The other advantages of microminiaturized systems include small sample size and reagent consumption, small power consumption, fast analysis due to small length scales [20, 21], increased flow control, parallel operation, reduced response time, batch fabrication and low cost [11]. This field also offers potential applications in the areas of biosensors, pacemakers, immunoisolation capsules, and drug delivery [22]. This chapter provides a broad overview on application of BioMEMS for studying cell-surface interactions as well as cell mechanics.

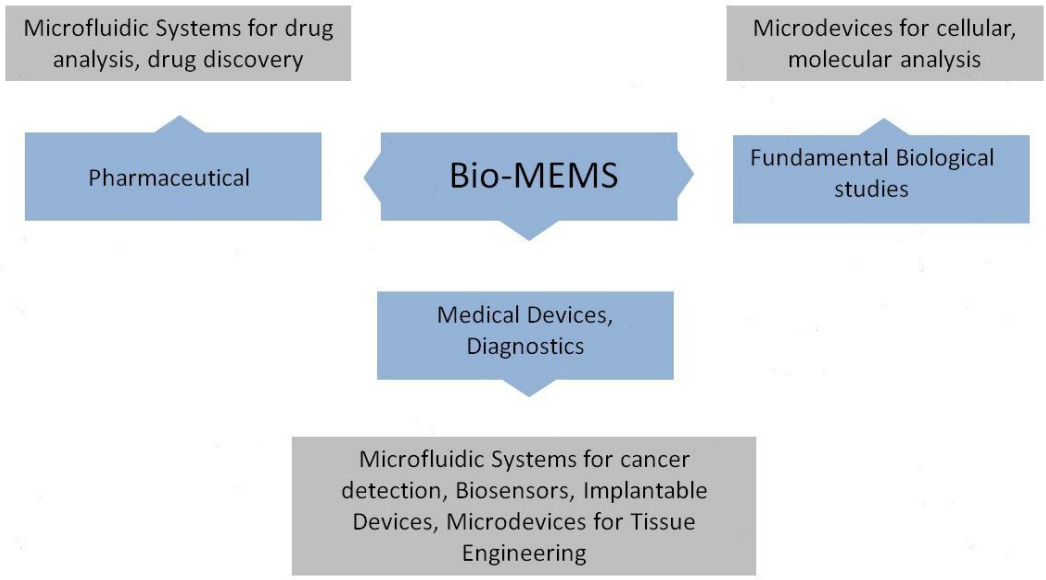

Figure 1-3 A block diagram showing major applications of the BioMEMS field.

1.3 Background on cell-substrate interaction

It is well established that surface topography with nano/microscale features influences the cell physiological behavior, morphology, and function [23, 24]. The cell-substrate interaction can be used as a signaling mechanism to accurately control the cell function. In depth investigation of cell-substrate interactions have potential applications in tissue engineering, designing biocompatible surfaces for prosthetics and medical implants as well as scientific biological studies.

The influence of surface topography was first noted by Harrison in 1914 [25] and resulted in the concept of "contact guidance" in which a cell aligns in the same direction as the surface grooves. Since that time, using microfabrication techniques, researchers have investigated cell responses to various precise topographical patterns including microgrooves fabricated in different materials such as silicon [26], quartz [27, 28], titanium-coated silicon [29, 30], poly-l-lactic (PLA) and polystyrene [31-34] and silicone [34] (Ex: Figure 1-4(A)). Most of these studies have been carried out to assess detailed effect of substrate topography on behavior of cell culture in order to influence the performance of medical implants. These studies further continued by researchers to explore whether the phenomenon of contact guidance is applicable in the field of tissue engineering and specifically creating *in vitro* tissue-engineered constructs (Ex: Figure 1-4(B,C)) [35-40].

In addition to microgrooved substrates, researchers have also investigated cell function on various other surface topographies including arrays of pillars and wells in silicon (Figure 1-4(D)) [41], arrays of pyramid shape microstructures in Polydimethylsiloxane (PDMS) (Figure 1-4(E)) [42], arrays of microwells in polystyrene (PS) with chemically modified surfaces [43], arrays of 3-D microstructures tailored in polystyrene (Figure 1-4(F)) [44], array of microholes and microgrooves fabricated in polycarbonate (Figure 1-4(G)) [45], network of ridges and grids in PDMS (Figure 1-4(H)) [46], needle like nano posts fabricated in silicon (Figure 1-4(I)) [47], arrays of micro-well in PDMS (Figure 1-4(J)) [48], 3-D surfaces fabricated in silicon with variable roughness and wettability (Figure 1-4(K)) [49] and array of independently deforming posts in PDMS (Figure 1-4(L)) [50, 51]. Table 1-1 summarized the previously developed nano/microscale topographies for cell-substrate interactions.

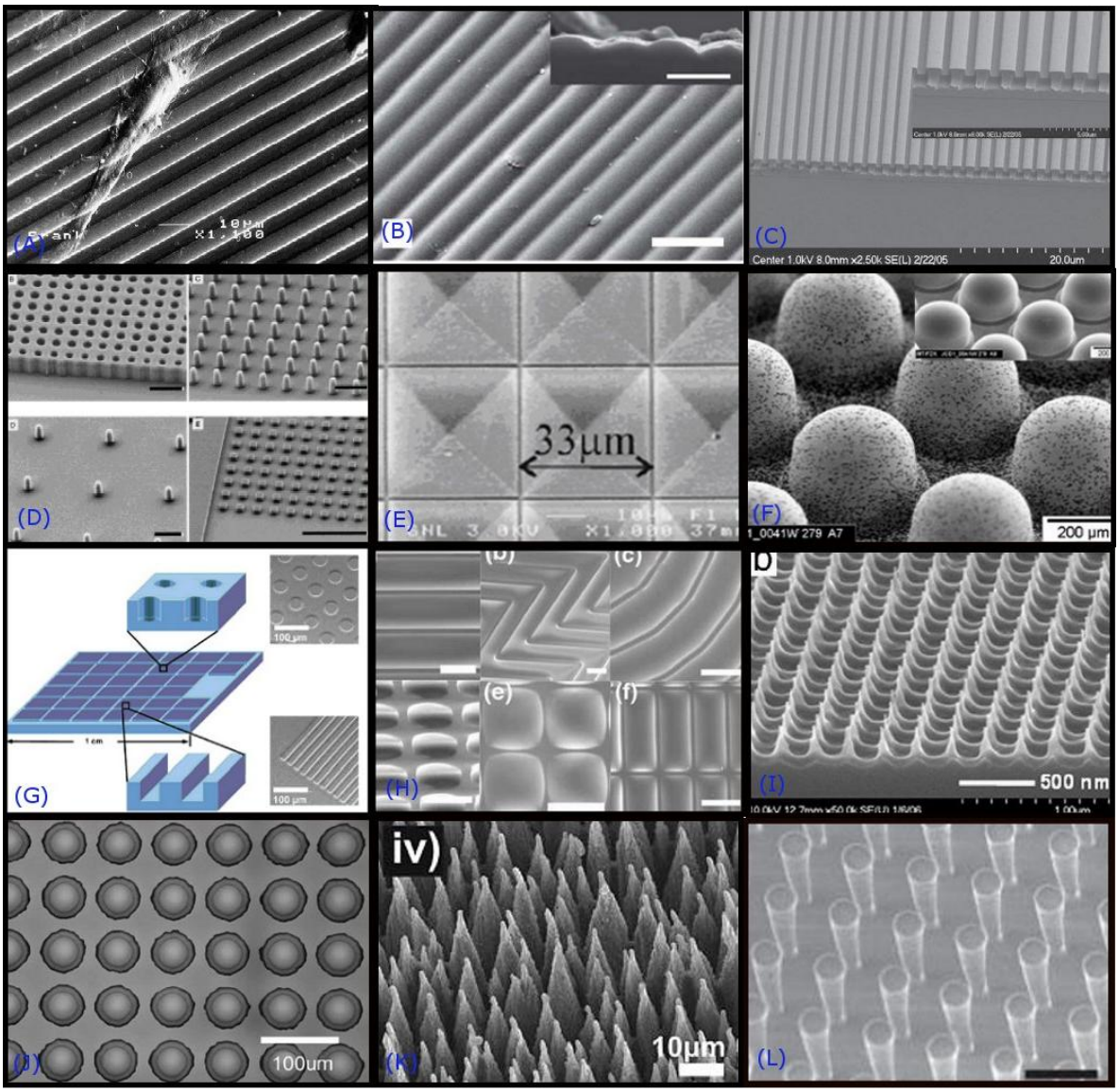

Figure 1-4 Some of the previously fabricated microstructures for cell-substrate interaction analysis including (A) microgrooves fabricated in polystyrene[34], (B) microgrooves fabricated in poly(glycerol-sebacate) (scale bars are 10 µm in the large figures and 5 µm in the insets)[39], (C) microgrooves fabricated in thermoplastic elastomer [40], (D) arrays of pillars and wells fabricated in silicon[41], (E) pyramid shaped microstructures fabricated in PDMS [42] (F) highly porous 3-D polymeric microstructures [44], (G) arrays of holes and grooves fabricated in polycarbonate [45], (H) of ridges and grids fabricated in PDMS (scale bars are 20 µm) [46], (I) needle like nano posts fabricated in silicon [47], (J) arrays of micro-well fabricated in PDMS [48], (K) 3-D rough surfaces fabricated in silicon [49] and (L) array of microposts fabricated in PDMS (scale bars represent 10 µm) [50]. Image Used under the Fair-Use Provision of Copyright Law.

Table 1-1 Summary of some of the studies on cell-substrate interaction

Cell Type	Substrate type	Substrate material	Focus of Study	Ref.
Rat dermal fibroblasts	Grooves	Silicon	Proliferation, elongation, alignment	[26]
BHK, MDCK, Chick embryo cerebral neurons	Grooves	Quartz	Elongation, alignment	[27]
Human gingival fibroblasts	Grooves	Titanium coated silicon	Cytoskeletal alignment and organization	[29]
Rat dermal fibroblasts	Grooves	Polystyrene	Elongation, alignment	[31]
Osteoblast-like rat bone marrow	Grooves	PLA, polystyrene	Proliferation, elongation, alkaline phosphatase activity	[33]
Vascular smooth muscle cells	Grooves	PDMS	Elongation, alignment	[35]
Mesenchymal stem cells	Grooves	Silicon	Elongation, alignment	[38]
Bovine aortic endothelial	Grooves	poly(glycerol–sebacate)	Elongation, alignment	[39]
Astrogilial cells	Pillars wells	Silicon	Attachment, adhesion	[41]
Rat osteoblast cells	pyramid shape	PDMS	Alkaline phosphatase activity, mineralization	[42]
MDCK II	wells	Polystyrene	Attachment, adhesion	[43]
Primary bovine aortic smooth muscle cells	Ridges grids	PDMS	Cell migration, cytoskeletal organization	[46]
Human foreskin fibroblasts cells	Needle shape nano posts	Silicon	Morphology, proliferation, alignment	[47]
Human colon carcinoma cell line (Caco-2)	wells	PDMS	Attachment, adhesion, metabolic activity	[48]
NIH/3T3 cells	Sharp spikes	Silicon	Attachment, adhesion, viability	[49]
Bovine pulmonary artery smooth muscle cells, NIH/3T3 cells	Posts	PDMS	Measurement of cell traction forces	[50]

Abbreviations: BHK: Baby hamster kidney, MDCK: Madin-Darby Canine Kidney, PLA: Poly-l-lactic acid, PDMS: Polydimethylsiloxane

1.4 Background on cell mechanics

It is well known that the cell structure, mechanical properties, and its biological functions are intrinsically linked [52, 53]. The deformability of the cells is mainly determined by its 3-D cytoskeletal structures which consist of a network of microtubules, actin filaments, and intermediate filaments (Section 1.1). The quantitative study of single cell biomechanics is an emerging field with translational applications in cancer diagnosis, orthopedics, cardiovascular and respiratory disease [52, 54, 55]. To date, numerous experimental and theoretical methods have been developed to better understand and describe the mechanical behavior of the cell.

1.4.1 Experimental techniques to measure mechanical properties of cells

Recent advances in micro and nanofabrication technologies have enabled to probe the mechanical properties of a single cell. To date, several techniques such as optical stretchers [56, 57], micropipette aspiration [58-60], magnetic beads [61, 62], scanning force microscopy [63, 64], and atomic force microcopy (AFM) [65-72] have been utilized to measure biomechanical properties of different cell lines and provide quantitative data regarding their deformation characteristics.

In optical stretchers method (Figure 1-5(a)), the cell is trapped inside a microfluidic device using two counter-propagating divergent laser beams. Consecutive images are obtained and recorded during the stretching and deformation of the cells. Consequently the images are analyzed to measure the magnitude of the deformation (variation in the cell aspect ratio) of the cell [56].

Micropipettes have been used extensively to measure the elastic properties and viscosity of the cell under controlled forces [73]. This method has been specifically employed to measure the mechanical properties of blood cells [74, 75] as well as articular cartilage and tissue structure cells [59, 60, 76]. In this method, cell is deformed by applying suction forces to the surface of the cells while attached to the micropipette. The major advantage of this method is that the force can be applied to the cells while they are in suspension. A typical micropipette aspiration system has been shown in Figure 1-5(b).

In magnetic beads method, a magnetic bead with functionalized surface is attached to the cell and twisted using a magnetic field to impose deformation on the cell body. The deformation information is then used to obtain the elastic or viscoelastic properties of the cells [77]. Figure 1-5(c) shows a bead bound to the surfaces of the cells to impose twisting force on the cell body [78].

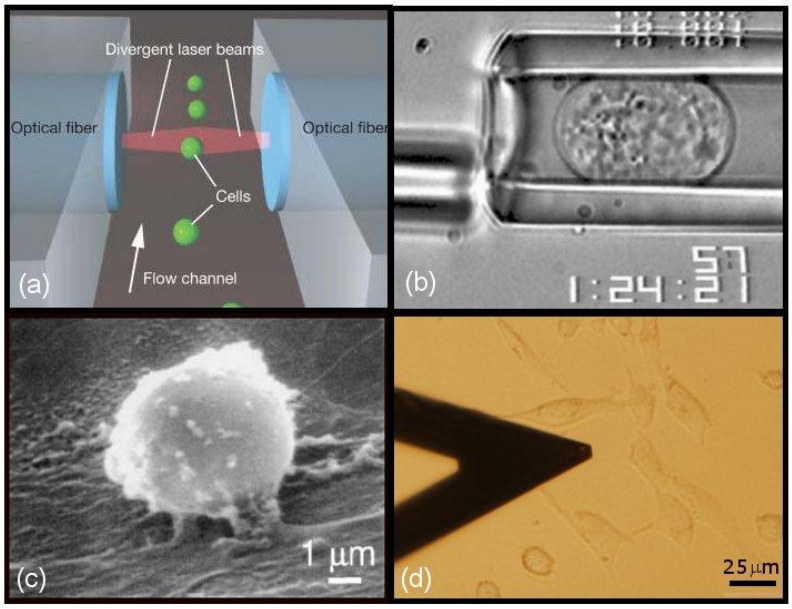

Figure 1-5 (a) optical stretcher [56, 57] (b) micropipette aspiration [60](c) magnetic twisting cytometry [62] and (d) atomic force microscopy methods to probe mechanical properties of the cell. Image Used under the Fair-Use Provision of Copyright Law.

AFM is a novel technique for high resolution imaging which was invented by Binnig in 1986 [79]. In this method, a tip at the free end of a cantilever induces force and generates a local deformation on the cell surface. This technique has been used extensively in biological studies in both imaging of cell surfaces under physiological conditions and in elasticity measurements by collecting force verses distance curves over specified location of the cell body (Figure 1-5(d)). In this dissertation, AFM method has been extensively used to measure the biomechanical prosperities of the cells (Young's modulus) under different growth conditions.

In addition to experimental methods, there has been several repots on development of various models such as the continuum model [80-82], soft glassy model (SGR) [62, 83-85], multiphasic model [52, 59, 76, 86], and tensegrity model [87] to analyze the cytoskeletal structures of the cell and its mechanical characteristics. Herein, we have frequently referred to the tensegrity

model to explain the differences in the adhesion characteristics of the normal and cancerous cells within the 3-D etched isotropic microstructures.

The tensegrity (tensional integrity) model was proposed by Donald E. Ingber in 1981 which considers a system known as "tensegrity architecture" for the cell structure. This model is a subclass of discrete cell models. Based on this model, cytoskeletal lattice (mainly actin filaments) carries preexisting tensile stress (prestress) which provides stability to the cell shape. The prestress within the cytoskeleton is balanced by the cell adhesion forces to the extracellular matrix and partly by internal compression cytoskeletal elements such as microtubules. Structural rigidity and stiffness of the tensegrity structures is proportional to its level of the prestress. Based on this model, the more the systems is under prestress, the more stable it is and the less it is favorable to deform under external load [87, 88]. So far, some experimental studies which have verified the hypothesis in the tensegrity model [89, 90].

1.5 Objective and outline of the dissertation

The main objective of this research is to develop three dimensional (3-D) isotropic silicon microstructures to conduct comprehensive analysis on cytoskeletal organization, adhesion pattern, morphology, growth and trapping efficiency of normal fibroblasts, non-malignant, and malignant breast cells (major cell types embedded within the human breast tumor microenvironment) interacting with the 3-D topographies. The main emphasis is on identification of cell biomechanical signatures which can be ultimately used to segregate between normal and cancerous cells. The motivation of this dissertation originated from the following fundamental questions:

- Whether the cells' response to the topographical patterns of their underlying substrate is dependent on the degree of their disease state?
- Whether the cells' cytoskeletal organization and its biomechanical properties are among the parameters which affect their behavior on nano/microscale topographies?
- Whether it is possible to maximize (augment) the differential response of normal and diseased cells by varying the geometrical features of the substrate or introducing chemical stimuli to the static culture condition?

- Whether it is ultimately possible to utilize cell-substrate interactions to create platforms for cell separation and cancer diagnosis applications?

Within the scope of this research, three different generations of isotropic microstructures were developed to achieve the desired objective. Furthermore, AFM was employed to directly measure the Young's modulus of the cells and to investigate the role of cell biomechanical properties on adhesion pattern and cytoskeletal organization of the cells on the 3-D microstructures. This dissertation is divided into four major sections which cover the experimental and theoretical work performed during the term of the completion of the project in the last four years. Most of the chapters of this document provide background information for the fields of interest and specific application. Below is a brief outline of the dissertation:

Chapter 2 (section one) covers development of the first generation of 3-D isotropic silicon microstructures and the utilization of these microenvironments for discriminating between normal human fibroblast (HS68) and metastatic human breast cancer cells (MDA-MB-231). The behavior and response of normal fibroblast and breast cancer cells were explored in terms of adhesion, growth and trapping in these artificial 3-D microenvironments having curved sidewalls. **Chapters 3 and 4** (section two) explain development of the second generation of the 3-D isotropic silicon microstructures for detailed investigation of the role of cell cytoskeletal organization and its biomechanical properties and morphology in differential adhesion patterns of normal human fibroblasts (HS68), normal human breast epithelial cells (MCF10A), and metastatic human breast cancer cells (MDA-MB-231) on the proposed microstructures. **Chapter 5** (section three) is focused on the effect of the SAHA anti-cancer drug on cell cytoarchitecture, morphology and adhesion pattern on the second generation of 3-D silicon microstructures. **Chapter 6** (section four) reports development of the third generation of 3-D isotropic microstructures for comprehensive analysis of the response of MDA-MB-231 and MCF10A cells to SAHA anti-cancer drug in a co-culture system. **Chapter 7** covers the influence of the composition of the growth medium on biomechanical properties of the MCF10A and MDA-MB-231 cells using AFM. **Chapter 8** presents the conclusion and outlook.

1.6 References

[1] B. Alberts, *et al.*, *Molecular Biology of the Cell*, Fifth ed. New York: Garland Science, Taylor & Francis Group, 2008.

[2] J. Howard, *Mechanics of Motor Proteins and the Cytoskeleton* Sunderland: Sinauer Associates, Inc., 2001.

[3] Y. Tsuda, *et al.*, "Torsional rigidity of single actin filaments and actin-actin bond breaking force under torsion measured directly by in vitro micromanipulation," *Proceedings of the National Academy of Sciences of the United States of America,* vol. 93, pp. 12937-12942, Nov 1996.

[4] R. Yasuda, *et al.*, "Direct measurement of the torsional rigidity of single actin filaments," *Journal of Molecular Biology,* vol. 263, pp. 227-236, Oct 1996.

[5] T. P. Stossel, "Contribution of actin to the structure of the cytoplasmic matrix," *Journal of Cell Biology,* vol. 99, pp. S15-S21, 1984.

[6] R. Ananthakrishnan, *et al.*, "Quantifying the contribution of actin networks to the elastic strength of fibroblasts," *Journal of Theoretical Biology,* vol. 242, pp. 502-516, Sep 2006.

[7] C. Rotsch and M. Radmacher, "Drug-induced changes of cytoskeletal structure and mechanics in fibroblasts: An atomic force microscopy study," *Biophysical Journal,* vol. 78, pp. 520-535, Jan 2000.

[8] F. Gittes, *et al.*, "Flexural Rigidity of Microtubules and Actin Filaments Measured from Thermal Fluctuations in Shape," *Journal of Cell Biology,* vol. 120, pp. 923-934, Feb 1993.

[9] N. Mucke, *et al.*, "Assessing the flexibility of intermediate filaments by atomic force microscopy," *Journal of Molecular Biology,* vol. 335, pp. 1241-1250, Jan 2004.

[10] H. Lodish, *et al.*, *Molecular cell biology*. New York: W. H. Freeman, 2000.

[11] A. Prokop, *et al.*, "NanoLiterBioReactor: Long-term mammalian cell culture at nanofabricated scale," *Biomedical Microdevices,* vol. 6, pp. 325-339, Dec 2004.

[12] K. Slater, "Cytotoxicity tests for high-throughput drug discovery," *Current Opinion in Biotechnology,* vol. 12, pp. 70-74, Feb 2001.

[13] G. Z. Weng, *et al.*, "Complexity in biological signaling systems," *Science,* vol. 284, pp. 92-96, Apr 1999.

[14] E. H. Davidson, *et al.*, "A genomic regulatory network for development," *Science,* vol. 295, pp. 1669-1678, Mar 2002.

[15] J. Drews, "Drug discovery: A historical perspective," *Science,* vol. 287, pp. 1960-1964, Mar 2000.

[16] C. Sander, "Genomic medicine and the future of health care," *Science,* vol. 287, pp. 1977-1978, Mar 2000.

[17] J. B. Gibbs, "Mechanism-based target identification and drug discovery in cancer research," *Science,* vol. 287, pp. 1969-1973, Mar 2000.

[18] H. Kitano, "Systems biology: A brief overview," *Science,* vol. 295, pp. 1662-1664, Mar 2002.

[19] T. H. Park and M. L. Shuler, "Integration of cell culture and microfabrication technology," *Biotechnology Progress,* vol. 19, pp. 243-253, Mar-Apr 2003.

[20] K. F. Jensen, "Microreaction engineering—is small better?," *Chemical Engineering Science,* vol. 56, pp. 293-303, Jan 2001.

[21] S. D. Senturia, *Microsystem Design*. Norwell: Kluwer Academic Publishers, 2001.

[22] A. C. R. Grayson, *et al.*, "A BioMEMS review: MEMS technology for physiologically integrated devices," *Proceedings of the IEEE,* vol. 92, pp. 6-21, Jan 2004.

[23] A. Curtis and C. Wilkinson, "Topographical control of cells," *Biomaterials,* vol. 18, pp. 1573-1583, Dec 1997.

[24] C. J. Bettinger, *et al.*, "Engineering Substrate Topography at the Micro- and Nanoscale to Control Cell Function," *Angewandte Chemie-International Edition,* vol. 48, pp. 5406-5415, 2009.

[25] R. G. Harrison, "Reaction of embryonic cells to solid structures," *Journal of Experimental Zoology,* vol. 17, pp. 521-544, 1914.

[26] E. T. denBraber, *et al.*, "Quantitative analysis of cell proliferation and orientation on substrata with uniform parallel surface micro-grooves," *Biomaterials,* vol. 17, pp. 1093-1099, Jun 1996.

[27] P. Clark, *et al.*, "Cell Guidance by Ultrafine Topography Invitro," *Journal of Cell Science,* vol. 99, pp. 73-77, May 1991.

[28] A. M. Rajnicek, *et al.*, "Contact guidance of CNS neurites on grooved quartz: influence of groove dimensions, neuronal age and cell type," *Journal of Cell Science,* vol. 110, pp. 2905-2913, Dec 1997.

[29] C. Oakley and D. M. Brunette, "The Sequence of Alignment of Microtubules, Focal Contacts and Actin-Filaments in Fibroblasts Spreading on Smooth and Grooved Titanium Substrata," *Journal of Cell Science,* vol. 106, pp. 343-354, Sep 1993.

[30] C. Oakley, *et al.*, "Sensitivity of fibroblasts and their cytoskeletons to substratum topographies: Topographic guidance and topographic compensation by micromachined grooves of different dimensions," *Experimental Cell Research,* vol. 234, pp. 413-424, Aug 1997.

[31] X. F. Walboomers, *et al.*, "Growth behavior of fibroblasts on microgrooved polystyrene," *Biomaterials,* vol. 19, pp. 1861-1868, Oct 1998.

[32] X. F. Walboomers, *et al.*, "Attachment of fibroblasts on smooth and microgrooved polystyrene," *Journal of Biomedical Materials Research,* vol. 46, pp. 212-220, Aug 1999.

[33] K. Matsuzaka, *et al.*, "Effect of microgrooved poly-l-lactic (PLA) surfaces on proliferation, cytoskeletal organization, and mineralized matrix formation of rat bone marrow cells," *Clinical Oral Implants Research,* vol. 11, pp. 325-333, Aug 2000.

[34] X. F. Walboomers, *et al.*, "Contact guidance of rat fibroblasts on various implant materials," *Journal of Biomedical Materials Research*, vol. 47, pp. 204-212, Nov 1999.

[35] S. Sarkar, *et al.*, "Vascular tissue engineering: microtextured scaffold templates to control organization of vascular smooth muscle cells and extracellular matrix," *Acta Biomaterialia*, vol. 1, pp. 93-100, Jan 2005.

[36] B. S. Zhu, *et al.*, "Alignment of osteoblast-like cells and cell-produced collagen matrix induced by nanogrooves," *Tissue Engineering*, vol. 11, pp. 825-834, May 2005.

[37] W. E. Johnson, *et al.*, "Topographical guidance of intervertebral disc cell growth in vitro: towards the development of tissue repair strategies for the anulus fibrosus," *European Spine Journal*, vol. 15, pp. S389-S396, Aug 2006.

[38] D. Zahor, *et al.*, "Organization of mesenchymal stem cells is controlled by micropatterned silicon substrates," *Materials Science & Engineering C-Biomimetic and Supramolecular Systems*, vol. 27, pp. 117-121, Jan 2007.

[39] C. J. Bettinger, *et al.*, "Micro fabrication of poly (glycerol-sebacate) for contact guidance applications," *Biomaterials*, vol. 27, pp. 2558-2565, Apr 2006.

[40] M. D. Guillemette, *et al.*, "Surface topography induces 3D self-orientation of cells and extracellular matrix resulting in improved tissue function," *Integrative Biology*, vol. 1, pp. 196-204, Feb 2009.

[41] A. M. P. Turner, *et al.*, "Attachment of astroglial cells to microfabricated pillar arrays of different geometries," *Journal of Biomedical Materials Research*, vol. 51, pp. 430-441, Sep 2000.

[42] H. H. Liao, *et al.*, "Response of rat osteoblast-like cells to microstructured model surfaces in vitro," *Biomaterials*, vol. 24, pp. 649-654, Feb 2003.

[43] M. R. Dusseiller, *et al.*, "An inverted microcontact printing method on topographically structured polystyrene chips for arrayed micro-3-D culturing of single cells," *Biomaterials*, vol. 26, pp. 5917-5925, Oct 2005.

[44] S. Giselbrecht, *et al.*, "3D tissue culture substrates produced by microthermoforming of pre-processed polymer films," *Biomedical Microdevices*, vol. 8, pp. 191-199, Sep 2006.

[45] J. L. Charest, *et al.*, "Myoblast alignment and differentiation on cell culture substrates with microscale topography and model chemistries," *Biomaterials*, vol. 28, pp. 2202-2210, Apr 2007.

[46] J. Y. Mai, *et al.*, "A microfabricated platform probing cytoskeleton dynamics using multidirectional topographical cues," *Biomedical Microdevices*, vol. 9, pp. 523-531, Aug 2007.

[47] C. H. Choi, *et al.*, "Cell interaction with three-dimensional sharp-tip nanotopography," *Biomaterials*, vol. 28, pp. 1672-1679, Mar 2007.

[48] L. Wang, *et al.*, "Influence of micro-well biomimetic topography on intestinal epithelial Caco-2 cell phenotype," *Biomaterials*, vol. 30, pp. 6825-6834, Dec 2009.

[49] A. Ranella, *et al.*, "Tuning cell adhesion by controlling the roughness and wettability of 3D micro/nano silicon structures," *Acta Biomaterialia,* vol. 6, pp. 2711-2720, Jul 2010.

[50] J. L. Tan, *et al.*, "Cells lying on a bed of microneedles: An approach to isolate mechanical force," *Proceedings of the National Academy of Sciences of the United States of America,* vol. 100, pp. 1484-1489, Feb 2003.

[51] Z. J. Liu, *et al.*, "Mechanical tugging force regulates the size of cell-cell junctions," *Proceedings of the National Academy of Sciences of the United States of America,* vol. 107, pp. 9944-9949, Jun 2010.

[52] M. R. K. Mofrad and R. D. Kamm, *Cytoskeletal Mechanics: Models and Measurements*. New York: Cambridge University Press, 2006.

[53] D. A. Fletcher and D. Mullins, "Cell mechanics and the cytoskeleton," *Nature,* vol. 463, pp. 485-492, Jan 2010.

[54] S. Suresh, "Biomechanics and biophysics of cancer cells," *Acta Materialia,* vol. 55, pp. 3989-4014, Jul 2007.

[55] G. Bao and S. Suresh, "Cell and molecular mechanics of biological materials," *Nature Materials,* vol. 2, pp. 715-725, Nov 2003.

[56] J. Guck, *et al.*, "Optical deformability as an inherent cell marker for testing malignant transformation and metastatic competence," *Biophysical Journal,* vol. 88, pp. 3689-3698, May 2005.

[57] J. Guck, *et al.*, "The optical stretcher: A novel laser tool to micromanipulate cells," *Biophysical Journal,* vol. 81, pp. 767-784, Aug 2001.

[58] K. A. Ward, *et al.*, "Viscoelastic properties of transformed cells: role in tumor cell progression and metastasis formation," *Biorheology,* vol. 28, pp. 301-13, 1991.

[59] F. Guilak, *et al.*, "The effects of osmotic stress on the viscoelastic and physical properties of articular chondrocytes," *Biophysical Journal,* vol. 82, pp. 720-727, Feb 2002.

[60] W. R. Trickey, *et al.*, "Determination of the Poisson's ratio of the cell: recovery properties of chondrocytes after release from complete micropipette aspiration," *Journal of Biomechanics,* vol. 39, pp. 78-87, 2006.

[61] S. M. Mijailovich, *et al.*, "A finite element model of cell deformation during magnetic bead twisting," *Journal of Applied Physiology,* vol. 93, pp. 1429-1436, 2002.

[62] B. Fabry, *et al.*, "Scaling the microrheology of living cells," *Physical Review Letters,* vol. 87, Oct 2001.

[63] S. Leporatti, *et al.*, "Cytomechanical and topological investigation of MCF-7 cells by scanning force microscopy," *Nanotechnology,* vol. 20, Feb 2009.

[64] M. Lekka, *et al.*, "Elasticity of normal and cancerous human bladder cells studied by scanning force microscopy," *European Biophysics Journal,* vol. 28, pp. 312-316, 1999.

[65] S. E. Cross, *et al.*, "Nanomechanical analysis of cells from cancer patients," *Nature Nanotechnology,* vol. 2, pp. 780-783, Dec 2007.

[66] E. M. Darling, *et al.*, "A thin-layer model for viscoelastic, stress-relaxation testing of cells using atomic force microscopy: Do cell properties reflect metastatic potential?," *Biophysical Journal,* vol. 92, pp. 1784-1791, Mar 2007.

[67] E. M. Darling, *et al.*, "Viscoelastic properties of human mesenchymally-derived stem cells and primary osteoblasts, chondrocytes, and adipocytes," *Journal of Biomechanics,* vol. 41, pp. 454-464, 2008.

[68] E. C. Faria, *et al.*, "Measurement of elastic properties of prostate cancer cells using AFM," *Analyst,* vol. 133, pp. 1498-1500, 2008.

[69] S. E. Cross, *et al.*, "AFM-based analysis of human metastatic cancer cells," *Nanotechnology,* vol. 19, Sep 2008.

[70] S. Iyer, *et al.*, "Atomic force microscopy detects differences in the surface brush of normal and cancerous cells," *Nature Nanotechnology,* vol. 4, pp. 389-393, Jun 2009.

[71] M. Nikkhah, *et al.*, "Evaluation of the Influence of Growth Medium Composition on Cell Elasticity," *Journal of Biomechanics,* vol. In Press, 2010.

[72] M. Nikkhah, *et al.*, "The cytoskeletal organization of breast carcinoma and fibroblast cells inside three dimensional (3-D) isotropic silicon microstructures," *Biomaterials,* vol. 31, pp. 4552-4561, Jun 2010.

[73] R. M. Hochmuth, "Micropipette aspiration of living cells," *Journal of Biomechanics,* vol. 33, pp. 15-22, Jan 2000.

[74] G. M. Artmann, *et al.*, "Micropipette aspiration of human erythrocytes induces echinocytes via membrane phospholipid translocation," *Biophysical Journal,* vol. 72, pp. 1434-1441, Mar 1997.

[75] F. Richelme, *et al.*, "Dynamic study of cell mechanical and structural responses to rapid changes of calcium level," *Cell Motility and the Cytoskeleton,* vol. 45, pp. 93-105, Feb 2000.

[76] F. Guilak and V. C. Mow, "The mechanical environment of the chondrocyte: a biphasic finite element model of cell-matrix interactions in articular cartilage," *Journal of Biomechanics,* vol. 33, pp. 1663-1673, Dec 2000.

[77] J. X. Chen, *et al.*, "Twisting integrin receptors increases endothelin-1 gene expression in endothelial cells," *American Journal of Physiology-Cell Physiology,* vol. 280, pp. C1475-C1484, Jun 2001.

[78] G. N. Maksym, *et al.*, "Mechanical properties of cultured human airway smooth muscle cells from 0.05 to 0.4 Hz," *Journal of Applied Physiology,* vol. 89, pp. 1619-1632, Oct 2000.

[79] G. Binnig, *et al.*, "Atomic Force Microscope," *Physical Review Letters,* vol. 56, pp. 930-933, 1986.

[80] G. A. Ateshian, *et al.*, "Continuum Modeling of Biological Tissue Growth by Cell Division, and Alteration of Intracellular Osmolytes and Extracellular Fixed Charge Density," *Journal of Biomechanical Engineering-Transactions of the ASME,* vol. 131, Oct 2009.

[81] D. E. Discher, *et al.*, "Simulations of the erythrocyte cytoskeleton at large deformation. II. Micropipette aspiration," *Biophysical Journal,* vol. 75, pp. 1584-1597, Sep 1998.

[82] G. T. Charras and M. A. Horton, "Determination of cellular strains by combined atomic force microscopy and finite element modeling," *Biophysical Journal,* vol. 83, pp. 858-879, Aug 2002.

[83] B. Fabry and J. J. Fredberg, "Remodeling of the airway smooth muscle cell: are we built of glass?," *Respiratory Physiology & Neurobiology,* vol. 137, pp. 109-124, Sep 2003.

[84] K. K. Mandadapu, *et al.*, "On the cytoskeleton and soft glassy rheology," *Journal of Biomechanics,* vol. 41, pp. 1467-1478, 2008.

[85] P. Sollich, "Rheological constitutive equation for a model of soft glassy materials," *Physical Review E,* vol. 58, pp. 738-759, Jul 1998.

[86] F. Guilak, "Compression-induced changes in the shape and volume of the chondrocyte nucleus," *Journal of Biomechanics,* vol. 28, pp. 1529-1541, Dec 1995.

[87] D. E. Ingber, "Tensegrity I. Cell structure and hierarchical systems biology," *Journal of Cell Science,* vol. 116, pp. 1157-1173, Apr 2003.

[88] D. E. Ingber, "Cellular tensegrity: defining new rules of biological design that govern the cytoskeleton," *Journal of Cell Science,* vol. 104, pp. 613-627, 1993.

[89] D. Stamenovic, *et al.*, "Experimental tests of the cellular tensegrity hypothesis," *Biorheology,* vol. 40, pp. 221-225, 2003.

[90] N. Wang, *et al.*, "Cell prestress. I. Stiffness and prestress are closely associated in adherent contractile cells," *American Journal of Physiology. Cell Physiology,* vol. 282, pp. C606-C616, Mar 2002.

2 Chapter Two: Attachment and Response of Human Fibroblast and Breast Cancer Cells to Three Dimensional Silicon Microstructures of Different Geometries

M. Nikkhah, et al., "Attachment and response of human fibroblast and breast cancer cells to three dimensional silicon microstructures of different geometries," Biomedical Microdevices, vol. 11, pp. 429-441, Apr 2009.

2.1 Introduction

Advances in microfabrication and microfluidic technologies have attracted significant attention as a means to create highly controllable microenvironments for cell biology research and to simulate *in vivo* growth situations more closely than traditional two dimensional (2-D) cell culture methods [2]. Biomedical devices created through microtechnology have been used to enhance our knowledge of cell-cell, cell-medium, and cell-substrate interactions. This information has broad applicability to the development of artificial tissues, biosensors, drug screening instrumentations, and cell sorting devices [3].

To date, a variety of other investigators have addressed the principles of cell-surface interactions and described cellular responses to differing substrate topographical patterns including arrays of microgrooves [4-15], arrays of pillars and wells [16-18], arrays of grooves and holes [19, 20], arrays of pyramid shape microstructures [21] and networks of ridges and girds [22]. Most of these microdevices were fabricated by an anisotropic etching process or soft lithography to form microstructures with vertical sidewalls, and were used to determine the crucial surface texture parameters for designing implantable prosthetic devices.

The microfabrication process presented here is distinct from previously reported work, and can be utilized to develop three-dimensional (3-D) microenvironments, precisely engineer the cell culture substrate topography, and extend the repertoire of possible surface geometries because the side-wall curvature can be controlled to varying degrees. The technique allows, several important cellular behaviors including deformability and adhesion to be tested by spatially controlling the curvature of the sidewalls within the 3-D microenvironments.

In summary we present the development of arrays of 3-D silicon microstructures consisting of isotropic microchambers interconnected with channels using a novel single-mask 3-D fabrication process for the development of microelectromechanical systems (MEMS) and microfluidics [23]. Next, we quantitatively assess the effect of the geometry of isotropic microchambers with varying width and depth on adhesion and growth behavior of normal human fibroblast cells and metastatic human breast cancer cells under static culture conditions. Specifically, we have investigated the effect of microchambers surface curvature on cell adhesion and the effect of microchambers depth on cell growth. This is the first description of a silicon substrate used as an *in vitro* model to simulate a human breast tumor microenvironment. Fibroblast cells are the principal cellular component of connective tissues matrix [24], and in patients, fibroblast cells are intimately embedded within breast tumor microenvironments [25, 26]. In any tumor biopsy, there is extensive contamination of breast tumor epithelial cells by fibroblasts, and an important research goal is to understand how fibroblast and breast tumor epithelial cells respond differentially to the silicon growth substrate and utilize this information to design microdevices for cancer research. Using our isotropic silicon substrates, we illustrate how cellular behaviors such as spreading and deformation change in healthy fibroblasts and cancerous breast epithelial cells in response to their substrate microenvironment. The application of this information is crucial for the design of new MEMS-based cancer cell separation, detection, and diagnostics technologies. The 3-D complex microenvironments can also lead into new instruments for *in vitro* drug efficacy monitoring [27].

2.2 Materials and methods

2.2.1 Device fabrication

The devices shown in Figure 2-1 were fabricated using MEMS technology from single-crystal silicon wafers. The fabrication method relies on the applicability of reactive ion etching (RIE) lag and its dependence on the geometrical patterns of the photomask layout [23] to etch silicon to different depths using a single isotropic etch step and to form arrays of microchambers interconnected with microchannels.

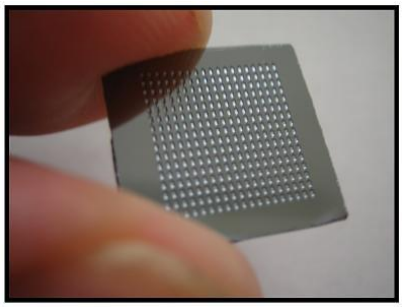

Figure 2-1 A photo image of the 1 cm^2 chips fabricated in silicon.

Figure 2-2 shows the fabrication process flow which started by the deposition of an 8000Å-thick oxide layer on a silicon wafer using plasma enhanced chemical vapor deposition (PECVD) technique. The wafer was then vapor-primed with hexamethyldisylazane (HMDS) and spun coated with approximately 2 µm of photoresist 1813. After patterning photoresist, the oxide layer was etched for 3 minutes using deep reactive ion etching (DRIE) CH_4/C_4F_8 plasma. Next, silicon was etched using DRIE SF_6 plasma to achieve final 3-D microstructures. The mask design consisted of square patterns with sizes of 4 ×10 µm^2. Due to RIE lag, areas under the bigger mask openings were etched more, thereby achieving 3-D geometries. After removing photoresist and the oxide layer, the wafer was diced into 1 cm^2 chips. The chips were cleaned using acetone and isopropanol, were rinsed in deionized water, and, finally, were air-dried.

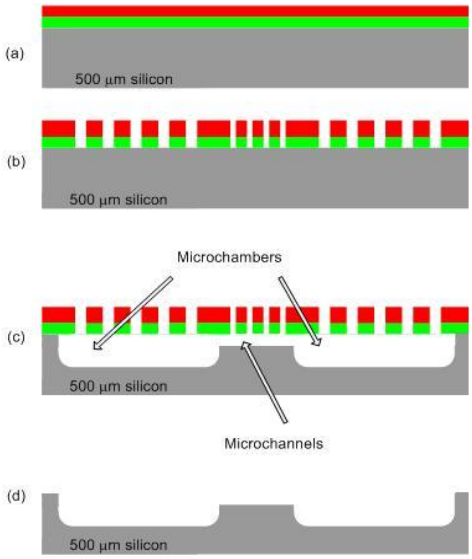

Figure 2-2 Process flow for the fabrication of 3-D cell culture substrates comprising arrays of isotropic microchambers interconnected with microchannels.

Figure 2-3 shows scanning electron microscopy (SEM) images of the fabricated silicon microstructures. Silicon was etched for five different etch times of 5, 10, 15, 20, and 30 minutes to investigate the effect of the curved sidewalls of the microchambers, resulted from isotropic silicon etching, and their corresponding depths on cellular behavior. As the etch time increased, the microchambers became wider and deeper. The width and depth of the microchambers were varied in the range of 215-308 µm and 25-126 µm, respectively.

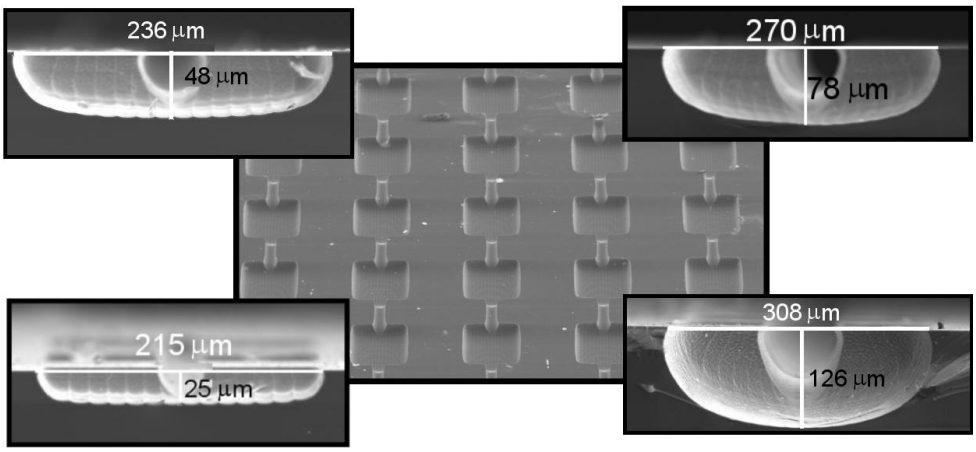

Figure 2-3 SEM images of the silicon microstructures composed of isotropic microchambers and microchannels. The corresponding widths of the microchambers for 5, 10, 15, 20 and 30 minute etch times are 215, 236, 270, 279, and 308 µm, respectively, and the corresponding depth are 25, 48, 78, 88 and 126 µm

It is notable that due to RIE lag, the depths of the microchambers were different from the interconnecting channels for each of the etching times. The curvature of the microchambers has been approximated assuming an elliptical shape for their cross sectional view. The curvature of an ellipse can be calculated using the following equation:

$$k(t) = \frac{ab}{\left(a^2 \sin^2(t) + b^2 \cos^2(t)\right)^{3/2}} \qquad 0 \le t \le 2\pi$$

where "a" and "b" denote half of the length of the major and minor axis, respectively. The variation of the curvature for different etch times has been shown in Figure 2-4 in the range of $-\pi/2 \le t \le 0$. In this figure, $t = -\pi/2$ corresponds to the flat surfaces at the bottom of the microchambers and $t = 0$ corresponds to the location on the sidewalls with maximum curvature. As the etch time increases, the microchambers become wider and deeper, however the curvature of the sidewalls decreases.

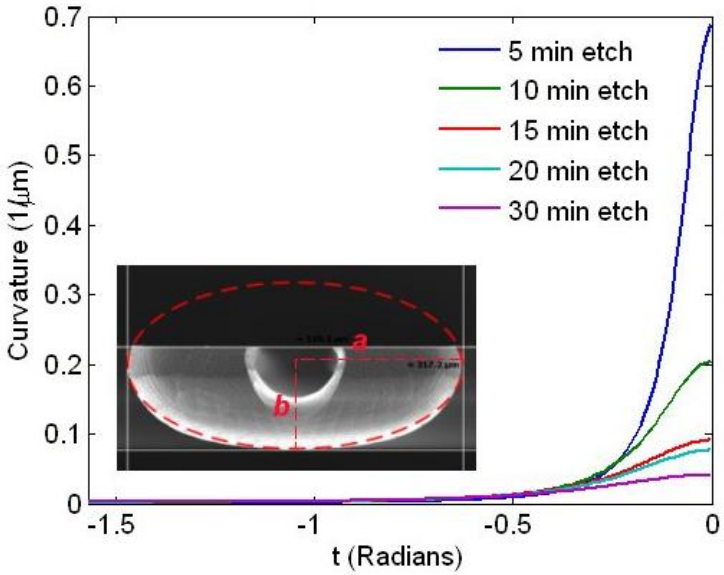

Figure 2-4 The curvatures of the microchambers for different etch times. The inset shows the elliptical shape approximation for the microchambers' cross sectional view.

2.2.2 Fibroblast and breast cancer cell culture

Both HS68 normal human fibroblasts and MDA-MB-231 human breast cancer cells used in this work were purchased from the American Type Culture Collections (ATCC). Cells were maintained in plastic T-75 cm^2 culture flasks in RPMI culture medium which contained 10% fetal bovine serum (FBS), 1 mM sodium pyruvate, and penicillin-streptomycin (100 Units/ml). Cells were grown at 37 °C in humidified 7% CO_2-93% air atmosphere. In order to avoid bubble formation on the microchambers during cell culture process, the chips were transferred to individual wells in a 12-well culture dishes and centrifuged with 3500 rpm for 15 minutes in the presence of culture medium. Cells were then added to the culture medium. After the desired culture period, Hoechst 33342 dye (6.6 µg/ml final concentration) was added to the culture medium for 10 minutes (37 °C). Hoechst 33342 is a cell-permeant DNA intercalator that labels nuclei in living cells. The chips were rinsed three times in Hank's Balanced Salt Solution and were fixed in 4% formaldehyde in phosphate-buffered saline for 15 minutes at room temperature. The chips were finally rinsed with water and air-dried

2.2.3 Measurement techniques

Fluorescence microscopy was performed at 365 nm excitation and 445 nm emission wavelengths to image blue nucleus staining (Hoechst 33342). For all etch times of 5, 10, 15, 20,

30 minutes, fluorescence images were obtained at ten different fields on each chip with 10X objective magnification. Each field included six microchambers and the flat surfaces between them. The fluorescence images inside the microchambers were obtained at two different depths of focus due to the curvature of their sidewalls. Samples were also imaged by confocal microscopy in the reflection mode. The confocal images inside the microchambers were taken at different depths of focus to construct Z-stack images. Cell nuclei were stained with Hoechst 33342 dye and actin was visualized using Alexa-488 phalloidin [18]. SEM was performed to assess the detailed effects of the etched microstructures on the cells' morphology. X-ray Photoelectron Spectroscopy (XPS) was used to provide detailed information on the surface composition and chemical state of the elements detected in the near surface for both the flat surfaces and etched microstructures. An X-ray beam spot of 100 µm was used to make sure that the detected signal only came from the area of interest. The number of cells inside each field was counted using the National Institutes of Health (NIH) imageJ software. The data were statistically analyzed using Prism GraphPad V.5 software. One-way ANOVA analysis was followed by linear-trend or Dunnett's multiple t-test post-tests. Alternatively, pair-wise comparisons between fibroblast and cancer cell ratios were performed using Bonferoni's t-test.

2.3 Results and Discussion

2.3.1 Fibroblast and cancer cells growth on flat surfaces

Both fibroblast cells and cancer cells were cultured on separate flat silicon and glass surfaces and their growth was compared as the control for the experiments. Following seeding at low density, fibroblast cells attached and spread on both surfaces within 6 hours. The corresponding time for cancer cells was about 24 hours. This process was visualized under an optical microscope. HS68 cells proliferated on silicon and glass surfaces with typical cell growth kinetics. Figure 2-5(a) demonstrates logarithmic, and plateau phase of fibroblast cell growth. There was not a significant difference in growth of these cells on a silicon substrate compared to the commonly used glass plates. Figure 2-5(b) demonstrates the logarithmic phase of the MDA-MB-231 cells growth on silicon and glass surfaces. Cancer cells tended to grow more on glass compared to silicon while having a similar growth rate on both substrates.

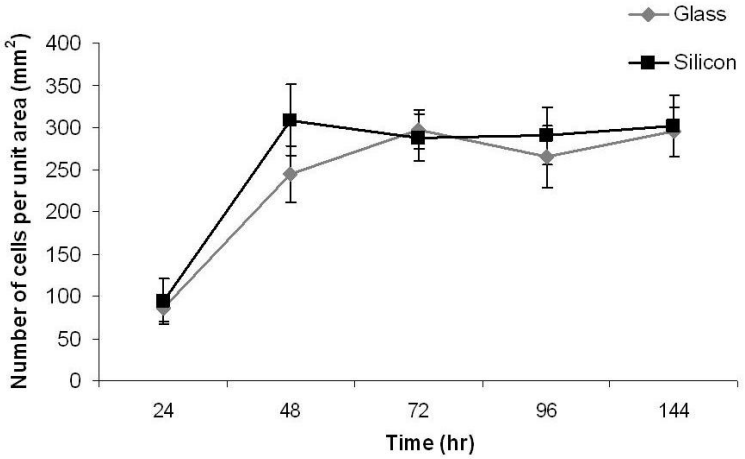

(a)

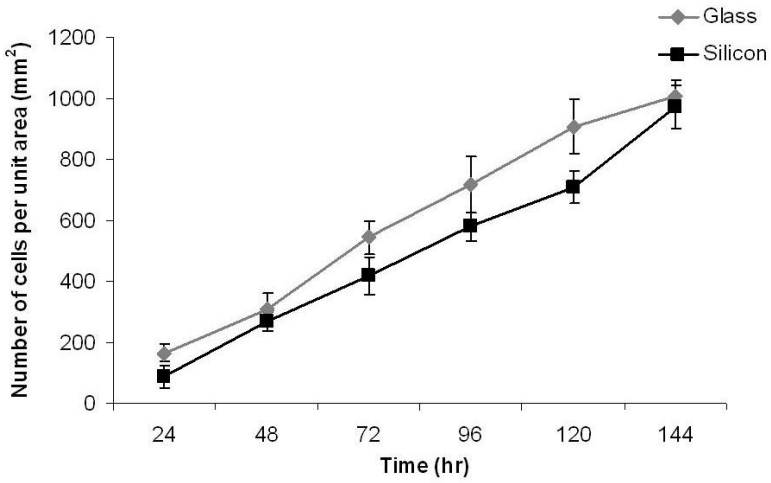

(b)

Figure 2-5 (a) Fibroblast and (b) cancer cells growth on flat silicon and glass surfaces as a function of time showing typical cell growth kinetics. Data shown are the mean and standard deviation of the cell #/mm2.

The logarithmic growth rate of breast cancer cells typically exceeds that of fibroblast cells because transformed cells bear oncogenic mutations [28]. Typically, cancer cells achieved higher cell densities than fibroblast cells and entered a steady-state period of growth after 144 hours of incubation. After 168 hours in culture, confluent monolayers of cells covered the smooth surfaces of the chip.

2.3.2 Cell adhesion on the curved sidewalls of 3-D microchambers

Attachment of fibroblast and cancer cells on curved sidewalls of the microchambers as well as the interconnecting microchannels was first assessed using SEM and confocal microscopy to visualize the nuclei and actin filaments. Figure 2-6 shows the SEM images of the microchambers and interconnecting channels and cross section of their sidewalls with the attached cells after 72 hours culture time.

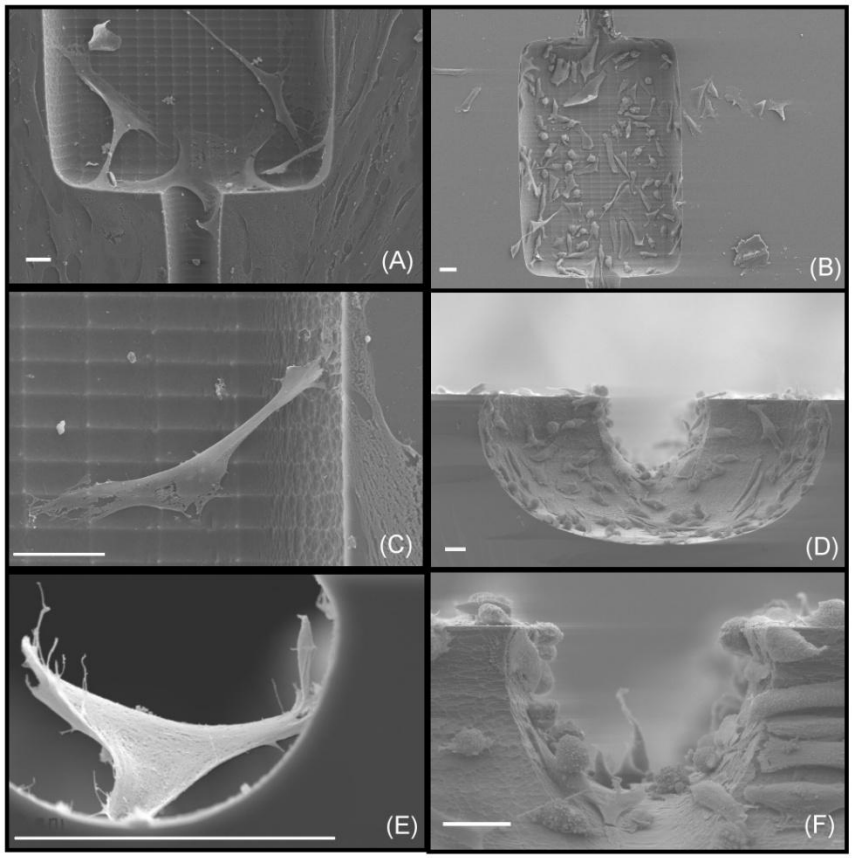

Figure 2-6 SEM images of fibroblast (A, C, E) and cancer (B, D, F) cells illustrating their attachment on the curved sidewalls of the microenvironments. Scale bars represent 20 µm.

For the most part, fibroblasts adhered to the surfaces with low curvature. This includes smooth flat surfaces, surfaces at the bottom of microchambers and also sidewalls with low curvature, i.e. 20 minutes and 30 minutes etched microchambers (Figure 2-4). Moreover, they stretched to avoid the curved sidewalls with high curvature (Figure 2-6(A,C,E)). From these images, it is clear that surface curvature plays a major role in the adhesion behavior of fibroblast cells. As seen in Figure 2-6(B,D,F), the breast cancer cells, unlike fibroblasts, formed stable

adhesions and attached to the corners and curved sidewalls of the microchambers regardless of their curvature. The cancer cells were also found inside the microchannels and deformed to adapt to the shape of the substrate geometry.

Confocal microscopy was performed after 72 hours of cell growth on silicon substrates. Figure 2-7 shows the actin filaments and nuclei distribution within fibroblast cells attached on the smooth flat surfaces (Figure 2-7(A)) and inside the microchambers (Figure 2-7(C,E)).

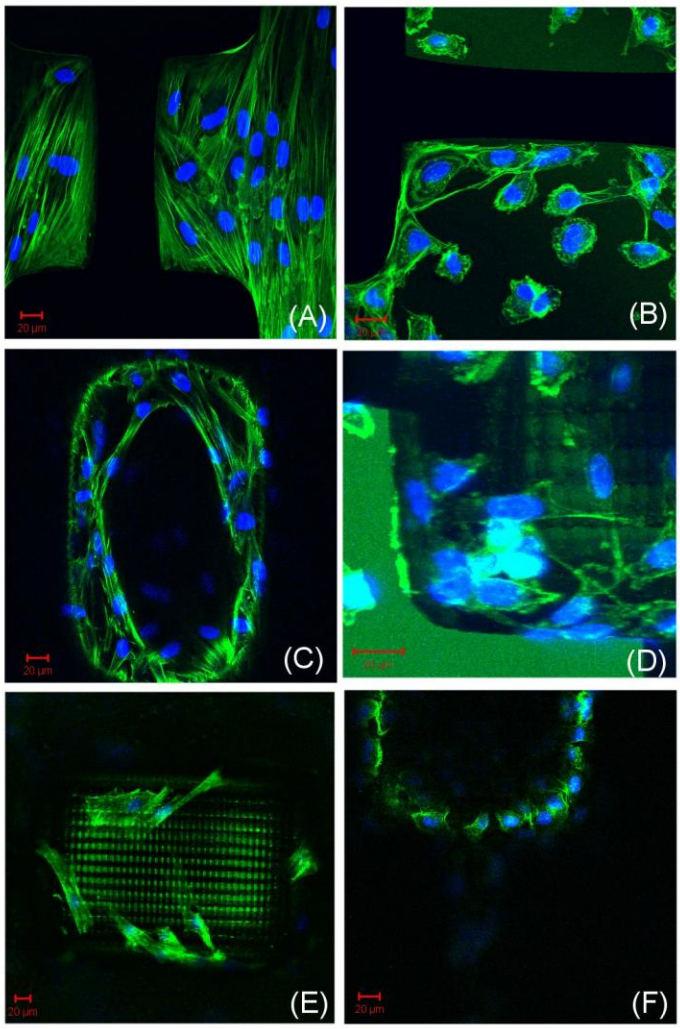

Figure 2-7 Confocal images from the nuclei of fibroblast (A, C, E) and cancer (B, D, F) cells and their actin filaments on flat surfaces and inside the etched microstructures.

On flat surfaces, the cells as well as their actin filaments were spread and oriented in one direction. The orientation of the actin filaments and nuclear shape changed and deformed when the cells were attached on the edges of the etched features. The fibroblast cells exhibited a flat

cytoskeleton structure and their actin filaments were distributed in long, thin and parallel bundles. As previously observed by SEM images, the fibroblast cells stretched to avoid curved sidewalls and in Figure 2-7(C) the actin filament distribution in the stretched cells can be seen.

Figure 2-7(B) shows the cytoskeleton structure and actin filaments of the breast cancer cells attached on flat silicon surfaces. It is well known that reorganization of cytoskeleton and alterations in actin filament structure occurs during malignant transformation of normal cells [29, 30]. These confocal images of human breast cancer cells attached on our silicon substrates clearly indicate such alterations in their actin network. The MDA-MB-231 cancer cells were generally rounded and their actin filaments were randomly distributed in short bundles throughout the cell body. The actin cytoskeleton in these cancer cells is clearly more poorly organized compared with that in the normal fibroblast cells. Figure 2-7(D,F) show the actin filaments and nuclei distribution of cells attached to the corners and on the curved sidewalls of the microchambers. The cancer cells can be seen to adapt their cytoskeleton to the curved geometry of the 3-D microstructures much more frequently than the fibroblasts.

We propose that the aforementioned differences in the adhesion behaviors of the breast cancer cells and normal human fibroblasts are likely due to differences in their biomechanical properties, mainly cytoskeleton stiffness. Fibroblast cells are less likely to distort their cytoskeleton structure and this can be the main reason for their stretching inside the isotropic microchambers. These cells do not deform, due to the stiffness of their cytoskeleton structure, to take the shape of the curved sidewalls of isotropic microchambers. Previous studies have also shown that actin filaments play a dominant role in cell elasticity and overall strength [31, 32] and that there is a three-fold decrease in the elasticity of malignantly transformed fibroblast cells compared to normal ones [33]. It is also expected that these cells sense the rigidity of the substrate like other cells [34]. They generate a mechanical force balance within their body to reach biomechanical equilibrium through stretching and avoiding the sidewalls while maintaining an organized cytoskeleton [35].

Breast cancer cells, on the other hand, do not tend to maintain an organized cytoskeleton structure due to random distribution of their actin filaments. The observed behavior of these cells

in the microenvironments can be a reflection of their metastatic nature and their easily deformable cytoskeleton structure [28].

In addition to the adhesion behavior of these cells, the effect of isotropic geometries on growth preference of the cancer and normal fibroblast cells was further investigated.

2.3.3 The growth of fibroblast cells on the isotropic microstructures

The number of fibroblasts was first screened using fluorescence microscopy to determine how etched microstructures with different dimensions affected their proliferation rate. Growth periods of 72 hours and 120 hours were chosen because at these time points, cells were well spread on the silicon substrates making it possible to obtain quantitative data. Figure 2-8(a) and Figure 2-8(b) show typical fluorescence images of the fibroblast nuclei spread on the silicon chips after two different culture times. Fibroblast cells tended to grow on both the flat surfaces and inside the microchambers regardless of the microchamber depth. After 120 hours in culture, the cells became overpopulated and formed confluent monolayer on the flat surfaces.

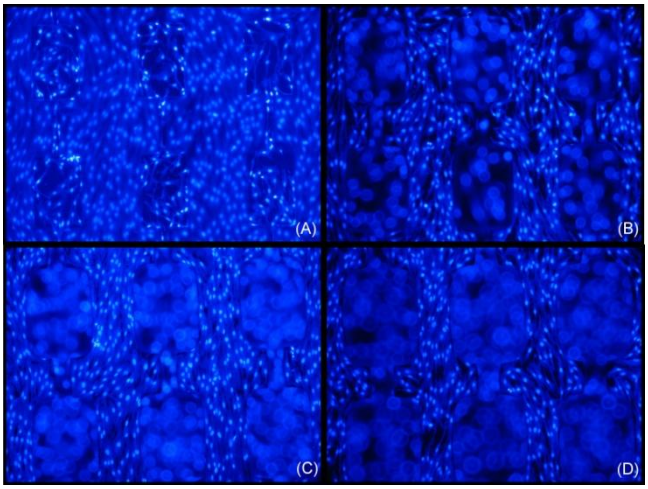

(a)

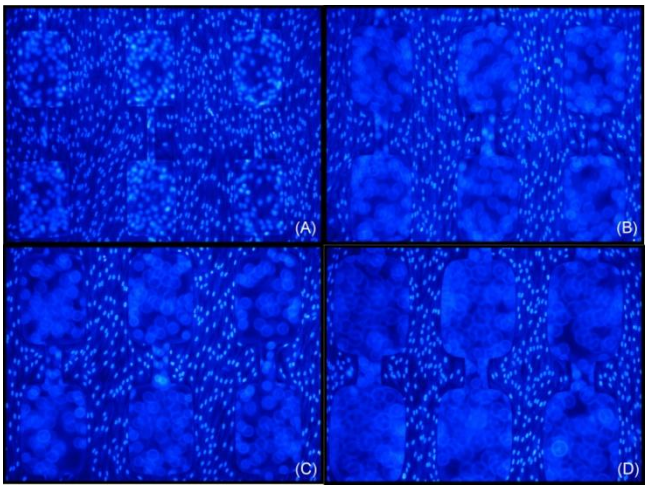

(b)

Figure 2-8 Fluorescence images of the fibroblast cells' nuclei spread on the silicon chips etched for 5(A), 15(B), 20 (C), and 30 (D) minutes after (a) 72 hours and (b) 120 hours of growth. The images are focused on the top flat surfaces.

Fibroblast cells were uniformly oriented on the flat surfaces; however, they were randomly oriented inside the isotropic microchambers (Figure 2-9(A-D)). Figure 2-10 shows the mean +/- standard deviation of the ratio of the number of fibroblast cells on flat surfaces to total number of cells within each field.

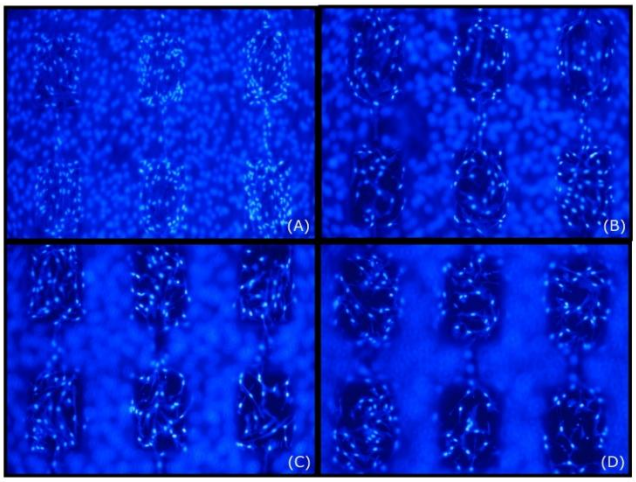

Figure 2-9 Fluorescence images of the fibroblast cells' nuclei distribution inside the microchambers etched for 5(A), 15(B), 20 (C), and 30 (D) minutes after 72 hours of growth. The images are focused inside the microchambers.

For both culture times, slightly more than half of the fibroblasts grew on the flat surfaces regardless of the depth of the microchambers. The shape of the fibroblasts growing on the flat surfaces and within the microchambers was similar. The data indicate that fibroblasts were able to grow on the bottom of microchambers as deep as 126µm, and this is evidence that the nutrients and oxygen reach the bottom of microchambers. In conclusion, fibroblasts rather uniformly distributed over the silicon substrates and the 3-D geometries did not elicit marked changes in their overall cell shape.

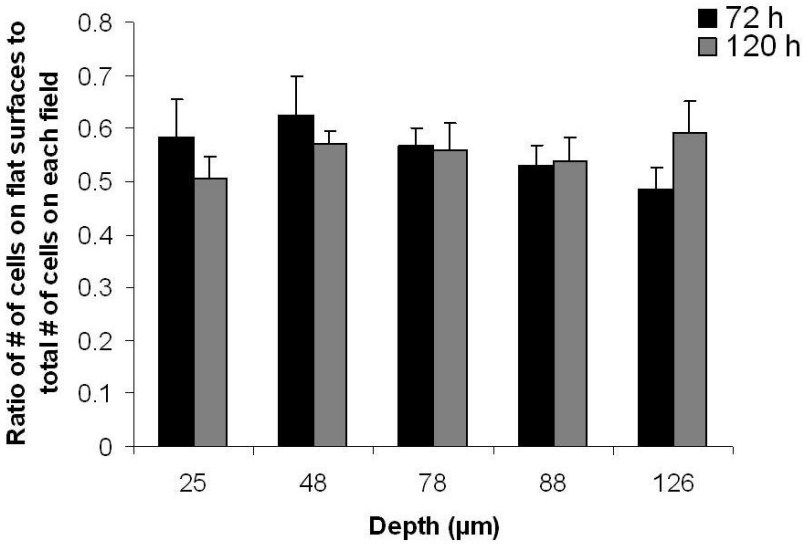

Figure 2-10 The Ratio of the number of fibroblast cells on flat surfaces to the total number of cells versus microchamber depth. Error bars represent one standard deviation.

2.3.4 The growth of human breast cancer cells on the isotropic microstructures

Figure 2-11(a) and Figure 2-11(b) show fluorescence images of breast cancer cell nuclei spread on the silicon chips after 72 hours and 120 hours of culture. After 72 hours growth in substrates with the more shallow microstructures (25 µm-deep structures), the cancer cells were populated everywhere (Figure 2-11(a)(A)). On substrates created using longer etch times so that the microchambers became deeper and wider, the population of the cancer cells on flat surfaces decreased, and instead, these cells tended to grow inside the microchambers (Figure 2-11(a)(B-D)).

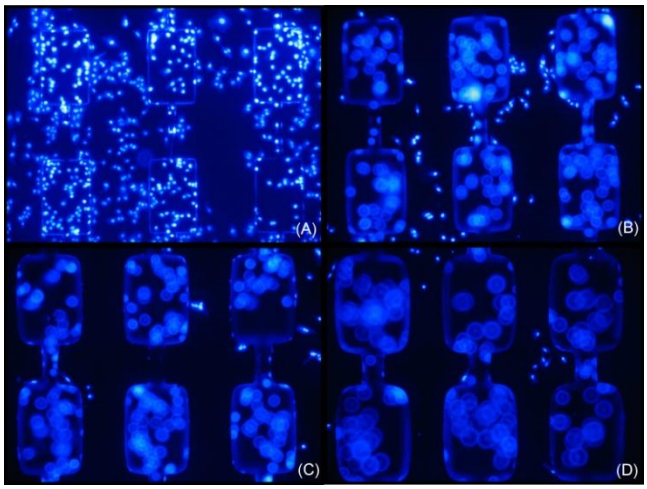

(a)

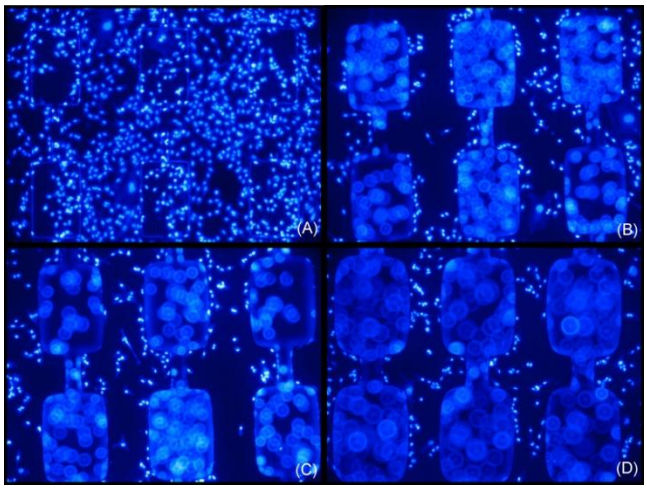

(b)

Figure 2-11 Fluorescence images of the cancer cells' nuclei spread on the silicon chips etched for 5(A), 15(B), 20 (C), and 30 (D) minutes after (a) 72 hours and (b) 120 hours of growth. The images are focused on the top flat surfaces.

A longer culture time did not change this behavior (Figure 2-11(b)(A)). As the microchambers became deeper, the population of the breast cancer cells on flat surfaces decreased further and their number inside the microchambers increased (Figure 2-11(b)(B-D)). The results suggest that MDA-MB-231 breast cancer cells reside preferentially within the deeper isotropic microstructures etched in our silicon microdevices.

Figure 2-12(a) shows the mean +/- standard deviation of the total number of cancer cells counted growing on ten different fields within each silicon chip versus microchamber depth.

After 72 hours culture time, the total number of cells per silicon chip decreased as the microchamber depth increased suggesting that there was a loss of cells attached to deeply etched silicon chips at this time point. However, in cultures maintained for 120 hours, the total number of breast cancer cells attached to the silicon chip was independent of the depth of microstructures. Figure 2-12(b) shows the mean +/- standard deviation of the ratio of the number of breast cancer cells on the smooth flat surfaces compared to the total number of cells within each field versus microchamber depth.

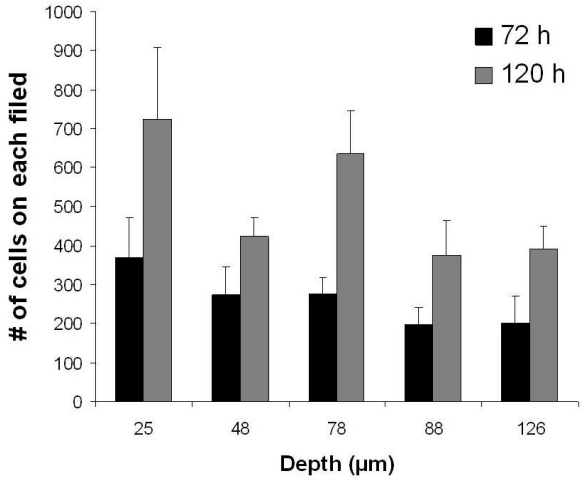

(a)

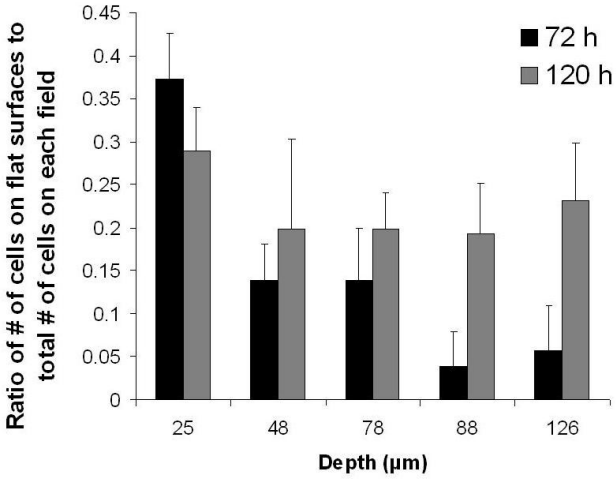

(b)

Figure 2-12 (a) The total number of cancer cells on each field versus microchamber depth (b) The ratio of the number of cancer cells on flat surfaces to the total number of cells to within each field versus the microchamber depth. Error bars represent one standard deviation.

These figures clearly indicate that for both culture times, when the microchamber depth exceeded 48 µm, fewer breast cancer cells grew on the flat surfaces. After 72 hours of culture on silicon chips containing microchambers with a depth of 88 µm, less than 5% of the breast cancer cells grew on the flat surfaces. Statistical analysis indicated that there was a significant decrease ($P<0.001$) in the ratio of the number of breast cancer cells on flat surfaces to the total number of cells within each field as the depth increased. These results indicate that significantly more breast cancer cells grew inside the microchambers deeper than 25 µm (5 minute etch) ($P<0.001$). Similarly, after 120 hours of culture on chips with microchambers having a depth greater than 48 µm, only about 20% of the cells grew on the flat surfaces. In conclusion, MDA-MB-231 breast cancer cells and HS68 fibroblast cells differ significantly in their responses to deeper microchambers etched into silicon. After 72 hours of culture, the ratio of the breast cancer cells on flat surfaces to those inside the microchambers deeper than 80 µm is almost one order of magnitude lower than the corresponding value for fibroblasts.

We have described how the adhesion and growth behavior of breast cancer cells was affected by the presented 3-D isotropic features and how this differed from normal fibroblasts. To establish that substrate geometry, not substrate chemistry was important in determining these behaviors, we compared the chemical composition of the flat silicon surfaces and the surfaces inside the microchambers (etched areas). Using XPS, we determined that the chemical composition of the entire silicon substrates remained unchanged during the fabrication process (Figure 2-13). The data eliminate the possibility that deposition of the etch byproducts occurred on silicon surfaces. As shown in Figure 2-13, the fabrication process did not change the chemical composition of the silicon surfaces as the etch time increased. Also, there was no alteration in the chemistry of the flat surfaces and the curved surfaces inside the microchambers (data not shown here). To further explore the mechanisms that might explain the preferential localization of breast cancer cells inside the microchambers, we tested the growth of the cancer cells on 20 minutes etched microchambers (Depth of 88 µm) at different time points of 12, 24, 48 and 72 hours of growth.

Figure 2-14 shows the number of the cells on flat surfaces as well as inside the microchambers for the selected time points. It is clearly seen that the colonization of the cancer cells inside the

microchambers starts as early as 12 hours. The growth rate inside the microchambers exceeds that of the flat surfaces and as reported earlier, at 72 hours, 95% of the breast cancer cells reside inside the microchambers.

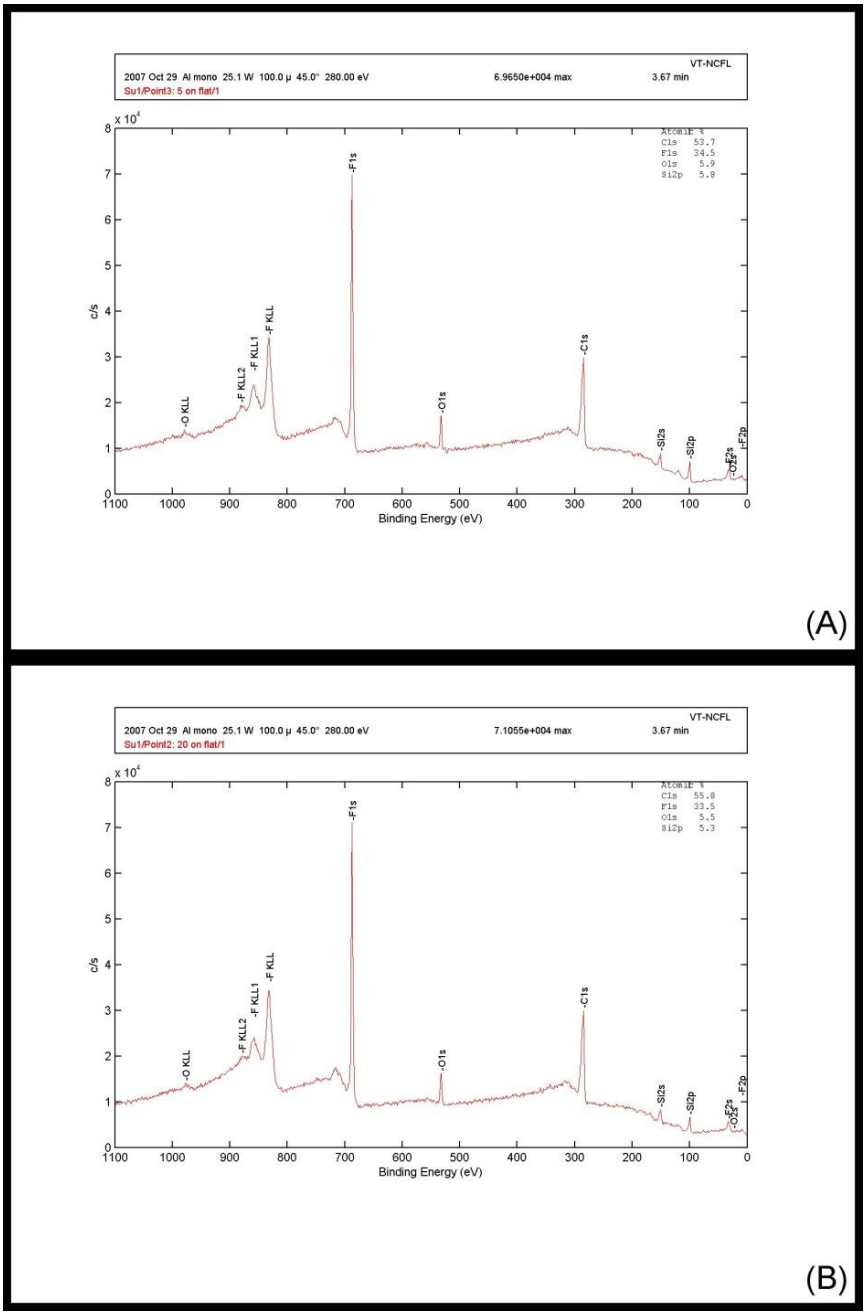

Figure 2-13 X-ray photoelectron spectrometry (XPS) of typical flat surfaces within each field of the silicon microstructures etched for 5 minutes (A) and 20 minutes (B).

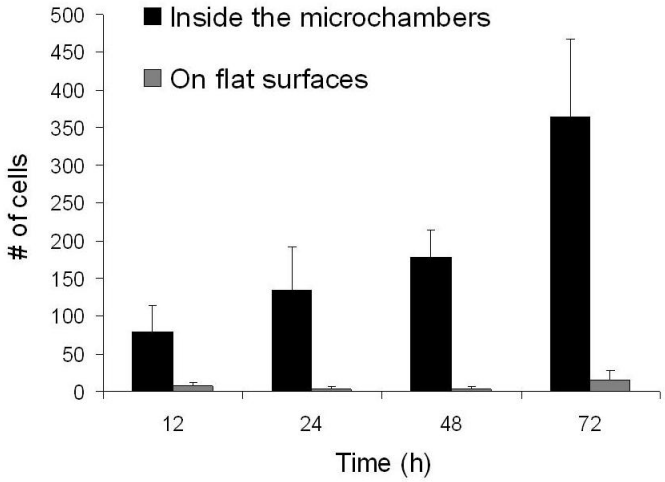

Figure 2-14 The total number of cancer cells on flat surfaces and inside the microchambers of 20 minutes etched microstructure (Depth of 88 µm) after 12, 24, 48 and 72 hours of growth. Error bars represent one standard deviation.

Detailed inspection of the attachment of the cancer cells on isotropic geometries based on SEM images and confocal microscopy showed that these cells sense and respond to the substrate geometry by adapting their shape to the curved sidewalls. The substrate-cell attachment complexes are known to connect directly with the cytoskeleton and communicate through the cytoskeleton to the cell nucleus; hence, inputs from cell attachment sites on the surfaces of the substrate microenvironment have the potential to trigger cytoskeleton reorganization, mechanical deformation and stress, and gene expression changes. This is a highly complex response which might induce cancer cells to chemically modify the deep microchamber environment further attracting additional cancer cells to a preferred microenvironment. The other possible explanation for this behavior is related to cytokine signaling. MDA-MB-231 breast cancer cells secrete interleukin-8 (IL-8), a cytokine which stimulates MDA-MB-231 cell invasiveness through controlled pore matrigel membranes [36]. By analogy, the accumulation of cancer cells within deep microchambers of the silicon microstructures might be a response to the release of IL-8, and mirror MDA-MB-231 behavior in matrigel migration assays. This hypothesis is currently under investigation

2.4 Conclusion

In this work, 3-D isotropic silicon microstructures, consisting of arrays of isotropic microchambers connected with channels, were developed to study the behavior of normal human fibroblast and human breast cancer cells in response to novel substrate geometries. These cell lines represent two cell types prevalent in human breast tumor microenvironments, and the work constitutes an important step in creating a 3-D silicon model system for investigating human breast tumor microenvironments *in vitro*. The devices presented here were fabricated using a single-mask, single-etch process. Breast cancer cells and fibroblasts had distinct attachment and adhesion properties. The breast cancer cells deformed and formed stable adhesion complexes to isotropic geometries while fibroblast cells maintained a more organized cytoskeletal structure which stretched to avoid curved sidewalls within these same substrates. Statistical analysis showed that the depth of the microchambers affected the distribution of breast cancer cells within the silicon chips. As the depth of the microchambers increased, the cancer cells tended to grow inside the microchambers. In contrast, normal fibroblasts were nearly evenly populated throughout the silicon chips.

The 3-D microstructures presented here, provide a model system for the study of biomechanical properties of cancer and normal cells, and for the design of microenvironments suitable for segregating normal and cancer cells. We can utilize this model system to test how electrical field stimulation, biochemical coatings to the 3-D microstructures, and multilevel microenvironments created by a two-step etch process enhance the separation of breast cancer cells from normal cells in a co-culture system. The ability to trap breast cancer cells within specified microenvironment compartments has practical application to cancer diagnosis, prognosis and treatment. The system also makes it possible to study the behavior and interactions of these cell types in mixed co-cultures which simulate an *in vivo* breast tumor microenvironment and can provide important insights into new breast cancer treatments.

2.5 References

[1] M. Nikkhah, *et al.*, "Attachment and response of human fibroblast and breast cancer cells to three dimensional silicon microstructures of different geometries," *Biomedical Microdevices*, vol. 11, pp. 429-441, Apr 2009.

[2] G. M. Walker, *et al.*, "Microenvironment design considerations for cellular scale studies," *Lab on a Chip,* vol. 4, pp. 91-97, 2004.

[3] T. H. Park and M. L. Shuler, "Integration of cell culture and microfabrication technology," *Biotechnology Progress,* vol. 19, pp. 243-253, Mar-Apr 2003.

[4] E. T. denBraber, *et al.*, "Quantitative analysis of cell proliferation and orientation on substrata with uniform parallel surface micro-grooves," *Biomaterials,* vol. 17, pp. 1093-1099, Jun 1996.

[5] X. F. Walboomers, *et al.*, "Contact guidance of rat fibroblasts on various implant materials," *Journal of Biomedical Materials Research,* vol. 47, pp. 204-212, Nov 1999.

[6] P. Clark, *et al.*, "Cell Guidance by Ultrafine Topography Invitro," *Journal of Cell Science,* vol. 99, pp. 73-77, May 1991.

[7] M. J. Dalby, *et al.*, "Nucleus alignment and cell signaling in fibroblasts: response to a micro-grooved topography," *Experimental Cell Research,* vol. 284, pp. 274-282, Apr 2003.

[8] A. M. Rajnicek, *et al.*, "Contact guidance of CNS neurites on grooved quartz: influence of groove dimensions, neuronal age and cell type," *Journal of Cell Science,* vol. 110, pp. 2905-2913, Dec 1997.

[9] C. Oakley and D. M. Brunette, "The Sequence of Alignment of Microtubules, Focal Contacts and Actin-Filaments in Fibroblasts Spreading on Smooth and Grooved Titanium Substrata," *Journal of Cell Science,* vol. 106, pp. 343-354, Sep 1993.

[10] C. Oakley, *et al.*, "Sensitivity of fibroblasts and their cytoskeletons to substratum topographies: Topographic guidance and topographic compensation by micromachined grooves of different dimensions," *Experimental Cell Research,* vol. 234, pp. 413-424, Aug 1997.

[11] X. F. Walboomers, *et al.*, "Attachment of fibroblasts on smooth and microgrooved polystyrene," *Journal of Biomedical Materials Research,* vol. 46, pp. 212-220, Aug 1999.

[12] K. Matsuzaka, *et al.*, "Effect of microgrooved poly-l-lactic (PLA) surfaces on proliferation, cytoskeletal organization, and mineralized matrix formation of rat bone marrow cells," *Clinical Oral Implants Research,* vol. 11, pp. 325-333, Aug 2000.

[13] X. F. Walboomers, *et al.*, "Growth behavior of fibroblasts on microgrooved polystyrene," *Biomaterials,* vol. 19, pp. 1861-1868, Oct 1998.

[14] B. Wojciakstothard, *et al.*, "Role of the Cytoskeleton in the Reaction of Fibroblasts to Multiple Grooved Substrata," *Cell Motility and the Cytoskeleton,* vol. 31, pp. 147-158, 1995.

[15] C. J. Bettinger, *et al.*, "Micro fabrication of poly (glycerol-sebacate) for contact guidance applications," *Biomaterials,* vol. 27, pp. 2558-2565, Apr 2006.

[16] Y. A. Rovensky, *et al.*, "Spreading of Mouse Fibroblasts on the Substrate with Multiple Spikes," *Experimental Cell Research,* vol. 197, pp. 107-112, Nov 1991.

[17] T. G. van Kooten and A. F. von Recum, "Cell adhesion to textured silicone surfaces: The influence of time of adhesion and texture on focal contact and fibronectin fibril formation," *Tissue Engineering*, vol. 5, pp. 223-240, Jun 1999.

[18] A. M. P. Turner, *et al.*, "Attachment of astroglial cells to microfabricated pillar arrays of different geometries," *Journal of Biomedical Materials Research*, vol. 51, pp. 430-441, Sep 2000.

[19] J. L. Charest, *et al.*, "Myoblast alignment and differentiation on cell culture substrates with microscale topography and model chemistries," *Biomaterials*, vol. 28, pp. 2202-2210, Apr 2007.

[20] M. R. Dusseiller, *et al.*, "An inverted microcontact printing method on topographically structured polystyrene chips for arrayed micro-3-D culturing of single cells," *Biomaterials*, vol. 26, pp. 5917-5925, Oct 2005.

[21] H. H. Liao, *et al.*, "Response of rat osteoblast-like cells to microstructured model surfaces in vitro," *Biomaterials*, vol. 24, pp. 649-654, Feb 2003.

[22] J. Y. Mai, *et al.*, "A microfabricated platform probing cytoskeleton dynamics using multidirectional topographical cues," *Biomedical Microdevices*, vol. 9, pp. 523-531, Aug 2007.

[23] K. Gantz, *et al.*, "Development of a comprehensive model for RIE-lag-based three-dimensional microchannel fabrication," *Journal of Micromechanics and Microengineering*, vol. 18, Feb 2008.

[24] D. Tarin and C. B. Croft, "Ultrastructural features of wound healing in mouse skin," *Journal of Anatomy*, vol. 105, pp. 189-190 1969.

[25] R. Kalluri and M. Zeisberg, "Fibroblasts in cancer," *Nature Reviews Cancer*, vol. 6, pp. 392-401, May 2006.

[26] N. A. Bhowmick, *et al.*, "Stromal fibroblasts in cancer initiation and progression," *Nature*, vol. 432, pp. 332-337, Nov 2004.

[27] J. S. Strobl, *et al.*, "Application of microengineered silicon chips to the study of human metastatic breast cancer and responses to histone deacetylase inhibitors," in *American Association for Cancer Research Special Conference on Advances in Breast Cancer Research: Genetics, Biology, and Clinical Applications*, San Diego, CA, 2007.

[28] R. A. Weinberg and R. Allan, *The Biology of Cancer*. New York: Garland Science, Taylor & Francis Group, 2007.

[29] A. Benzeev, "The cytoskeleton in cancer cells," *Biochimica Et Biophysica Acta*, vol. 780, pp. 197-212, 1984.

[30] K. M. K. Rao and H. J. Cohen, "Actin cytoskeletal network in aging and cancer," *Mutation Research*, vol. 256, pp. 139-148, Mar-Nov 1991.

[31] Y. Tseng and D. Wirtz, "Mechanics and multiple-particle tracking microheterogeneity of alpha-actinin-cross-linked actin filament networks," *Biophysical Journal*, vol. 81, pp. 1643-1656, Sep 2001.

[32] T. P. Stossel, "Contribution of actin to the structure of the cytoplasmic matrix," *Journal of Cell Biology,* vol. 99, pp. S15-S21, 1984.

[33] C. Rotsch and M. Radmacher, "Drug-induced changes of cytoskeletal structure and mechanics in fibroblasts: An atomic force microscopy study," *Biophysical Journal,* vol. 78, pp. 520-535, Jan 2000.

[34] D. E. Discher, *et al.*, "Tissue cells feel and respond to the stiffness of their substrate," *Science,* vol. 310, pp. 1139-1143, Nov 2005.

[35] D. E. Ingber, "Cellular tensegrity: defining new rules of biological design that govern the cytoskeleton," *Journal of Cell Science,* vol. 104, pp. 613-627, 1993.

[36] C. Yao, *et al.*, "Interleukin-8 modulates growth and invasiveness of estrogen receptor-negative breast cancer cells," *International Journal of Cancer,* vol. 121, pp. 1949-1957, Nov 2007.

3 Chapter 3: Cytoskeletal Role in Differential Adhesion Patterns of Normal Fibroblasts and Breast Cancer Cells inside Silicon Microenvironments

This chapter is produced from [1] with permission from Springer.

M. Nikkhah, et al., "Cytoskeletal role in differential adhesion patterns of normal fibroblasts and breast cancer cells inside silicon microenvironments," Biomedical Microdevices, vol. 11, pp. 585-595, Jun 2009.

3.1 Introduction

Recent reports have emphasized that cellular functions are controlled by their surrounding microenvironment [2, 3] including substrate topography, surface chemistry, soluble factors, and signals from neighboring cells. Microengineered environments can facilitate quantitative analysis of the effects of microscale surface topography on individual cell growth, adhesion, migration, and mechanics. They can also be used to explore how cell-cell interactions influence the aforementioned cellular behaviors [4, 5]. Understanding cell-surface interactions *in vitro* has broad applicability in cell-based biosensors, tissue engineering, prosthetics, and medical implants.

The influence of surface topography on cellular behavior was first noted by Harrison [6] and led to the concept of “contact guidance” in which cells align in the direction of surface grooves. Advances in microelectromechanical systems (MEMS) technology have made it possible to observe cellular responses to a variety of precise topographical patterns including microgrooves fabricated from silicon [7], silicone [8], quartz [9-11], titanium-coated silicon [8, 12, 13], polystyrene [14-16], silica [17] and ploy (glycerol-sebacate) [18], arrays of pillars and wells [19-21], arrays of grooves and holes fabricated in silicon [22] and polystyrene [23], arrays of pyramid microstructures fabricated in silicone [24] and networks of ridges and grids fabricated in PDMS [25]. Some of the aforementioned studies have focused on the critical role of cytoskeletal components, actin microfilaments and microtubules in cell alignment [13, 17]. Both mechanical loading and microgrooved surface topographies promote cytoskeletal reorganization and affect the behavior of fibroblast cells [26, 27]. Cytoskeletal proteins play an important role in tissue engineering by mediating the cellular response to different substrates.

The devices described in the previously cited literature involve microstructures with vertical sidewalls. However, extracellular matrix (ECM) proteins are well known to form a complex interconnecting network and a 3-D surface topography [28]. We previously reported development of arrays of 3-D silicon microstructures consisting of isotropic microchambers interconnected with channels in order to asses the adhesion and growth behavior of normal human fibroblast cells (HS68) and human breast cancer cells (MDA-MB-231) [29]. These cells represent key cell types in human breast tumor microenvironments [30] (Chapter 2). The main focus in our previous work was the growth behavior of these cell lines inside isotropic microstructures; however, we found that these cells exhibited differential adhesion to the microstructures with curved sidewalls. In this chapter, we explore in detail whether the differential adhesion of these two cell types to isotropic architectures is dependent on their cytoskeletal structure and biomechanical properties. For this purpose, we developed new 3-D isotropic silicon microstructures using our novel fabrication technology [31]. These microenvironments can be potentially used as novel platforms to study cytoskeletal organization of various cell lines in a 3-D architecture.

3.2 Materials and methods

3.2.1 Device fabrication

The final devices shown in Figure 3-1 were fabricated from single-crystal silicon wafers. The fabrication process is similar to our previous work relying on the applicability of RIE lag and its dependence on geometrical patterns of the photomask layout to etch silicon to different depths [29].

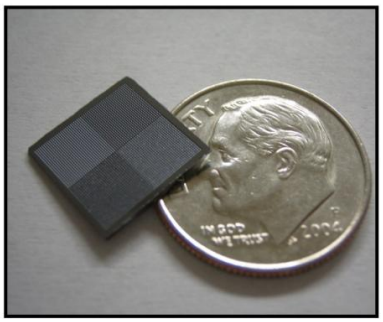

Figure 3-1 Photo image of the fabricated devices in silicon. The cell culture substrate comprises star and circular-shaped microchambers.

Figure 3-2 shows different layouts of the photomask design; the openings for the star-shaped microchambers are rectangular with the dimension in the range of 2 µm×2 µm to 10 µm×10 µm (Figure 3-2(A,B)). The openings for the circular-shaped microchambers are circular rings with a diameter of 5µm and with variable spacing raging from 2µm to 6µm (Figure 3-2(C,D)). Briefly, the fabrication process starts by depositing 8000Å-thick PECVD oxide layer on a silicon wafer.

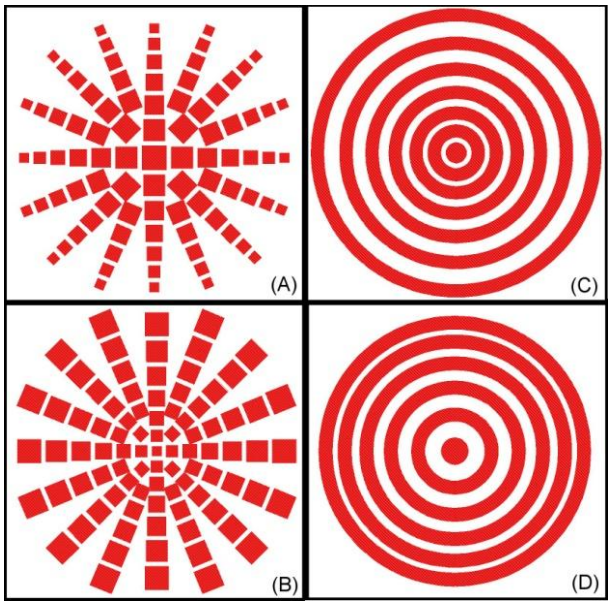

Figure 3-2 Photo mask layout comprising four different features for star (A, B) and circular-shaped microchambers (C, D). The openings for the star-shaped microchambers are rectangular with the dimension in the range of 2 µm×2 µm to 10 µm×10 µm. The openings for the circular-shaped microchambers are circular rings with a diameter of 5µm and with variable spacing ranging from 2µm to 6 µm.

After spinning and patterning photoresist, the oxide layer was etched for 3 minutes using DRIE CH4/C4F8 plasma. Next, silicon was etched using DRIE SF6 plasma to form complex arrays of features composed of star and circular-shaped microchambers. Due to RIE lag, areas under the bigger mask openings were etched more, thereby achieving 3-D microstructures. After removing photoresist the oxide layer is subsequently removed using DRIE.

Figure 3-3 shows the scanning electron microcopy (SEM) images of the microchambers with varying cross sectional shapes. The depth of the microchambers varies between 60-70 µm and the width ranges between 150-170 µm. Table 1 summarizes the etching parameters. It is notable that the described fabrication technique provides localized rough edges on the curved sidewalls and on the bottom surface of the microchambers. In the star patterns, the rough edges formed on

the sidewalls (Figure 3-3(A)) while in the circular-shaped microchambers, the rough edges were localized on the bottom of the microchambers in the form of concentric rings (Figure 3-3(B)).

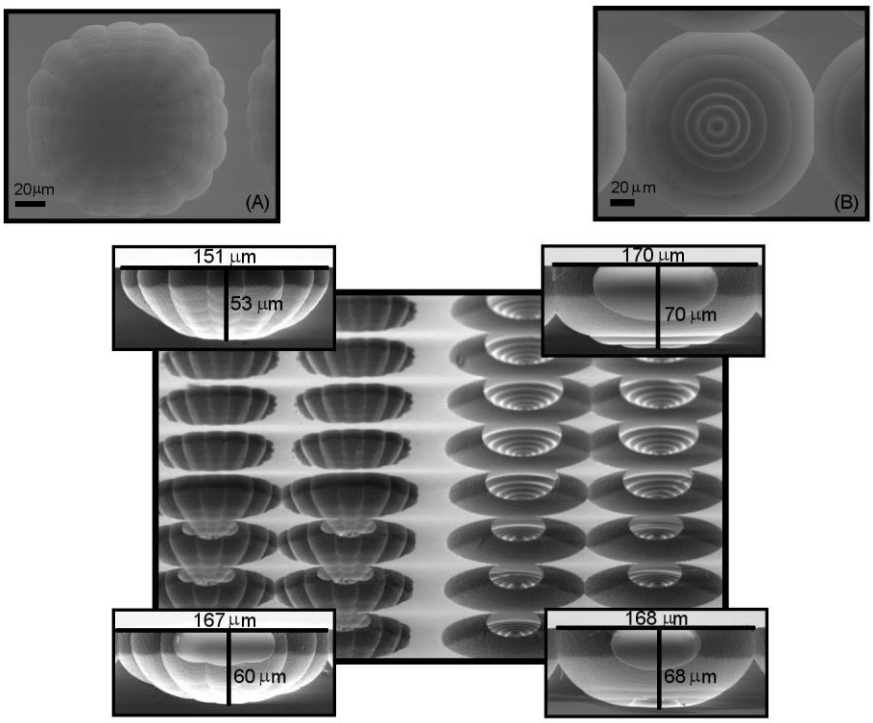

Figure 3-3 SEM images of the (3-D) silicon substrates comprising star and circular-shaped microchambers with the corresponding top view images. With the proposed fabrication technology, scalloped edges can be formed on the curved sidewalls and the bottom surface of the microchambers.

The final fabricated wafer is diced into 1 cm^2 chips, each chip contains the etched microstructures surrounded by un-etched flat surfaces (Figure 3-1). This provides the ability to compare the control experiments on flat surfaces and the results on the etched microstructures under the same cell culturing conditions. Chips were cleaned using acetone and isopropanol, rinsed in deionized water, and, finally, air-dried prior to cell culture experiments.

Table 3-1: Etching parameters for the isotropic geometries

	SF_6 Flow rate (sccm)	Pressure (mbar)	Coil power (W)	Etching time (min)
Etching parameters	300	4.5e-02	1800	10

3.2.2 Cell culture and reagents

HS68 normal human fibroblasts and MDA-MB-231 human breast cancer cells were purchased from the American Type Culture Collection (ATCC). Cells were maintained in plastic T-75 cm^2 culture flasks in RPMI culture medium which contained 10% fetal bovine serum (FBS), 1 mM sodium pyruvate, and penicillin-streptomycin (100 Units/ml). Cells were grown at 37 °C in a humidified 7% CO_2-93% air atmosphere. Cells were fixed in a 50%-ethanol-5% formaldehyde-0.1% crystal violet solution in normal saline for 10 minutes prior to imaging. After 72 hours of growth, cytochalasin D (final concentration of 10 µM) [32] was added to the culture medium for either 10 or 30 minutes prior to fixation.

3.2.3 Microscopy and immunofluorescence for cytoskeletal organization

Optical microscopy was performed using a digital-video optical microscope7 with a 2000 maximum magnification for cell counting on flat silicon and glass surfaces. Confocal microscopy8 was performed in the reflection mode to image the actin cytoskeletal structures. Cell nuclei were stained with Hoechst 33342 dye and actin was visualized using Alexa Fluor-488 phalloidin [21]. The confocal images inside the microchambers were taken at different depths of focus to construct Z-stack images. SEM was also performed to assess the detailed effects of the etched microstructures on the cells' morphology. After fixation of the culture with 3.7% formaldehyde in phosphate buffered saline (PBS) for 10 minutes, samples were critical point dried and sputter-coated with a thin layer of gold palladium prior to SEM imaging.

3.2.4 Quantification of cell number, cell length and cell morphology

SEM images were obtained at nine different fields of star and circular-shaped microchambers within each chip. Each field included 24 microchambers and their adjacent flat surfaces. The selected fields almost cover the entire fabricated substrate. These images were used to count the number of fibroblast cells inside the etched features before and after adding Cytochalasin D.

Cell length measurements on flat surfaces were performed using the National Institutes of Health (NIH) ImageJ (v. 1.41) software. The cell length was quantified as the distance between farthest end points of the cell. To quantify the cell length inside etched microchambers, we assumed an ellipsoid shape for the etched microchambers with an equation of $\frac{x^2}{a^2}+\frac{y^2}{b^2}+\frac{z^2}{c^2}=1$,

where ”*a*” and “*b*” are the equatorial radii and “c” refers to the polar radius (microchamber depth). For the star-shaped microchambers, a=80 µm, b=80 µm, c=55 µm, whereas for the circular-shaped microchambers, a=82.5 µm, b=82.5 µm, c=70 µm. The x and y coordinates of the end points of the cell were measured from the top view images using ImageJ software. Then the z coordinate of the corresponding points was measured using the ellipsoid equation stated above. Finally the cell length is measured using the standard line equation in 3-D space $l = \sqrt{(x_2 - x_1)^2 + (y_2 - y_1)^2 + (z_2 - z_1)^2}$.

For fibroblast cell shape analysis, three different morphologies of round, spread and stretched were assumed. The spread cells are those in which the cell body has a uniform contact with the sidewalls of the microchamber while the stretched ones anchor to different location of the microchambers and do not have contact with the sidewalls. The average aspect ratio (*Max(length/width)*) of stretched and spread cells was measured to be 26.6±13.8 and 3.7±1.8 respectively.

3.2.5 Statistical analysis

Two-way ANOVA analysis was performed using Prism v.59 to study the effect of etched geometries on cell length and to assess the statistical significance of the effect of cytochalasin D on the morphology of cells growing in circular and star-shaped microchambers.

3.3 Results

Figure 3-4 compares the length of fibroblast and cancer cells on flat surfaces as well as inside the etched microstructures. An average length of 88±23 µm (n=100) and 33±11 µm (n=100) was measured for fibroblast and cancer cells, respectively. HS68 fibroblast cells are significantly longer ($p<0.001$) than the MDA-MB-231 breast cancer cells on flat surfaces and all the etched geometries. Both cell types distributed with random orientation within the etched microstructures (data not shown).

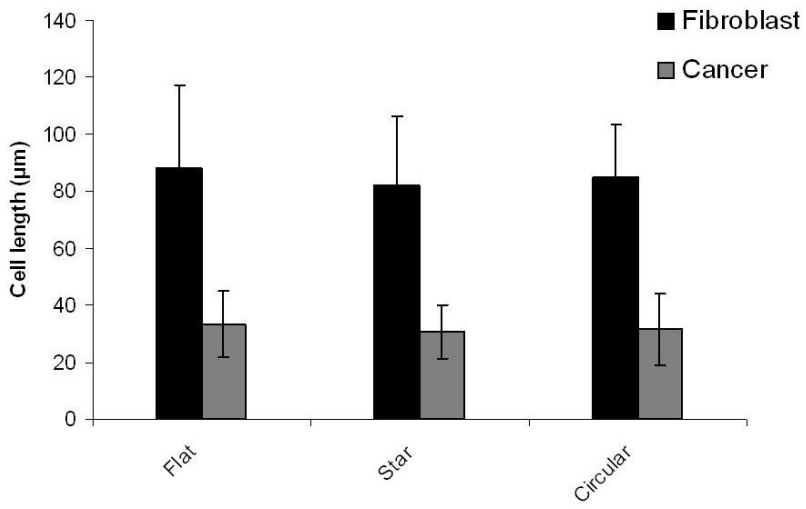

Figure 3-4 Fibroblast and cancer cell length on flat surfaces and inside the star and circular-shaped microchamber.

Figure 3-5(A-F) shows the SEM images of untreated control fibroblast cells inside the etched features revealing the tendency of fibroblasts to stretch inside the isotropic microchambers to avoid curved sidewalls. Cancer cells, on the other hand, attached to the curved sidewalls of the microchambers (Figure 3-5(G-L)). The cross-sectional views clearly demonstrate that cancer cells adapted their shape to fit the curved sidewalls and their adhesion behavior was less responsive to the substrate geometrical pattern compared to that of normal fibroblast cells. This observation is in agreement with our observation in previous chapter on different isotropic microenvironments.

To examine whether cell cytoskeletal structure plays a major role in the adhesion behavior of these two cell lines we disrupted the actin cytoskeleton with cytochalasin D. Confocal microscopy was performed after 72 hours of cell grown on flat silicon substrates to visualize the disruption of the actin cytoskeleton for different treatment times of 10 and 30 minutes and to show the dynamics of cell cytoskeleton alteration. Figure 3-6 illustrates the actin cytoskeleton and nuclei distribution in fibroblasts attached to flat silicon surfaces. The actin filaments were distributed in long, thin bundles with parallel or cross-link distribution (Figure 3-6(A,B)).

After10 minutes of treatment with cytochalasin D, there were persistent actin filament bundles through the cell body (Figure 3-6(C,D)). However after 30 minutes of treatment, the dense mesh and long fibers of actin were entirely disrupted throughout the cell body (Figure 3-6(E,F)).

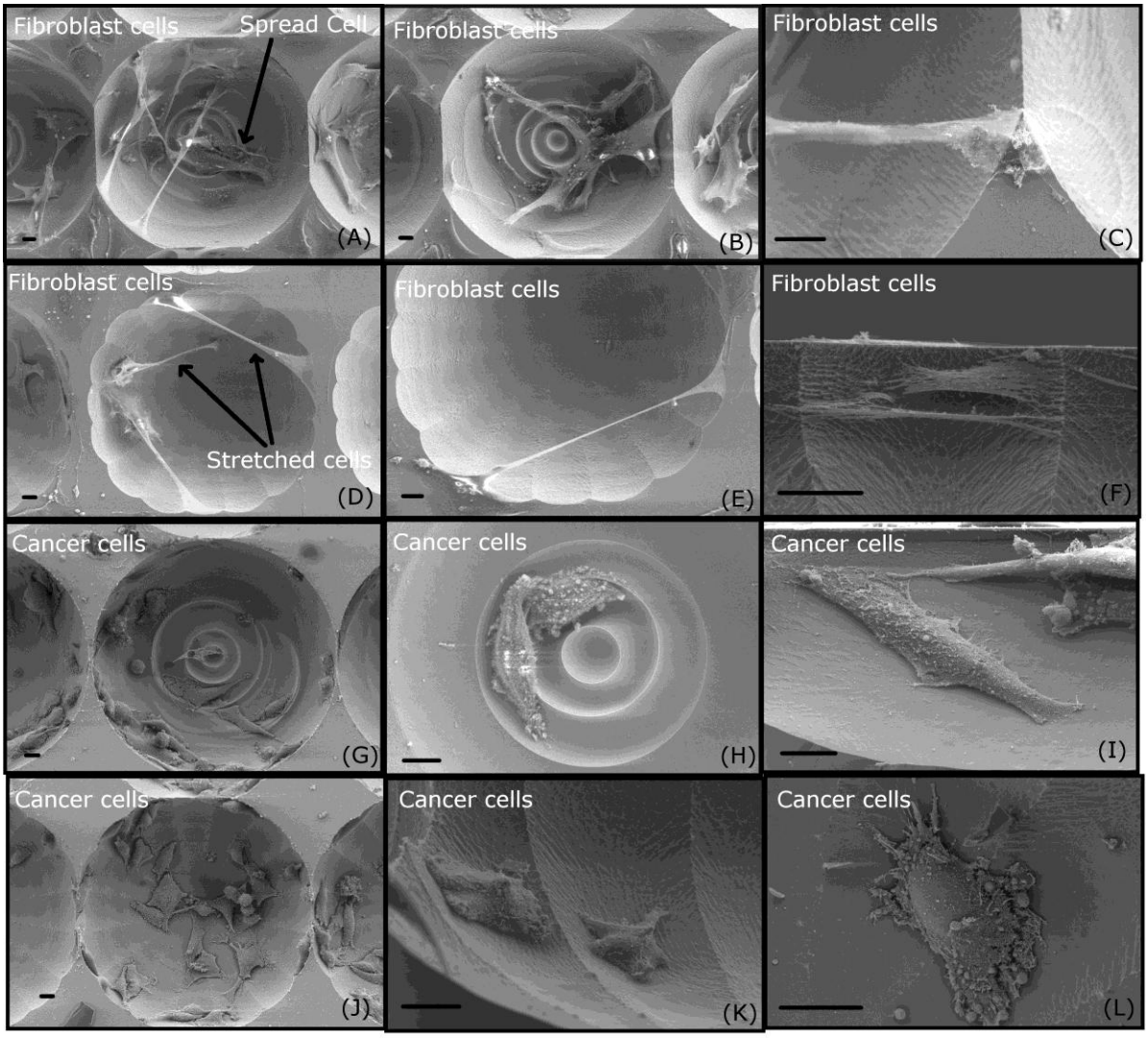

Figure 3-5 SEM images of the HS68 normal fibroblast and MDA-MB-231 human breast cancer cells inside the etched features. Fibroblast cells stretch to avoid curved sidewalls of isotropic microchambers. Cancer cells attach and spread on isotropic microchambers and deform to take the shape of the curved sidewalls. These cells are less discriminating on the substrate geometrical pattern. Scale bars represent 10µm.

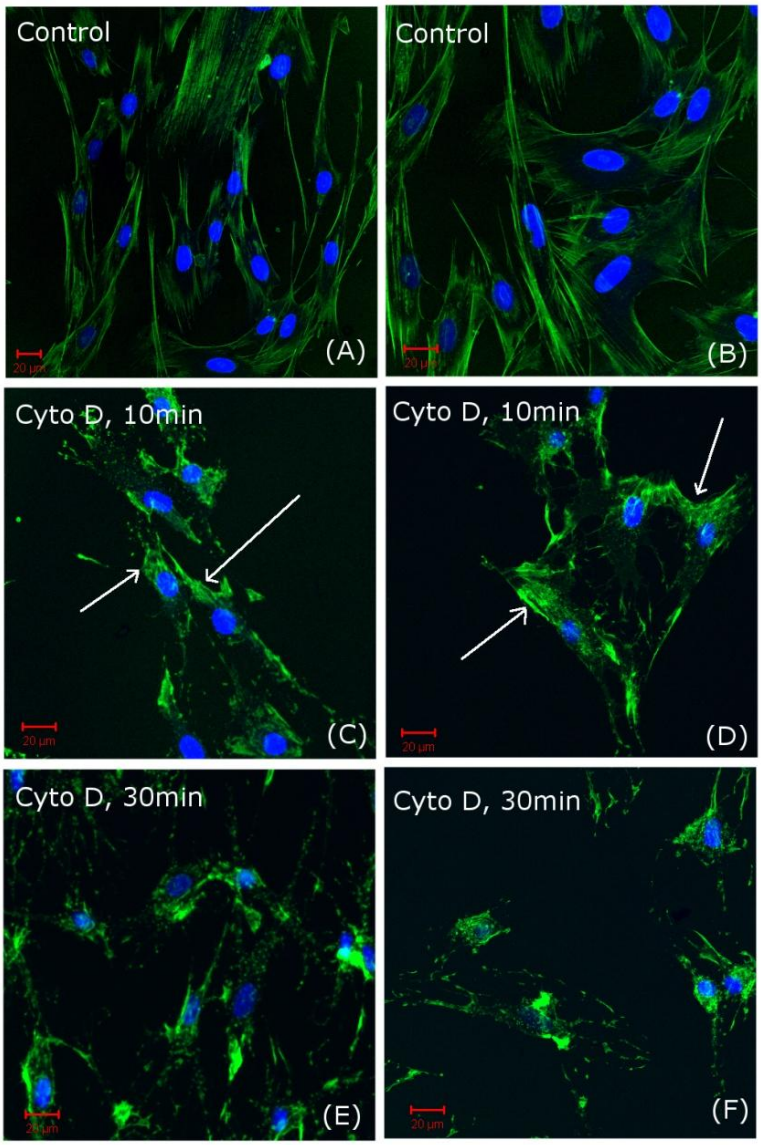

Figure 3-6 Confocal images showing the distribution of the actin and nuclei of the HS68 fibroblast cells attached to flat surfaces in their normal state (A,B) and after adding cytochalasin D for 10 (C, D) and 30 minutes (E,F). After 10 minutes, some stress fibers were observed within the cytoskeleton of the cells (arrows). After 20 minutes, the dense mesh and long fibers of actin were entirely disrupted through the cell body. Scale bars represent 20 µm.

Figure 3-7 shows the actin cytoskeleton of the MDA-MB-231 cancer cells attached to flat silicon surfaces. The actin cytoskeleton of the cancer cells was organized differently compared to fibroblast cells. The cancer cells showed no actin filament formation. The actin cytoskeletal of cancer cells, attached to silicon was distributed in the form of concentric rings around the nuclei. The actin cytoskeleton of cancer cells was completely disrupted after 10 minutes treatment with cytochalasin D (Figure 3-7(C,D)).

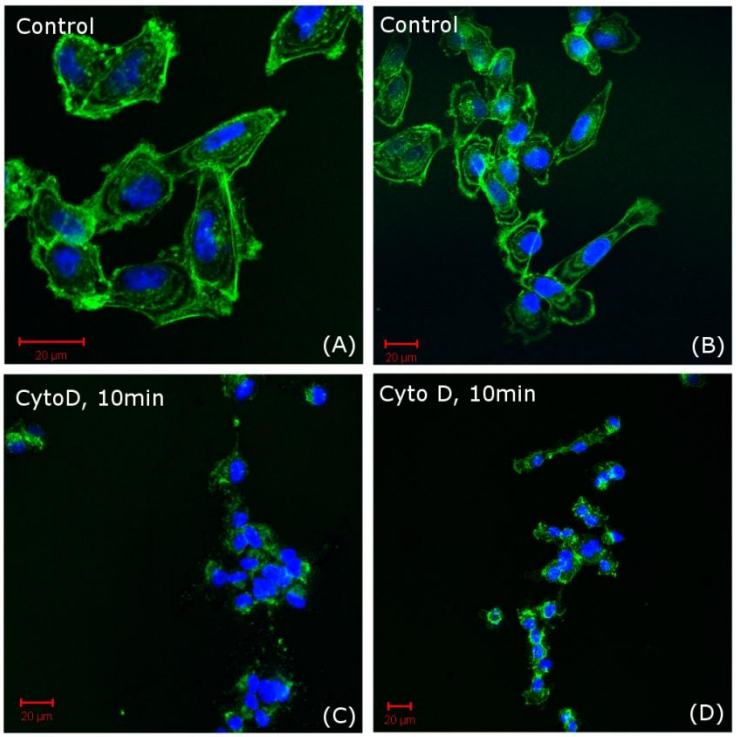

Figure 3-7 Confocal images showing the distribution of the actin and nuclei of the MDA-MB-231 breast cancer cells in their normal state (A,B) and 10 minutes after adding cytochalasin D (C,D). Scale bars represent 20 µm. In control condition, the actin cytoskeleton of MDA-MB-231 cells was distributed in a form of concentric rings around the cell's nuclei. After 10 minutes treatment with cytochalasin D the actin cytoskeleton is completely disrupted. Scale bars represent 20 µm.

Figure 3-8 shows the SEM images of the fibroblast and cancer cells attached inside the etched features after treatment with cytochalasin D. After 10 minutes in the presence of cytochalasin D, some fibroblast cells lost their stretching behavior and well spread and adapted to the curved sidewalls (Figure 3-8(A-C)). After 30 minutes, however, the majority of the cells lost their stretching behavior and rounded up indicating that these cells lost almost all their entire stress fibers consistent with the confocal microscopy observations (Figure 3-8(D-F)). At this state, the average length of the rounded fibroblast cells excluding the dendritic extensions was measured to be approximately 16±2 µm (n=20). On the other hand, cancer cells became more rounded after treatment with cytochalasin D and there was not a significant change in their adhesion behavior (Figure 3-8(G-I)). Similar to their original state, they attached to the curved sidewalls of the microchambers. At this state, the length of these cells was measured to be approximately 17±2 µm (n=20).

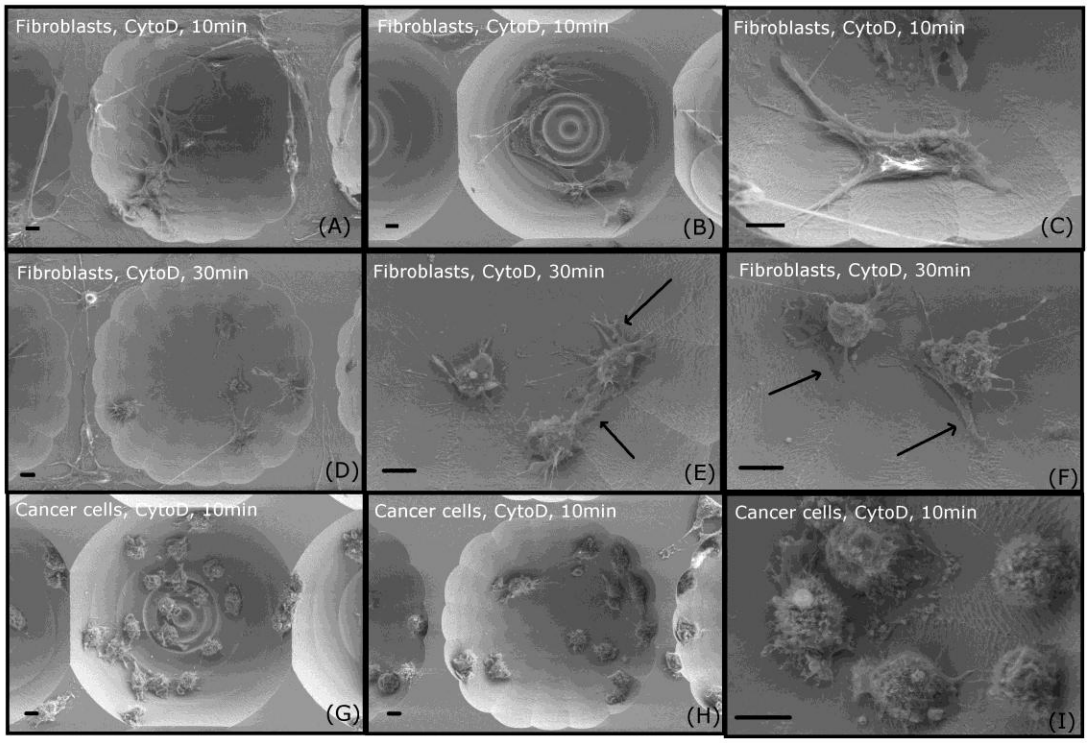

Figure 3-8 SEM images of the HS68 fibroblast and MDA-MB-231 cancer cells after adding cytochalasin D. After 10 minutes of disrupting actin cytoskeleton, fibroblast cells lost their anchorage dependent adhesion to the etched microstructures. While after 30 minute, the morphology of these cells altered toward rounded morphology and their adhesion became more like that of the cancer cell. Arrows show the dendritic extension of the cells. Addition of cytochalasin D to cancer cell cuased the morphology of these cells to become more rounded while there was mot a significant alteration in their adhesion behavior to the curved sidewalls. Scale bars represent 10 µm.

Figure 3-9 shows the quantitative data regarding the effect of cytochalasin D on fibroblasts for both 10 and 30 minutes treatment times. After 10 minutes disruption of actin cytoskeleton, 35±7% of the cells significantly ($P<0.001$) lost their anchorage dependent adhesion inside the etched features and spread on the curved sidewalls. However, 30 minutes treatment with cytochalasin D significantly ($P<0.001$) altered the morphology of 70±7% of fibroblast cells toward rounded morphology associated with dendritic extensions. In such state, their adhesion became more like that of the cancer cells; that is adapting to the etched microstructures and taking the shape of the curved sidewalls.

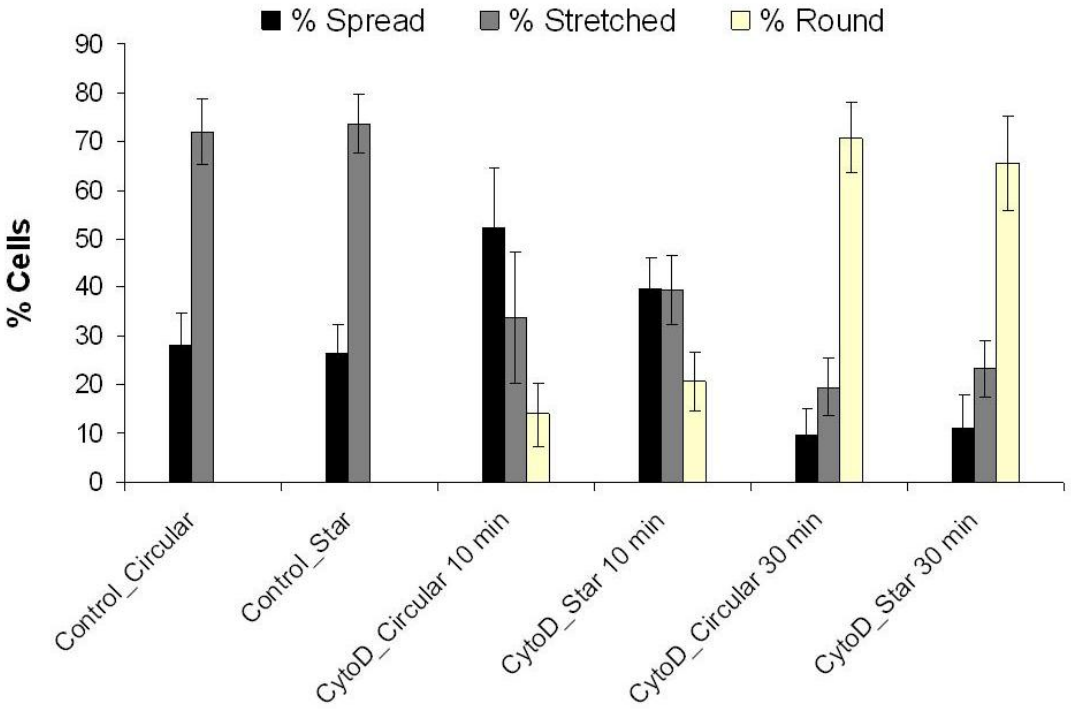

Figure 3-9 Quantitative data showing the effect of the cytochalasin D on fibroblast cell morphology 10 and 30 minutes after adding cytochalasin D. The data show that after 30 minutes, there is a significant change in fibroblast cell morphology from stretched in their normal state to round (associated with dendritic extension).

3.4 Discussion

It is well known that cells sense the stiffness and the geometry of their substrate, and modulate their cytoskeletal organization and adhesion in response to the substrate [33]. Much of the previous work on substrate stiffness has been conducted using 2-D routine planar culture surfaces [34]. With respect to the substrate geometry, researchers have explored the role of cytoskeleton on cell alignment using microgrooved substrates [7-17]. Herein, we investigated the distinctive behavior of HS68 normal fibroblast cells and MDA-MB-231 human breast cancer cells on 3-D silicon isotropic environments and investigated whether cytoskeletal structure (i.e. actin filaments) influenced their adhesion.

Fibroblast cells adhered well to the silicon substrate due to the abundance of parallel and cross-link formation of actin filaments. These cells tended to maintain an organized cytoskeleton and a state of high tension produced by formation of stress fibers, lamellipodia, and focal

adhesions. This limited the ability of these cells to bend inside the microchambers and adapt to the curved sidewalls. Under these conditions, the whole cell body is a pre-stressed tensegrity structure where the actin cytoskeleton is in tension and the microtubules are in compression [35]. The high tension within the actin cytoskeleton is balanced by both the microtubules compression and cell adhesion to the rigid silicon substrate. The balance between cytoskeletal pre-stress and the mechanical force within the cell body is the key determinant of cell shape stability [36] (i.e., stretching and avoiding the sidewalls).

After 10 minutes treatment with cytochalasin D, some actin stress fibers were still present in the cell cytoskeletal structure. However, by 30 minutes, fibroblast cells lose their entire actin filaments (i.e. stress fibers) and consequently their cytoskeletal pre-stress. This primarily results in a significant alteration in their morphology towards shape instability. It is well known that the mechanical structure of the cells, such as their elasticity and overall strength, is dominated by actin filaments [37-39]. Specifically, there is a direct linear correlation between the cell stiffness and the amount of cellular pre-stress [40]. Disruption of the cell cytoskeleton causes a major reduction in cell stiffness [41]. Therefore, after adding cytochalasin D, these cells transform to a low tensional state, their stiffness significantly decreases, and therefore, they easily deform to adapt themselves with the curved shape of 3-D microstructures – similar to the behavior observed in breast cancer cells. Such adaptation is a sign of their weak cytoskeleton after adding cytochalasin D. It is worth mentioning that low tensional state of fibroblast cells has been considered previously as the major cause for the round/bipolar or dendritic morphology of these cells in 3-D collagen matrices [42]. Although not a direct correlation between collagen matrices and our isotropically etched silicon substrates, the round/dendritic morphology of the fibroblasts after adding cytochalasin D in our experiments comes from the same origin; i.e., cells' low tensional state by disrupting actin microfilaments.

In contrast to normal fibroblast cells, the absence of stress fibers was evident in the cytoskeletal structure of cancer cells. This suggests that the adhesion of the cancerous cells to the silicon substrate is not as strong as normal fibroblast cells. Previously it was also reported that the presence of stress fibers is necessary for cell adhesion to the substrate [43, 44]. Cancer cells adopted with round and spread shapes on flat and curved sidewalls. Addition of cytochalasin D

caused these cells to become more rounded while it did not significantly change their adhesion behavior to the 3-D microstructures. This can be explained by the fact that even in their original state, these cells, attached to silicon substrates, did not possess actin stress fibers within their cytoskeletal structure. One characteristics of cells after oncogenic transformation is the loss of anchorage dependent growth [45]. Transformed cells are less responsive to surface rigidities [46], while the normal cells probe substrate rigidity as a mechanical feedback to modulate their shape and growth. Since destabilization of the stress fibers and focal adhesion in malignant cells enhances the migration process [34], it can be concluded that the observed behavior of MDA-MB-231 cells on the fabricated 3-D microstructures is a reflection of the metastatic nature of these cells and the failure of their impaired cytoskeleton to generate contractile forces on silicon substrates.

In summary, our research results support the hypothesis that differential response of normal and cancer cells to the various compartments of the 3-D silicon microenvironments is a reflection of differences in their cytoskeletal pre-stress and consequently their biomechanical properties. Previously, the use of scanning force microscopy (SFM) [47] and optical tweezers [48] provided quantitative measurements of the alterations in mechanical properties of cancer cells compared to normal cells. In general, these techniques showed that metastatic cancer cells are significantly softer and less resistant to deformation compared to normal cells, supporting our hypothesis. Although such instrumentation provides valuable quantitative measurements of cellular mechanical properties, we propose the precise surface topographical patterns etched into silicon provide another approach to evaluate biomechanical properties of different cell lines and specifically predict their stiffness under normal and diseased conditions. These microengineered structures can also be used to assess dynamic cytoskeleton responses, and show promise for applications in the identification of drugs able to restore normal cytoskeleton function [49]. Our future work will be focused on live measurement of dynamical changes in cytoskeletal structure of normal and cancer cells on the proposed microstructures.

3.5 Conclusion

In this chapter, we studied the behavior of individual HS68 normal human fibroblast and MDA-MB-2131 metastatic human breast cancer cells under static cell culture conditions in 3-D

silicon microstructures. Our findings demonstrated the contrasting behaviors of normal and cancer cells in the fabricated 3-D microenvironments. Fibroblast cells tended to stretch and maintained a more organized cytoskeleton. The cancer cells were less discriminating in response to the substrate geometry and deformed to take the shape of the curved sidewalls of isotropic microchambers. Treatment of the fibroblast cells with cytochalasin D, significantly altered their morphology and adhesion inside the etched features. However the adhesion of cancer cells to the curved microstructures was not significantly altered after disrupting their cytoskeleton using cytochalasin D. Our results suggest that differences in the cytoskeleton predominated by actin structures and biomechanical properties of these cells play a major role in their differential adhesion to various compartments of the etched silicon microstructures. The presented 3-D microstructures constitute a versatile platform to evaluate biomechanical properties of different cell types and to design novel cell-based assays including anti-cancer drug testing. The utility of these microstructures can be enhanced through the integration of additional electrical and fluidic components.

3.6 References

[1] M. Nikkhah, *et al.*, "Cytoskeletal role in differential adhesion patterns of normal fibroblasts and breast cancer cells inside silicon microenvironments," *Biomedical Microdevices,* vol. 11, pp. 585-595, Jun 2009.

[2] C. E. Semino, *et al.*, "Functional differentiation of hepatocyte-like spheroid structures from putative liver progenitor cells in three-dimensional peptide scaffolds," *Differentiation,* vol. 71, pp. 262-270, Jun 2003.

[3] T. Takezawa, "A strategy for the development of tissue engineering scaffolds that regulate cell behavior," *Biomaterials,* vol. 24, pp. 2267-2275, Jun 2003.

[4] P. Clark, *et al.*, "Topographical control of cell behaviour.1. Simple step cues," *Development,* vol. 99, pp. 439-448, Mar 1987.

[5] P. Clark, *et al.*, "Topographical control of cell behavior .2. multiple grooved substrata," *Development,* vol. 108, pp. 635-644, Apr 1990.

[6] R. G. Harrison, "The reaction of embryonic cells to solid structures," *Journal of Experimental Zoology,* vol. 17, pp. 521–544, 1914.

[7] E. T. denBraber, *et al.*, "Quantitative analysis of cell proliferation and orientation on substrata with uniform parallel surface micro-grooves," *Biomaterials,* vol. 17, pp. 1093-1099, Jun 1996.

[8] X. F. Walboomers, *et al.*, "Contact guidance of rat fibroblasts on various implant materials," *Journal of Biomedical Materials Research,* vol. 47, pp. 204-212, Nov 1999.

[9] P. Clark, *et al.*, "Cell Guidance by Ultrafine Topography Invitro," *Journal of Cell Science,* vol. 99, pp. 73-77, May 1991.

[10] A. M. Rajnicek, *et al.*, "Contact guidance of CNS neurites on grooved quartz: influence of groove dimensions, neuronal age and cell type," *Journal of Cell Science,* vol. 110, pp. 2905-2913, Dec 1997.

[11] M. J. Dalby, *et al.*, "Nucleus alignment and cell signaling in fibroblasts: response to a micro-grooved topography," *Experimental Cell Research,* vol. 284, pp. 274-282, Apr 2003.

[12] C. Oakley and D. M. Brunette, "The Sequence of Alignment of Microtubules, Focal Contacts and Actin-Filaments in Fibroblasts Spreading on Smooth and Grooved Titanium Substrata," *Journal of Cell Science,* vol. 106, pp. 343-354, Sep 1993.

[13] C. Oakley, *et al.*, "Sensitivity of fibroblasts and their cytoskeletons to substratum topographies: Topographic guidance and topographic compensation by micromachined grooves of different dimensions," *Experimental Cell Research,* vol. 234, pp. 413-424, Aug 1997.

[14] X. F. Walboomers, *et al.*, "Growth behavior of fibroblasts on microgrooved polystyrene," *Biomaterials,* vol. 19, pp. 1861-1868, Oct 1998.

[15] X. F. Walboomers, *et al.*, "Attachment of fibroblasts on smooth and microgrooved polystyrene," *Journal of Biomedical Materials Research,* vol. 46, pp. 212-220, Aug 1999.

[16] K. Matsuzaka, *et al.*, "Effect of microgrooved poly-l-lactic (PLA) surfaces on proliferation, cytoskeletal organization, and mineralized matrix formation of rat bone marrow cells," *Clinical Oral Implants Research,* vol. 11, pp. 325-333, Aug 2000.

[17] B. Wojciakstothard, *et al.*, "Role of the Cytoskeleton in the Reaction of Fibroblasts to Multiple Grooved Substrata," *Cell Motility and the Cytoskeleton,* vol. 31, pp. 147-158, 1995.

[18] C. J. Bettinger, *et al.*, "Micro fabrication of poly (glycerol-sebacate) for contact guidance applications," *Biomaterials,* vol. 27, pp. 2558-2565, Apr 2006.

[19] Y. A. Rovensky, *et al.*, "Spreading of Mouse Fibroblasts on the Substrate with Multiple Spikes," *Experimental Cell Research,* vol. 197, pp. 107-112, Nov 1991.

[20] T. G. van Kooten and A. F. von Recum, "Cell adhesion to textured silicone surfaces: The influence of time of adhesion and texture on focal contact and fibronectin fibril formation," *Tissue Engineering,* vol. 5, pp. 223-240, Jun 1999.

[21] A. M. P. Turner, *et al.*, "Attachment of astroglial cells to microfabricated pillar arrays of different geometries," *Journal of Biomedical Materials Research,* vol. 51, pp. 430-441, Sep 2000.

[22] J. L. Charest, *et al.*, "Myoblast alignment and differentiation on cell culture substrates with microscale topography and model chemistries," *Biomaterials,* vol. 28, pp. 2202-2210, Apr 2007.

[23] M. R. Dusseiller, *et al.*, "An inverted microcontact printing method on topographically structured polystyrene chips for arrayed micro-3-D culturing of single cells," *Biomaterials,* vol. 26, pp. 5917-5925, Oct 2005.

[24] H. H. Liao, *et al.*, "Response of rat osteoblast-like cells to microstructured model surfaces in vitro," *Biomaterials,* vol. 24, pp. 649-654, Feb 2003.

[25] J. Y. Mai, *et al.*, "A microfabricated platform probing cytoskeleton dynamics using multidirectional topographical cues," *Biomedical Microdevices,* vol. 9, pp. 523-531, Aug 2007.

[26] W. A. Loesberg, *et al.*, "The effect of combined cyclic mechanical stretching and microgrooved surface topography on the behavior of fibroblasts," *Journal of Biomedical Materials Research Part A,* vol. 75A, pp. 723-732, Dec 2005.

[27] W. A. Loesberg, *et al.*, "The effect of combined hypergravity and microgrooved surface topography on the behaviour of fibroblasts," *Cell Motility and the Cytoskeleton,* vol. 63, pp. 384-394, Jul 2006.

[28] R. Timpl, "Macromolecular organization of basement membranes," *Current Opinion in Cell Biology,* vol. 8, pp. 618-624, Oct 1996.

[29] M. Nikkhah, *et al.*, "Attachment and response of human fibroblast and breast cancer cells to three dimensional silicon microstructures of different geometries," *Biomedical Microdevices,* vol. 11, pp. 429-441, Apr 2009.

[30] R. Kalluri and M. Zeisberg, "Fibroblasts in cancer," *Nature Reviews Cancer,* vol. 6, pp. 392-401, May 2006.

[31] K. Gantz, *et al.*, "Development of a comprehensive model for RIE-lag-based three-dimensional microchannel fabrication," *Journal of Micromechanics and Microengineering,* vol. 18, Feb 2008.

[32] L. D. Kojic, *et al.*, "Raft-dependent endocytosis of autocrine motility factor is phosphatidylinositol 3-kinase-dependent in breast carcinoma cells," *Journal of Biological Chemistry,* vol. 282, pp. 29305-29313, Oct 2007.

[33] D. E. Discher, *et al.*, "Tissue cells feel and respond to the stiffness of their substrate," *Science,* vol. 310, pp. 1139-1143, Nov 2005.

[34] G. Giannone and M. P. Sheetz, "Substrate rigidity and force define form through tyrosine phosphatase and kinase pathways," *Trends in Cell Biology,* vol. 16, pp. 213-223, Apr 2006.

[35] D. E. Ingber, "Cellular tensegrity: defining new rules of biological design that govern the cytoskeleton," *Journal of Cell Science,* vol. 104, pp. 613-627, Mar 1993.

[36] D. E. Ingber, "Tensegrity I. Cell structure and hierarchical systems biology," *Journal of Cell Science,* vol. 116, pp. 1157-1173, Apr 2003.

[37] T. P. Stossel, "Contribution of actin to the structure of the cytoplasmic matrix," *Journal of Cell Biology,* vol. 99, pp. S15-S21, 1984.

[38] Y. Tseng and D. Wirtz, "Mechanics and multiple-particle tracking microheterogeneity of alpha-actinin-cross-linked actin filament networks," *Biophysical Journal,* vol. 81, pp. 1643-1656, Sep 2001.

[39] R. Ananthakrishnan, *et al.*, "Quantifying the contribution of actin networks to the elastic strength of fibroblasts," *Journal of Theoretical Biology,* vol. 242, pp. 502-516, Sep 2006.

[40] N. Wang, *et al.*, "Cell prestress. I. Stiffness and prestress are closely associated in adherent contractile cells," *American Journal of Physiology. Cell Physiology,* vol. 282, pp. C606-C616, Mar 2002.

[41] C. Rotsch and M. Radmacher, "Drug-induced changes of cytoskeletal structure and mechanics in fibroblasts: An atomic force microscopy study," *Biophysical Journal,* vol. 78, pp. 520-535, Jan 2000.

[42] S. Rhee and F. Grinnell, "Fibroblast mechanics in 3D collagen matrices," *Advanced Drug Delivery Reviews,* vol. 59, pp. 1299-1305, Nov 2007.

[43] L. Lewis, *et al.*, "The Relationship of Fibroblast Translocations to Cell Morphology and Stress Fiber Density," *Journal of Cell Science,* vol. 53, pp. 21-36, 1982.

[44] T. Soranno and E. Bell, "Cytostructural Dynamics of Spreading and Translocating Cells," *Journal of Cell Biology,* vol. 95, pp. 127-136, 1982.

[45] M. Stoker, *et al.*, "Anchorage and growth regulation in normal and virus-transformed cells " *International Journal of Cancer,* vol. 3, pp. 683–693, 1968.

[46] H. B. Wang, *et al.*, "Substrate flexibility regulates growth and apoptosis of normal but not transformed cells," *American Journal of Physiology. Cell Physiology,* vol. 279, pp. C1345-C1350, Nov 2000.

[47] M. Lekka, *et al.*, "Elasticity of normal and cancerous human bladder cells studied by scanning force microscopy," *European Biophysics Journal,* vol. 28, pp. 312-316, 1999.

[48] J. Guck, *et al.*, "Optical deformability as an inherent cell marker for testing malignant transformation and metastatic competence," *Biophysical Journal,* vol. 88, pp. 3689-3698, May 2005.

[49] J. S. Strobl, *et al.*, "Application of microengineered silicon chips to the study of human metastatic breast cancer and responses to histone deacetylase inhibitors," in *American Association for Cancer Research Special Conference on Advances in Breast Cancer Research: Genetics, Biology, and Clinical Applications*, San Diego, CA, 2007.

4 Chapter Four: The Cytoskeletal Organization of Breast Carcinoma and Fibroblast Cells inside Three Dimensional (3-D) Isotropic Silicon Microstructures

This chapter is produced from [1] with permission from Elsevier.

M. Nikkhah, et al., " The cytoskeletal organization of breast carcinoma and fibroblast cells inside three dimensional (3-D) isotropic silicon microstructures," Biomaterials, vol. 31, pp. 4552-4561, Jun 2010.

4.1 Introduction

Cell cytoskeleton is a highly dynamic polymeric network which defines the cell shape and its mechanical rigidity [2]. Any change in the cytoskeletal structure can affect the interaction of cells with their surrounding microenvironments [3]. Biological events in normal cells such as embryonic development, tissue growth and repair, and immune responses as well as cancer cell motility and invasiveness are dependent upon or regulated by cytoskeletal reorganization and the biomechanical properties of the cytoskeleton [2, 4-6]. Understanding how the cell cytoskeleton reorganizes during its interaction with the surrounding environment is a fundamental biological question with applications to tissue engineering [7] and cancer diagnosis and therapy [8].

The extracellular matrix (ECM) proteins *in vivo* form a complex and textured interconnecting network and a three dimensional (3-D) surface topography [9, 10]. Cells are exposed to several mechanical, chemical and three-dimensional topographical stimuli, which modulate their behaviors such as migration, growth, and adhesion. With advances in micro- and nano-fabrication technology, researchers have been able to create substrates comprised of precise micro- and nano- topographical and chemical patterns in order to mimic more *in vivo* microenvironments for biological and medical applications. These studies have provided valuable information on several cellular processes such as migration [11-13], cytoskeletal organization [13, 14], contact guidance [15-17] and differentiation [18] on the proposed micro- and nano-environments. However, many of the previous approaches have relied on using either microstructures comprising anisotropic geometries (grooves) [19-22], or polymeric fibrous

networks [23]. It is well known that 3-D microenvironments influence cell functions to a great extent and are different from standard two-dimensional (2-D) culture environments [24, 25].

We previously reported the development of 3-D silicon microstructures which comprised of curved isotropic surfaces to characterize and compare the growth and adhesion behavior of normal fibroblast and metastatic human breast cancer cells [26, 27] (Chapters 2 and 3). The isotropy of the curved surfaces determined by an approximately constant curvature is an excellent characteristic of our microstructures since it can be used for understanding the mechanism of deformation, adhesion and force balance within the cytoskeleton of different cells. This eliminates variability in the cell behavior introduced by the geometrical anisotropy of the microstructures. In this chapter, by building upon our previous work, we are interested in studying the biological behavior of the cell lines obtained from metastatic breast tumor pleural effusions, normal fibrocystic mammary epithelium, and normal fibroblasts inside 3-D isotropic microstructures. Breast carcinoma frequently originate with cells that normally line the milk ducts within the mammary gland [28]. It is also well known that inside the body fibroblast cells are intimately embedded within the breast microenvironment [29]. In invasive breast carcinoma, the tumor cells fill the duct, and the basement membrane, which normally separates the ductal epithelial cells from the stromal elements, primarily the fibroblasts, is disrupted resulting in close juxtaposition of carcinoma cells and the fibroblast cells of the breast stroma. This structural reorganization constitutes a critical pathobiological transition leading to disease progression [30].

Herein, we present the detailed cytoskeletal organization and adhesion mechanism of normal breast epithelial cells, metastatic breast cancer cells and fibroblast cells, three key cellular components embedded in any breast tumor microenviroenment [29], inside the 3-D silicon microstructures. The role of actin cytoskeleton in the cell adhesion behavior was established in our previous study [26]. In this work we explored the contribution of the cellular elasticity, focal adhesion complexes, and microtubules on the adhesion characteristics of the cells inside the isotropic (curved) 3-D microstructures. The role of microtubules in fibroblasts behavior on 2-D rigid surfaces and 3-D collagen matrices has been addressed before [31], but is relatively understudied in human breast cancer cells, where they might significantly impact pathological

cell behaviors such as adhesion, migration and metastasis. We used atomic force microcopy (AFM) indentation to quantitatively measure cellular elasticity.

The results of the current research can provide important diagnostic and prognostic markers unique to the tumor, which could ultimately be used to develop new tools for the detection and treatment of breast cancer.

4.2 Materials and methods

4.2.1 Silicon device fabrication

Figure 4-1(a,b) shows the photo image of the fabricated microdevice and the corresponding scanning electron microscopy (SEM) images. The fabrication process of 3-D silicon microstructure is similar as described in previous chapters. It relies on the application of reactive ion etching (RIE) lag and its dependence on geometrical patterns of the photomask layout to etch silicon to different depths [26]. Briefly, the fabrication process was started by depositing 8000Å-thick plasma enhanced chemical vapor deposition (PECVD) oxide layer on a silicon wafer. After spinning and patterning photoresist, the oxide layer was etched for 3 minutes using deep reactive ion etching (DRIE) CH_4/C_4F_8 plasma. Next, silicon was etched using DRIE SF_6 plasma to form complex arrays of features composed of star- and circular-shaped microchambers. After removing photoresist, the oxide layer was subsequently removed using DRIE. As shown in the SEM images of the microchambers, the depth of the microchambers varies between 60-70 µm and the width ranges between 150-170 µm. It is notable that the described fabrication technique provides localized rough edges on the curved sidewalls and on the bottom surface of the microchambers. In the star patterns, the rough edges formed on the sidewalls (Figure 4-1(b), top left inset) while in the circular-shaped microchambers, the rough edges were localized on the bottom of the microchambers in the form of concentric rings (Figure 4-1(b), top right inset).

4.2.2 Cell culture preparation and reagents

Normal human fibroblast cells (HS68), normal human breast epithelial cells (MCF10A), and metastatic human breast cancer cells (MDA-MB-231) investigated in this work were purchased from the American Type Culture Collection (ATCC). MDA-MB-231 and HS68 cells were maintained in plastic T-75 cm^2 culture flasks in RPMI culture medium, which contained 5% fetal

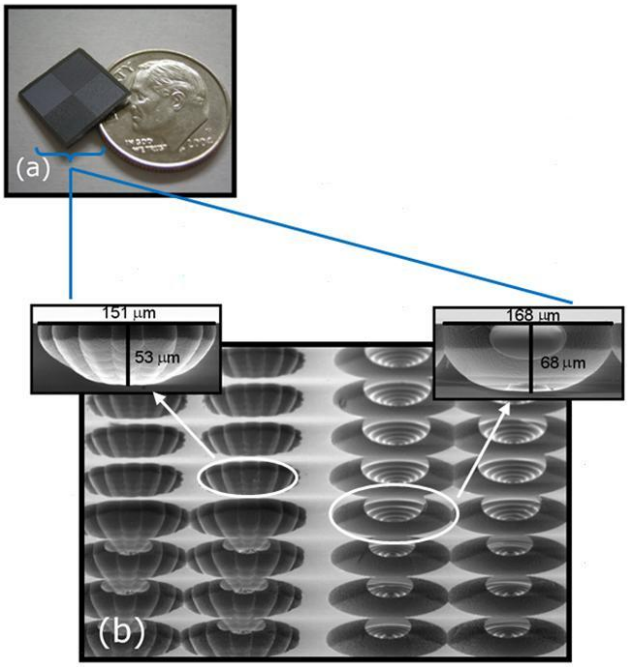

Figure 4-1 Photo image of the fabricated devices in silicon. (b) SEM images of the 3-D silicon microstructures comprising star and circular shape microchambers. With the fabrication technology utilized, scalloped edges can be formed on the curved sidewalls and the bottom surface of the microchambers.

bovine serum (FBS), 1 mM sodium pyruvate, and penicillin-streptomycin (100 Units/ml). MCF10A cells were grown in plastic T-75 cm^2 culture flasks using Hams F12:DMEM (50:50) (Mediatech), 2.5 mM L-glutamine (Mediatech), 20 ng/ml epidermal growth factor (EGF) (Sigma), 0.1 µg/ml cholera toxin (CT) (Sigma), 10 ug/ml insulin (Sigma), 500 ng/ml hydrocortisone (Sigma) and 5% horse serum (Atlanta Biologicals). For adhesion analysis, all the cells were grown for 48 h at 37°C in humidified 7% CO2-93% air atmosphere after plating at a density of 1.1×10^4cells/mm^2on 3-D silicon microstructures in RPMI culture medium which contained 10% FBS. After 48 hours of growth, nocodazole was added to the culture medium for either 30 minutes or 3 hours prior to fixation for confocal imaging to illustrate cell adhesion alteration inside the isotropic substrates.

4.2.3 Immunofluorescence for cytoskeletal organization and focal adhesions

We assessed the formation of focal adhesion complexes and actin cytoskeleton in cells attached to the 3-D isotropic microstructures using confocal microscopy (ZEISS-LSM-510 META) in the reflection mode after tagging the complexes with vinculin, a protein prominent in

focal adhesions in both fibroblast and breast cells [32, 33]. For vinculin staining, 3% paraformaldehyde (PF) solution in 250mM Tris, pH 7.2 was used to fix the cells on the 3-D silicon microstructures for 10 minutes. Then the cells were exposed to 6% PF solution with 0.25% Triton X-100 in PBS for another 10 minutes to permeabilize the cell membrane. A monoclonal mouse anti-vinculin antibody (Abcam) was diluted 1/100 in 2% chicken serum albumin in PBS and added to the samples for 30 minutes. Next, rhodamine conjugated goat anti-mouse secondary antibody (Invitrogen) was diluted 1/300 in 2% chicken serum albumin in PBS and added to the samples for 30 minutes. The actin cytoskeleton was stained using, AlexaFlour-488 phalloidin (Invitrogen)(10 U/ml in 140 mM NaCl-6% bovine serum albumin in 40 mM Tris, pH 7.2). Following the vinculin and actin staining, the samples were rinsed three times in PBS and mounted on ProLong Gold antifade reagent with DAPI (Invitrogen) for final imaging.

For microtubules staining, cells were fixed as described above for vinculin staining. A mouse monoclonal anti-β-Tubulin I+II antibody (Sigma) was diluted 1/750 in 2% chicken serum albumin in PBS for HS68 cells, and 1/1000 in 2% chicken serum albumin in PBS for MCF10A and MDA-MB-231 cells and added to the samples for 30 minutes. After washing the cells, rhodamine conjugated goat anti-mouse secondary antibody (Invitrogen) was diluted 1/300 in 2% chicken serum albumin in PBS and added to the samples for 30 minutes. Fluorescence microcopy (Nikon Eclipse 80i) was performed to image the microtubules.

4.2.4 Scanning electron microscopy (SEM)

SEM was also performed to investigate the detailed effects of the etched features on the cellular morphology and adhesion characteristics. Following 48 hours of growth, cells were fixed in 3.7% formaldehyde in PBS for 10 minutes. The samples were critical-point-dried and sputter-coated with a thin layer of gold palladium prior to SEM imaging.

4.2.5 Atomic force microscopy and Hertz's model

Due to the technical difficulty in measurements of the cells' Young's modulus on silicon surfaces, the AFM experiments were performed on the cells attached on the Collagen IV (Sigma) coated 25 mm round glass coverslips. Cells were plated with the density of 3×10^4 cells/ml on glass coverslips and incubated for 24h prior to experimentation. Atomic force microscopy from Asylum Research Corporation (Santa Barbara, CA), MFP-3D-Bio, was used for force

measurement. The AFM was combined with an inverted optical and fluorescence microscope (Olympus IX71) for precise positioning of the AFM tip on the samples and monitoring its movement during force application. For MDA-MB-231 cells, optical microscopy was used to guide and locate the AFM cantilever tip on the center of the cells while for MCF10A and HS68 cells, fluorescence microscopy was used for better visualization and locating the tip on the center of the cell. For this purpose, MCF10A and HS68 cells were labeled for 25 minutes in serum-free medium containing 1µl/ml of the membrane permeable fluorescent vital dye Cell Tracker Orange (Invitrogen). Soft V-shaped silicon nitride cantilevers, TR400PSA (Olympus), with the nominal length of 200µm and a spring constant of 0.02 N/m were used in this study. The spring constant was experimentally measured using thermal noise fluctuations. A glass sphere (Duke Scientific) with nominal diameter of ~10µm was attached to the cantilever tip to reduce any nonlinearity in deforming stress and avoid damaging the sample (Figure 4-2 top right inset). SEM was used to measure the exact diameter and the location of the glass attached to the tip. All the measurements were carried out using a standard fluid cell (Asylum Research) at room temperature.

After plating the cells, 20mM HEPES was added to the cell culture medium to maintain a physiological pH during the experimentation. The pH of the culture medium was measured to be 7.2 after adding HEPES. The measurements were carried out at the center of the cell with the tip velocity of 0.5µm/s.

The cells' Young's modulus was computed by using the Hertz's model [34, 35]. According to the model, the relationship between the applied force, F, and the indentation depth, δ, can be expressed as:

$$F = \frac{4\sqrt{R}}{3(1-\nu^2)} E\delta^{3/2} \qquad (4\text{-}1)$$

where R is the radius of the tip, and E and ν are the Young's modulus and Poisson's ratio of the indented cell, respectively. The indentation, δ, is usually interpreted as the difference in the relative changes of the piezo-stack movement and cantilever deflection and, thus, can be expressed as:

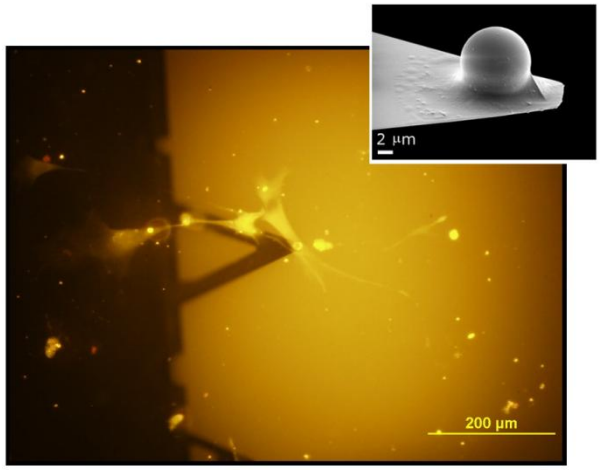

Figure 4-2 Single cell indentation experiment using AFM. The cells were indented using a silicon nitride cantilever. A glass sphere (Duke Scientific) with nominal diameter of ~10 µm was attached to the cantilever tip to reduce any nonlinearity in deforming stress and avoid damaging the sample (Top right inset).

$$\delta = (z - z_0) - (d - d_0) \tag{4-2}$$

z_0 and d_0 are the piezo-stack height and cantilever deflection at the contact point, respectively. One of the difficulties in using Hertz's model is finding the initial contact point between the cell and the tip of the cantilever. By following the approach proposed by Guo et al. [36], this difficulty can be overcome by employing the linear version in δ of the Hertz's model to define the contact point. Equation (4-1) can be rewritten as

$$F^{2/3} = \left[\frac{4\sqrt{R}}{3(1-\nu^2)}E\right]^{2/3}\delta \tag{4-3}$$

and, consequently, by substituting equation (4-2) into equation (4-3), one gets:

$$F^{2/3} = \left[\frac{4\sqrt{R}}{3(1-\nu^2)}E\right]^{2/3}(z-d) - \left[\frac{4\sqrt{R}}{3(1-\nu^2)}E\right]^{2/3}(z_0 - d_0) \tag{4-4}$$

Equation (4-4) can be regarded as the equation of a line in the plane $(F^{2/3}, z-d)$. The Young's modulus can then be directly calculated from the linear slope of $F^{2/3}$ and the contact point, $(z_0 - d_0)$, can be then calculated from the intercept of equation (4-4) by using the following equations:

$$S = \left[\frac{4\sqrt{R}}{3(1-\nu^2)} E \right]^{2/3}, \qquad E = \left[\frac{3(1-\nu^2)}{4\sqrt{R}} \right] S^{3/2} \tag{4-5}$$

$$C = -\left[\frac{4\sqrt{R}}{3(1-\nu^2)} E \right]^{2/3} (z_0 - d_0), \qquad (z_0 - d_0) = -C/S \tag{4-6}$$

The Poisson's ration ν is assumed to be 0.5 in accordance with the incompressibility assumption usually employed for cells and soft tissues [37]. All the data analysis and curve fitting of the Hertz's model to the collected force-indentation data were performed using MATLAB 7.0 software.

4.2.6 Cell area measurement and statistical analysis

Cell area measurements were performed on the flat surfaces surrounding the etched cavities on each silicon chip using fluorescence images and the National Institutes of Health (NIH) ImageJ (v. 1.41) software. For MCF10A cells, the area of a cluster of the cells was measured and divided by the number of the cells within the cluster to obtain the average area of a single cell.

A two-sample independent t-test was performed using Graph Pad Prism 5.0 statistical software to compare the cell area its Young's modulus obtained with AFM.

4.3 Results

In the first set of experiments, we examined the adhesion behavior of the cells to the 3-D silicon microstructures using SEM and confocal imaging. Figure 4-3 shows SEM images of the cells attached inside the etched features. These images demonstrate that the fibroblasts mostly developed tension and were stretched inside the etched features (Figure 4-3(a-c)) while both MCF10A and MDA-MB-231 cells deformed and adapted their shape to the curved sidewalls of isotropic geometries (Figure 4-3(d-i)).

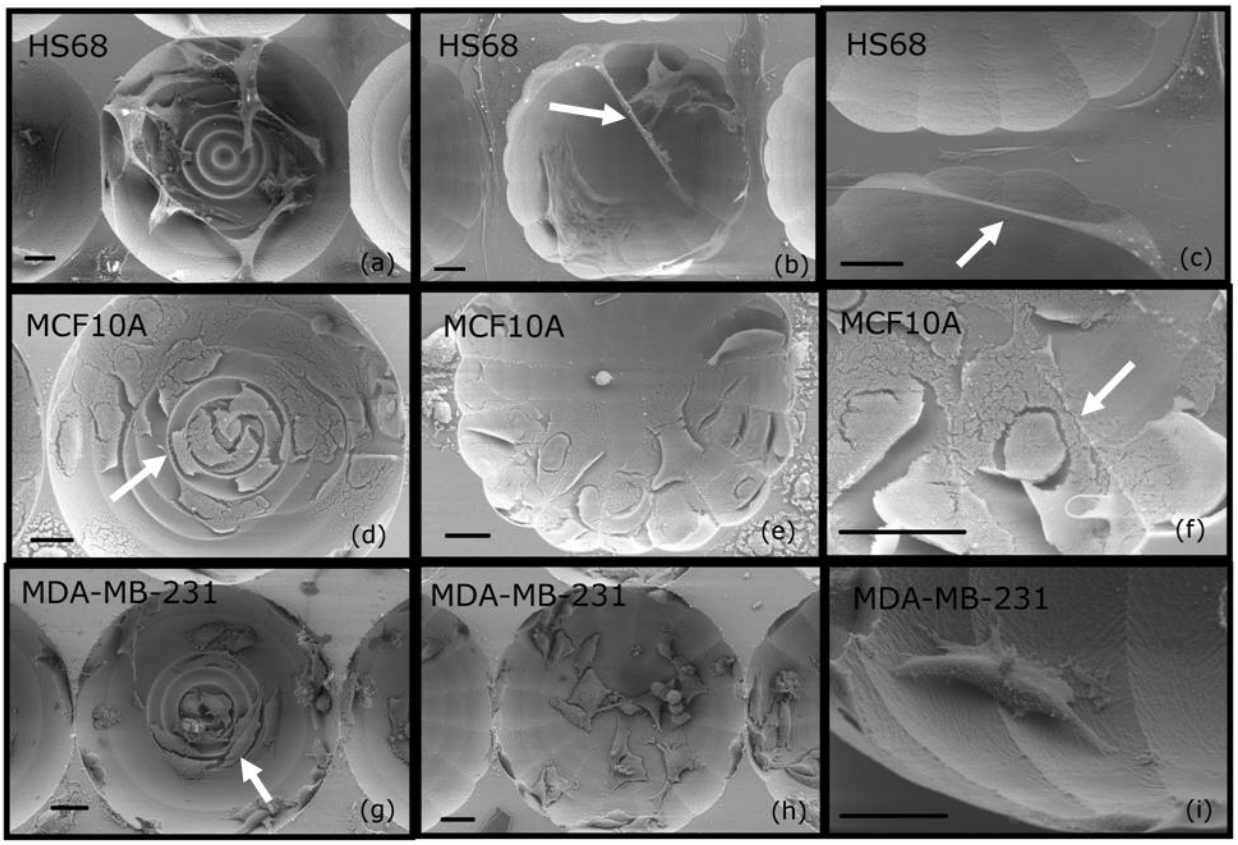

Figure 4-3 SEM images of the HS68 fibroblasts (a-c), MCF10A (d-f), and MDA-MB-231 (g-i) cells inside the isotropic microstructures. Fibroblasts mostly stretched inside the etched features while both MCF10A and MDA-MB-231 cells deformed and adapted their shape to the curved sidewalls of isotropic geometries. Scale bars represent 20 µm

Figure 4-4 shows the confocal images of the HS68, MCF10A and MDA-MB-231 cells attached inside the etched features. The confocal images inside the microchambers were taken at different depths of focus to construct 3-D Z-stack images. These images clearly indicate the stretching behavior of the fibroblast cells inside the microchambers thus confirming our previous observations using SEM imaging technique (Figure 4-4(a-d)). The side view of the stretched fibroblast cells within isotropic microchambers is shown in Figure 4-4(c) (arrow). Fibroblast cells protrude lamellipodia while attached inside the isotropic microchambers. Formation of several vinculin-containing focal adhesions (red-stain) on the anchoring sites of the fibroblast cells to the isotropic microstructures is clear from these images (Figure 4-4(c,d)). On the other hand, both MCF10A and MDA-MB-231 cells adapted their cytoskeleton to the curved sidewalls of the isotropic microchambers. Figure 4-4(g,k) shows the side view of deformed MCF10A and MDA-MB-231 confirming that these cells adopt the curvature of the isotropic sidewalls. Figure

4-4(h) shows the formation of the vinculin-containing focal adhesions of MCF10A cells around the ring edges at the bottom of the etched cavities. MCF10A cells maintained their cell-cell junction on the curved surfaces inside the etched features as well as on flat areas around the periphery of the etched features (Figure 4-4(e,f)).

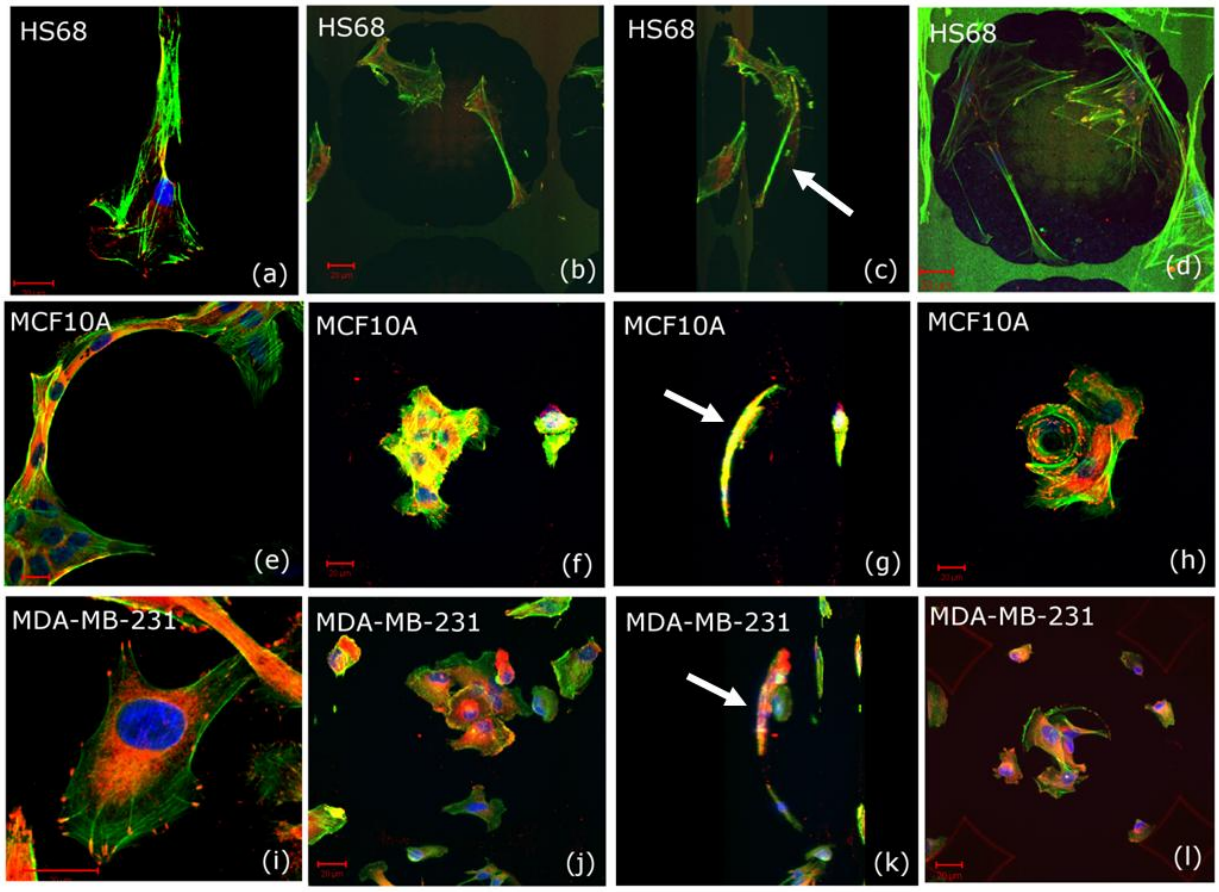

Figure 4-4 Planar and 3-D confocal images of the HS68 fibroblasts (a-d), MCF10A (e-h), and MDA-MB-231 (i-l) cells attached on flat surfaces and inside the etched features. Actin cytoskeleton is stained in green and vinculin is stained in red. Image (c) shows the side view of image (b); arrow identifies the stretched fibroblast cells. Images (g,k) show the side view of images (f,j) respectively; arrows identify deformed MCF10A and MDA-MB-231 cells inside the isotropic microchambers. Scale bars represent 20 µm.

To assess the role of cytoskeletal stiffness in differential adhesion characteristics of the cells to the 3-D isotropic microstructures, the Young's modulus of the cells was measured using AFM and Hertz's model. The Hertz's model was accurately fit to the experimental data to obtain Young's modulus (R^2~0.98). The population of elasticity measurements (Young's modulus, E) of the cells was not normally distributed according to Shapiro-Wilks test and was best described

by log-normal distributions having a shift toward lower modulus (Figure 4-5). HS68 cells had a broad distribution peak compared to both MCF10A and MDA-MB-231 cells. The peak modulus of HS68, MCF10A and MDA-MB-231 was located at 1.15 kPa, 0.43 kPa and 0.2 kPa, respectively. Table 4-1 shows the summary of elasticity measurements of the cells. Distinct biomechanical properties were observed among the three cell types. Given the same amount of average force exerted on the cell body, the indentation depths for MCF10A and MDA-MB-231 cells were higher than for fibroblast cells (Table 4-1). The AFM data suggests that the fibroblast cells are significantly stiffer (P<0.0001) than both MCF10A and MDA-MB-231 cells.

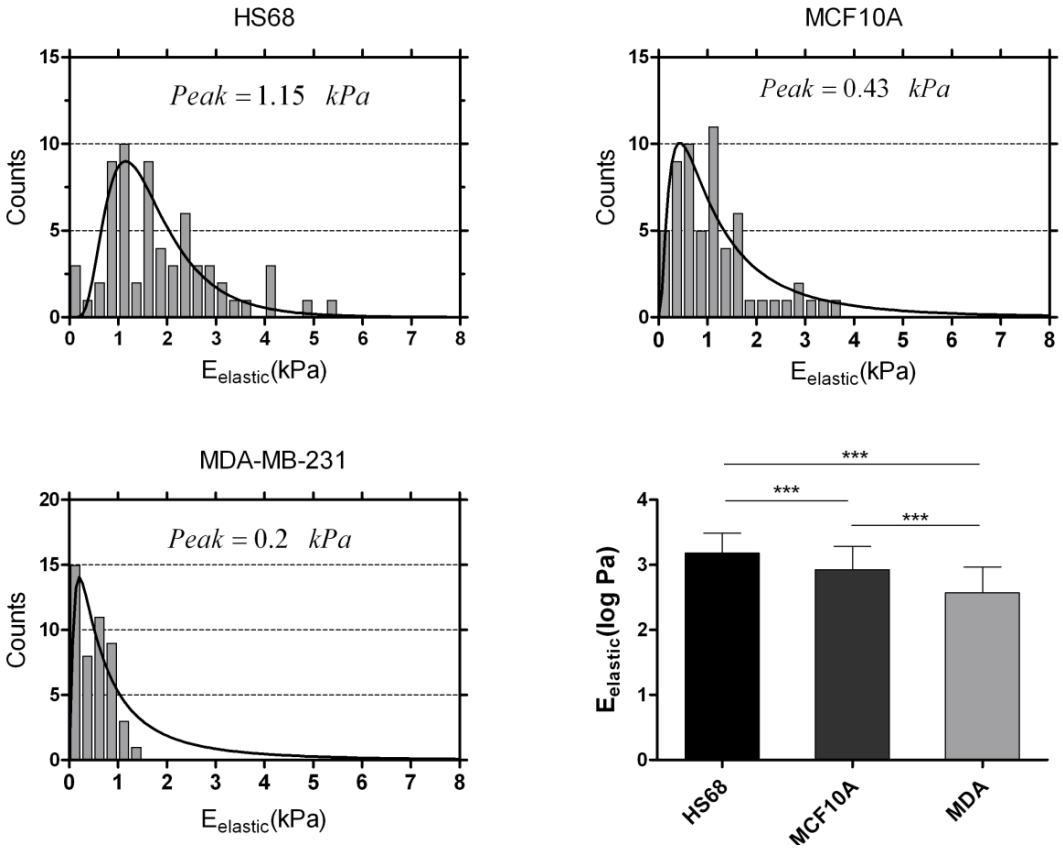

Figure 4-5 HS68 fibroblast, MCF10A and MDA-MB-231 population elasticity. The cells elastic modulus were best described by log-normal distributions. Bottom right figure shows the log transformed data indicating that fibroblast cells had the largest elastic moduli, followed by MCF10A cells then MDA-MB-231 (p<0.0001).

Table 4-1 Elastic parameters for normal human fibroblast cells (HS68), normal human breast epithelial cells (MCF10A) and metastatic human breast cancer cells (MDA-MB-231).

Cell	n	$E_{elastic}$	Ave. Force(nN)	Ave. Indentation(nm)
HS68	64	1.86±1.13	0.38±0.15	184.5±126.4
MC10A	59	1.13±0.84	0.38±0.07	262.8±146.7
MDA-MB-231	47	0.51±0.35	0.41±0.12	428±237.6

Data are presented mean ± standard deviation

Although, the AFM analysis confirmed that MCF10A cells were significantly ($p<0.0001$) stiffer than the MDA-MB-231 cells, these cells behaved similarly in terms of adhesion inside the etched features. These observations and measurements led us to speculate that microtubules may also play a role in adhesion of the cells to the 3-D silicon substrates. To test this hypothesis, we disrupted the microtubules by nocodazole treatments for either 30 minutes or 3 hours. Prior to visualization of cytoskeletal organization and adhesion of the cells inside the etched features at these time points, fluorescence microcopy was performed to visualize the disruption of microtubules by nocodazole. Figure 4-6 illustrates the microtubule organization in HS68, MCF10A and MDA-MB-231 cells before and after treatment with nocodazole. This figure clearly demonstrates that after 3 hours, microtubules are completely disrupted throughout the cell body in all the cell types.

With respect to cytoskeletal organization of the cells inside the etched features, after 30 minutes of nocodazole, most of the actin fibers of HS68 fibroblast cells retracted and only a few of them remained stretched inside the etched cavities (Figure 4-7(b)). After 3 hours of treatment with nocodazole, these cells lost their stretched morphology inside the etched cavities (Figure 4-7(c)). Although actin stress fibers and focal adhesions to the substrate were maintained, the cell shape adopted a rounded morphology while the cell area remained unchanged (Figure 4-8). These finding are consistent with previous work [31] with human foreskin fibroblasts attached to collagen coated glass coverslips after treatment with nocodazole.

MCF10A cells adhesion to the isotropic microchambers did not significantly change in response to nocodazole at either the 30 minutes or 3 hours time point (Figure 4-7(e,f)). These cells maintained their cell-cell junctions and their cell area (Figure 4-8) after treatment with nocodazole suggesting that microtubules do not contribute significantly to the maintenance of MCF10A cell shape and adhesion to the isotropic microchambers.

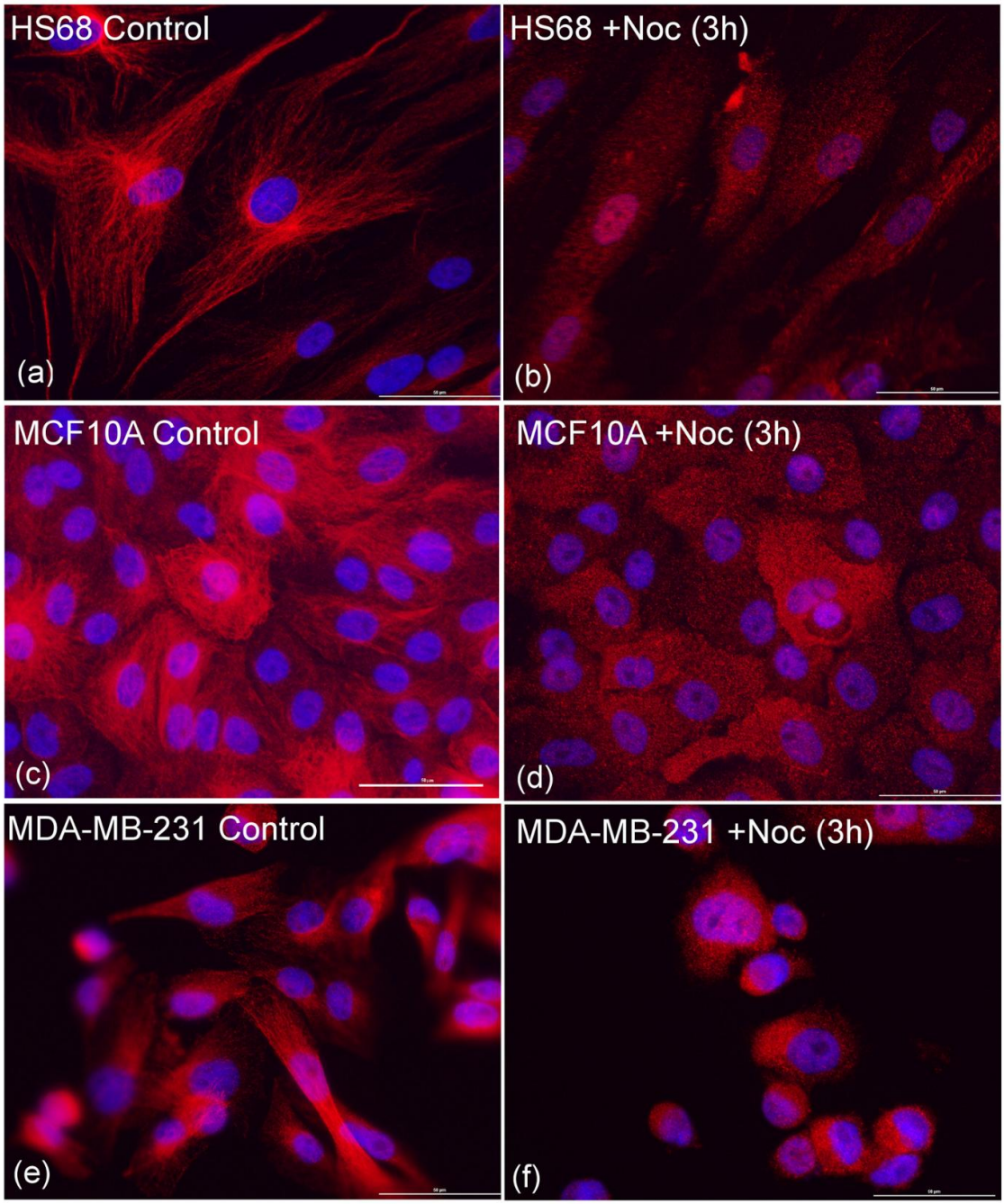

Figure 4-6 Fluorescence images showing the distribution of microtubules and nuclei in HS68 (a,b), MCF10A (c,d) and MDA-MB-231 (e,f) cells before and after treatment with nocodazole (3 hours). Nocodazole completely disrupted microtubules in all cell types. Scale bars represent 50 µm.

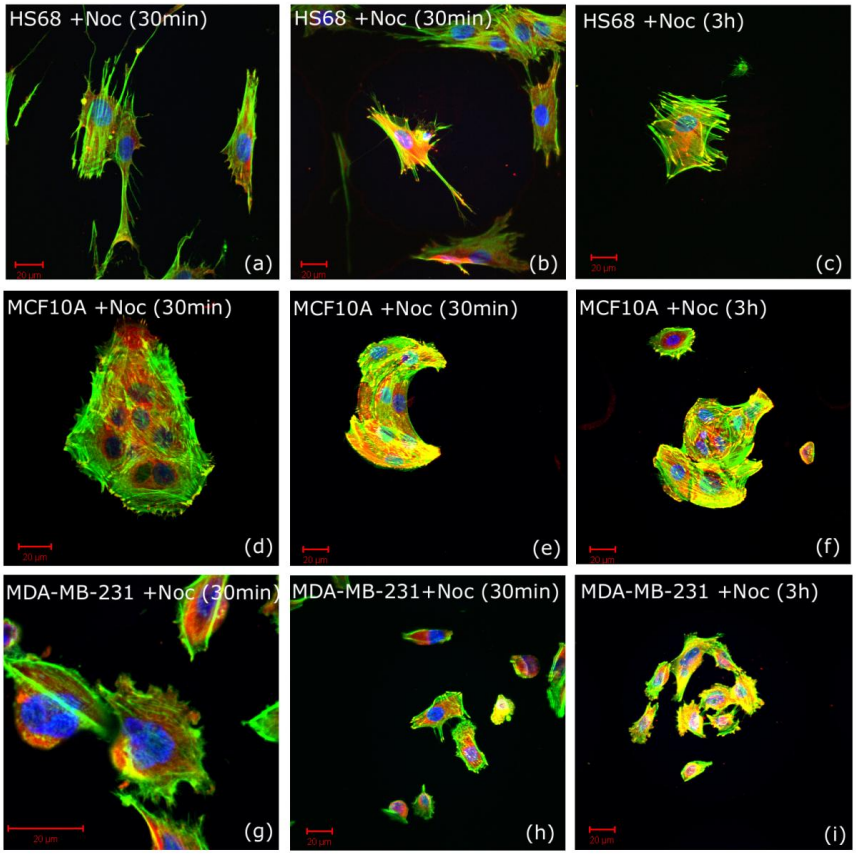

Figure 4-7 Confocal images of HS68 fibroblasts (a-c), MCF10A (d-f), and MDA-MB-231 (g-i) cells attached on flat surfaces and inside the etched features after adding nocodazole. Actin cytoskeleton is stained in green and vinculin is stained in red. Images (a,d,g) show the cells attached on flat surfaces. Images (b,c) show HS68 fibroblast cells after 30 minutes and 3 hours of nocodazole treatment. After 3 hours cells lost their stretching behavior and adopted rounded morphology. MCF10A and MDA-MB-231 cell adhesion to the isotropic microchambers did not significantly alter in response to nocodazole (e-f, h-i). Scale bars represent 20 µm.

In MDA-MB-231 cells, after 30 minutes of treatment with nocodazole, the lamellipodia formed were smaller in size compared to control cells, and the cell morphology was dominated by lamellipodial extensions. The adhesion behavior of the cells remained unchanged (adapting to the curved sidewalls of isotropic microchambers) after 30 minutes and 3 hours treatment with nocodazole (Figure 4-7(h,i)). However, the cells became rounded and the cell area significantly decreased ($P<0.02$) in response to nocodazole after 3 hours (Figure 4-8)[*].

[*] Supplementary movies associated with this chapter can be found at [1] M. Nikkhah, *et al.*, "The cytoskeletal organization of breast carcinoma and fibroblast cells inside three dimensional (3-D) isotropic silicon microstructures," *Biomaterials*, vol. 31, pp. 4552-4561, Jun 2010.

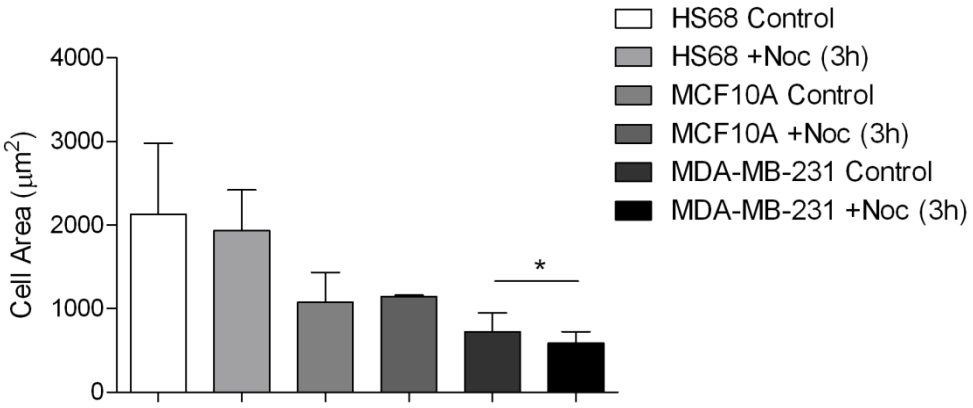

Figure 4-8 HS68, MCF10A and MDA-MB-231 cell area measured using NIH ImageJ software. HS68 and MCF10A cell area were not significantly changed in response to nocodazole. However, MDA-MB-231 cell area was significantly ($p<0.02$) decreased after nocodazole treatment. Data are presented mean ± standard deviation (n=20).

4.4 Discussion

With the advances in micro/nano fabrication technologies, numerous studies have investigated the effect of the surface topography on various cell behaviors such as migration [12, 13], differentiation [18] and cytoskeletal organization [13, 14]. Although these studies have reported valuable data in terms of biological functions of the cells, the proposed substrates are limited on anisotropic micro/nano structures or polymeric fibrous networks. In this study, the detailed cytoskeletal organization and adhesion behavior of three types of cells embedded in human breast tumor microenvironment in 3-D isotropic silicon microstructures was investigated by combining SEM, confocal microscopy and AFM. With respect to normal human fibroblast cells (HS68) and metastatic human breast cancer cells (MDA-MB-231), the results of the current work were in good agreement with our previous findings in which we investigated the interaction of these cells with 3-D isotropic microstructures [26, 27]. In our earlier work, we demonstrated that actin cytoskeleton plays a significant role in the stretching behavior of fibroblastic cells inside the microstructures having curved surfaces [26]. Disruption of the actin cytoskeleton of the fibroblast cells using cytochalasin D caused a significant alteration in the adhesion behavior of these cells in which they adopted the curved sidewalls of isotropic geometries [26]. Herein, the different behavior exhibited by these cells on 3-D microstructures was then correlated to their biomechanical properties (i.e. elasticity). AFM analysis confirmed that the average Young's

modulus of fibroblast cells was significantly greater than the average Young's modulus of normal human breast epithelial cells (MCF10A) and metastatic breast cancer cells (MDA-MB-231). Knowing that the actin cytoskeleton is a major determinant of the cell overall strength [38, 39], the AFM results confirm our previous finding which suggested that cell stiffness affects the adhesion behavior of the cells to the 3-D isotropic architecture.

It is also well known that the cellular cytoskeleton influences their biomechanical behavior including interactions with supporting substrates and neighboring cells [2, 6]. The tensegrity theory has been very successful in describing the complex mechanical behavior of adherent cells. According to this theory, the cell can be viewed as a tensional structure in which actin filaments bear tensile loads and microtubules bear compression loads [40]. The prestress, defined as the tensile stress in the cytoskeleton prior to application of an external load, is determined by actin filaments and balanced by microtubules and attachments to substrates or other cells. The theory predicts that the prestress in cells is proportional to their stiffness which is in agreement with experimental observations [41]. As indicated by the tensegrity theory and results of our AFM experiments, the prestress in the HS68 cells is higher than in MCF10A and MDA-MD-231 cells.

The Young's modulus of MCF10A cells was found to be significantly greater than the Young's modulus of MDA-MB-231 cells. With respect to breast cancer, earlier studies compared the elasticity of MCF10A and human cancerous breast cells (MCF7), and established that MCF7 cells are softer than MCF10A cells [42-44]. Our findings showing a decrease in cell stiffness in metastatic MDA-MB-231 cells compared to the normal breast cell line MCF10A concur with the previous work [45-47]. However, we also noted that although the MCF10A cells were significantly stiffer and had a higher prestress compared to MDA-MB-231 cells, the adhesion behavior of these two cell types inside the 3-D isotropic microstructures was in fact similar. Both breast cell lines, as opposed to normal fibroblasts, were able to adapt to the curved surfaces. This suggested that in addition to cytoskeletal prestress, focal adhesion complexes, other cytoskeletal components and cell morphology (which affects the magnitude of contractile forces [14]) influence the adhesion pattern and adaption of the cells to the 3-D microstructures. This paper in particular investigated the role of microtubules and attachments through the vinculin-containing focal adhesions to the substrate.

In the HS68 cells, vinculin staining was concentrated in the cell periphery, locations where the cells anchored to the isotropic geometries. Disruption of the microtubules by nocodazole (3 hours) inhibited the stretching behavior of the fibroblast cells within the etched features and caused these cells conform to the 3-D microstructures. Rhee et al. [31] showed that the microtubules are required for polarization of fibroblast cells attached on collaged coated coverslips and not for the cell spreading. Thus, within the context of the tensegrity theory, these findings confirm that prestress within the cytoskeleton of the fibroblast cells is mainly balanced by the microtubules.

It was quite evident by the pattern of vinculin staining that the distribution of the focal contacts was different in MCF10A and MDA-MB-231 cells compared to HS68 cells. Furthermore, no significant difference in the adhesion behavior of MCF10A and MDA-MB-231 cells were observed after disrupting their microtubules. The experimental data suggested that in breast cells, microtubules had a minor effect, if any, in the adhesion pattern to the 3-D microstructures, and this was in marked contrast to what was observed in fibroblast cells. Our observations also suggest that the differential adhesion behavior of these cell types within the etched features was influenced by the organization and the density of the adhesion sites. Although MCF10A cells were stiffer (having higher prestress) than MDA-MB-231 cells, the higher prestress could be balanced by their interaction with the substrate rather than by microtubules. In addition, the higher prestress in MCF10A cells deprived of microtubules could be partially balanced through connection points with neighboring cells and cell-cell junctions. It must be noted that the difference in the focal adhesions among the cell lines can be related to the effect of growth factors and serum which causes activation of small GTP-binding protein, Rho, and cytoskeletal tension [14, 48, 49]. This subject, however, is beyond the scope of the current work. Other investigators dissolved the microtubules in other types of fibroblasts by using the same drug [50, 51]. However, in the cited studies, the cells were in contact with collagen gels and matrices and, hence, the disruption of the microtubules also produced deformation of the collagen.

4.5 Conclusion

In this work we investigated the role of major cytoskeletal fibers namely, actin filaments and microtubules as well as focal adhesions proteins (vinculin) and cell biomechanical properties in

adhesion behavior of the cells inside 3-D silicon microstructures. HS68 fibroblast cell stretched inside the etched features, while both MCF10A and MDA-MB-231 cells adopted the curved surfaces of isotropic microchambers. In stretched HS68 cells, vinculin-containing focal adhesions were observed on anchoring sites to the etched features. MCF10A and MDA-MB-231 cells exhibited more diffuse Vinculin within the cell body. AFM indentation confirmed that HS68 cells were significantly stiffer than MCF10A and MDA-MB-231 cells. Upon microtubules disruption, HS68 fibroblast cells lost their stretching behavior inside the etched cavities and adopted a rounded morphology whereas the adhesion behavior and cell-cell junctions of MCF10A and MDA-MB-231 cells remained unchanged. Overall, the results of the current study demonstrated that cytoskeletal tension (prestress) and microtubules in HS68 cells, the adhesion strength to the substrate and cell-cell junction in MCF10A cells, and deformability and soft cytoskeletal structure in MDA-MB-231 cells, are the dominant factors defining their behavior inside the isotropic microstructure. Therefore, by carefully engineering the geometry of the substrate, it would be possible to differentiate the response of the cells based on their adhesion and stiffness signatures. The 3-D isotropic silicon microstructures have also the potential to investigate the detailed cytoskeletal organization and the mechanism of force balance in different cell types under healthy and diseased conditions and can lead to the development of label-free cell separation and diagnostics platforms based upon the cell biomechanical and cytoskeletal organization signatures .

4.6 References

[1] M. Nikkhah, *et al.*, "The cytoskeletal organization of breast carcinoma and fibroblast cells inside three dimensional (3-D) isotropic silicon microstructures," *Biomaterials*, vol. 31, pp. 4552-4561, Jun 2010.

[2] M. R. K. Mofrad and R. D. Kamm, *Cytoskeletal Mechanics: Models and Measurements*. New York: Cambridge University Press, 2006.

[3] L. G. Alexopoulos, *et al.*, "The biomechanical role of the chondrocyte pericellular matrix in articular cartilage," *Acta Biomaterialia*, vol. 1, pp. 317-325, May 2005.

[4] K. M. K. Rao and H. J. Cohen, "Actin cytoskeletal network in aging and cancer," *Mutation Research*, vol. 256, pp. 139-148, Mar-Nov 1991.

[5] O. Thoumine and A. Ott, "Comparison of the mechanical properties of normal and transformed fibroblasts," *Biorheology*, vol. 34, pp. 309-326, Jul-Oct 1997.

[6] G. Bao and S. Suresh, "Cell and molecular mechanics of biological materials," *Nature Materials,* vol. 2, pp. 715-725, Nov 2003.

[7] T. Wakatsuki, *et al.*, "Cell mechanics studied by a reconstituted model tissue," *Biophysical Journal,* vol. 79, pp. 2353-2368, Nov 2000.

[8] S. Suresh, "Biomechanics and biophysics of cancer cells," *Acta Biomaterialia,* vol. 3, pp. 413-438, Jul 2007.

[9] M. M. Stevens and J. H. George, "Exploring and engineering the cell surface interface," *Science,* vol. 310, pp. 1135-1138, Nov 2005.

[10] R. Timpl, "Macromolecular organization of basement membranes," *Current Opinion in Cell Biology,* vol. 8, pp. 618-624, Oct 1996.

[11] A. Mata, *et al.*, "Analysis of connective tissue progenitor cell behavior on polydimethylsiloxane smooth and channel micro-textures," *Biomedical Microdevices,* vol. 4, pp. 267-275, Dec 2002.

[12] E. K. F. Yim, *et al.*, "Nanopattern-induced changes in morphology and motility of smooth muscle cells," *Biomaterials,* vol. 26, pp. 5405-5413, Sep 2005.

[13] J. Y. Mai, *et al.*, "A microfabricated platform probing cytoskeleton dynamics using multidirectional topographical cues," *Biomedical Microdevices,* vol. 9, pp. 523-531, Aug 2007.

[14] J. L. Tan, *et al.*, "Cells lying on a bed of microneedles: An approach to isolate mechanical force," *Proceedings of the National Academy of Sciences of the United States of America,* vol. 100, pp. 1484-1489, Feb 2003.

[15] X. F. Walboomers, *et al.*, "Contact guidance of rat fibroblasts on various implant materials," *Journal of Biomedical Materials Research,* vol. 47, pp. 204-212, Nov 1999.

[16] X. F. Walboomers, *et al.*, "Attachment of fibroblasts on smooth and microgrooved polystyrene," *Journal of Biomedical Materials Research,* vol. 46, pp. 212-220, Aug 1999.

[17] P. Clark, *et al.*, "Cell Guidance by Ultrafine Topography Invitro," *Journal of Cell Science,* vol. 99, pp. 73-77, May 1991.

[18] J. L. Charest, *et al.*, "Myoblast alignment and differentiation on cell culture substrates with microscale topography and model chemistries," *Biomaterials,* vol. 28, pp. 2202-2210, Apr 2007.

[19] J. L. Charest, *et al.*, "Combined microscale mechanical topography and chemical patterns on polymer cell culture substrates," *Biomaterials,* vol. 27, pp. 2487-2494, Apr 2006.

[20] W. B. Tsai, *et al.*, "Fibronectin modulates the morphology of osteoblast-like cells (MG-63) on nano-grooved substrates," *Journal of Materials Science-Materials in Medicine,* vol. 20, pp. 1367-1378, Jun 2009.

[21] W. B. Tsai and J. H. Lin, "Modulation of morphology and functions of human hepatoblastoma cells by nano-grooved substrata," *Acta Biomaterialia,* vol. 5, pp. 1442-1454, Jun 2009.

[22] M. J. Dalby, *et al.*, "Nucleus alignment and cell signaling in fibroblasts: response to a micro-grooved topography," *Experimental Cell Research,* vol. 284, pp. 274-282, Apr 2003.

[23] C. M. Hwang, *et al.*, "Controlled cellular orientation on PLGA microfibers with defined diameters," *Biomedical Microdevices,* vol. 11, pp. 739-746, Aug 2009.

[24] A. Abbott, "Cell culture: Biology's new dimension," *Nature,* vol. 424, pp. 870-872, Aug 2003.

[25] D. R. Albrecht, *et al.*, "Probing the role of multicellular organization in three-dimensional microenvironments," *Nature Methods,* vol. 3, pp. 369-375, May 2006.

[26] M. Nikkhah, *et al.*, "Cytoskeletal role in differential adhesion patterns of normal fibroblasts and breast cancer cells inside silicon microenvironments," *Biomedical Microdevices,* vol. 11, pp. 585-595, Jun 2009.

[27] M. Nikkhah, *et al.*, "Attachment and response of human fibroblast and breast cancer cells to three dimensional silicon microstructures of different geometries," *Biomedical Microdevices,* vol. 11, pp. 429-441, Apr 2009.

[28] P. P. Rosen, *et al.*, *Breast pathology: diagnosis by needle core biopsy,* 2nd ed.: Lippincott Williams & Wilkins, 2005.

[29] R. Kalluri and M. Zeisberg, "Fibroblasts in cancer," *Nature Reviews Cancer,* vol. 6, pp. 392-401, May 2006.

[30] C. Jedeszko, *et al.*, "Fibroblast Hepatocyte Growth Factor Promotes Invasion of Human Mammary Ductal Carcinoma In situ," *Cancer Research,* vol. 69, pp. 9148-9155, Dec 2009.

[31] S. Rhee, *et al.*, "Microtubule function in fibroblast spreading is modulated according to the tension state of cell-matrix interactions," *Proceedings of the National Academy of Sciences of the United States of America,* vol. 104, pp. 5425-5430, Mar 2007.

[32] C. T. Brew, *et al.*, "Indole-3-carbinol inhibits MDA-MB-231 breast cancer cell motility and induces stress fibers and focal adhesion formation by activation of Rho kinase activity," *International Journal of Cancer,* vol. 124, pp. 2294-2302, May 2009.

[33] M. Swierczewska, *et al.*, "Cellular response to nanoscale elastin-like polypeptide polyelectrolyte multilayers," *Acta Biomaterialia,* vol. 4, pp. 827-837, Jul 2008.

[34] H. Hertz, "On the elastic contact of elastic solids," *J. Reine Angew. Math,* vol. 92, pp. 156–171, 1881.

[35] S. P. Timoshenko and J. N. Goodier, "Theory of Elasticity ", 3rd ed. New York: McGraw-Hill Companies, 1970.

[36] S. L. Guo and B. B. Akhremitchev, "Packing density and structural heterogeneity of insulin amyloid fibrils measured by AFM nanoindentation," *Biomacromolecules,* vol. 7, pp. 1630-1636, May 2006.

[37] K. D. Costa, "Single-cell elastography: Probing for disease with the atomic force microscope," *Disease Markers,* vol. 19, pp. 139-154, 2004.

[38] T. P. Stossel, "Contribution of actin to the structure of the cytoplasmic matrix," *Journal of Cell Biology,* vol. 99, pp. S15-S21, 1984.

[39] R. Ananthakrishnan, *et al.*, "Quantifying the contribution of actin networks to the elastic strength of fibroblasts," *Journal of Theoretical Biology,* vol. 242, pp. 502-516, Sep 2006.

[40] M. R. King, *Principles of cellular engineering: understanding the biomolecular interface*. Burlington: Elsevier Academic Press, 2005.

[41] N. Wang, *et al.*, "Cell prestress. I. Stiffness and prestress are closely associated in adherent contractile cells," *American Journal of Physiology. Cell Physiology,* vol. 282, pp. C606-C616, Mar 2002.

[42] Y. C. Kim, *et al.*, "Biomechanical analysis of cancerous and normal cells based on bulge generation in a microfluidic device," *Analyst,* vol. 133, pp. 1432-1439, 2008.

[43] Q. S. Li, *et al.*, "AFM indentation study of breast cancer cells," *Biochemical and Biophysical Research Communications,* vol. 374, pp. 609-613, Oct 2008.

[44] H. W. Hou, *et al.*, "Deformability study of breast cancer cells using microfluidics," *Biomedical Microdevices,* vol. 11, pp. 557-564, Jun 2009.

[45] S. E. Cross, *et al.*, "AFM-based analysis of human metastatic cancer cells," *Nanotechnology,* vol. 19, Sep 2008.

[46] S. E. Cross, *et al.*, "Nanomechanical analysis of cells from cancer patients," *Nature Nanotechnology,* vol. 2, pp. 780-783, Dec 2007.

[47] J. Guck, *et al.*, "Optical deformability as an inherent cell marker for testing malignant transformation and metastatic competence," *Biophysical Journal,* vol. 88, pp. 3689-3698, May 2005.

[48] X. D. Ren, *et al.*, "Regulation of the small GTP-binding protein Rho by cell adhesion and the cytoskeleton," *Embo Journal,* vol. 18, pp. 578-585, Feb 1999.

[49] M. ChrzanowskaWodnicka and K. Burridge, "Rho-stimulated contractility drives the formation of stress fibers and focal adhesions," *Journal of Cell Biology,* vol. 133, pp. 1403-1415, Jun 1996.

[50] S. Rhee and F. Grinnell, "Fibroblast mechanics in 3D collagen matrices," *Advanced Drug Delivery Reviews,* vol. 59, pp. 1299-1305, Nov 2007.

[51] J. J. Tomasek and E. D. Hay, "Analysis of the role of microfilaments and microtubules in acquisition of bipolarity and elongation of fibroblasts in hydrated collagen gels," *Journal of Cell Biology,* vol. 99, pp. 536-549, 1984.

5 Chapter Five: Actions of the Anti-Cancer Drug Suberoylanilide Hydroxamic Acid (SAHA) on Human Breast Cancer Cytoarchitecture in Silicon Microstructures

J. S. Strobl, M. Nikkhah*, and M. Agah., "Actions of the Anti-Cancer Drug Suberoylanilide Hydroxamic Acid (SAHA) on Human Breast Cancer Cytoarchitecture in Silicon Microstructures", Biomaterials, vol. 31, pp. 7043-7050, Sep 2010, * Equal Contribution.*

5.1 Introduction

Applications of micro and nanotechnology in cancer research aim to improve detection, diagnosis and treatment of this devastating disease. Research topics range from nanoparticle-based therapeutics and imaging, robotic-based tumor detection, to the design of microdevices to perform fundamental studies of tumor cell biology [2]. In this regard, a number of laboratories including our own are engaged in the fabrication of microdevices to analyze human mammary cancer cell biology [3-7] and drug sensitivity [8].

A large body of work has established that the material composition of microdevices merits careful consideration because the cell-substrate plays an important role in the behavior of mammary cells [9-12]. For example, implantation of cells into soft microenvironments composed of extracellular matrix protein gels most closely simulates an *in vivo* condition, and in these three-dimensional (3-D) cultures, normal mammary cells adopt spherical and duct-like structures while transformed cells express a less malignant phenotype [13]. In comparison, mammary cell growth in traditional two-dimensional (2-D) cell culture on stiff surfaces such as plastic or glass promotes formation of focal adhesion complexes, cell spreading and cell motility [12]. The effect of modulating the surface stiffness and integrin binding sites on mammary cells grown in 2-D cell culture systems has also been investigated using uniformly protein coated surfaces, micro-patterning of peptides, floating collagen gels, polyacrylamide gels of varying cross-linking density, and PDMS [12, 14, 15]. Collectively, these investigations confirm the exquisite sensitivity of mammary cells to the nature of their contacts with the growth surface.

Silicon is a stiff material suitable for adhesion of mammary cells [3, 6, 7]. Furthermore silicon microdevices can be fabricated with growth surfaces containing a wide-variety of precise arrayed features including arrays of microgrooves [16] and pillars and wells [17]. We previously reported development of 3-D silicon microstructures using a single mask, single etch step fabrication process [3, 6, 7] (Chapters 2, 3 and 4); the fabrication method relies on the application of reactive ion etching (RIE) lag to etch silicon to different depths to create precise isotropic topographical patterns with features ranging in size from 10-200 µm. These structures impose upon cells a variety of topological challenges to adhesion, spreading, and cell motility.

In this work, we used the MDA-MB-231 cell culture model of highly metastatic human breast cancer [18] which is also representative of "triple-negative" breast tumors which are refractory to many standard cancer therapies [19]. The effect of SAHA, a new anti-cancer drug also known as Vorinostat, on cell attachment to flat silicon substrates and to 3-D silicon microarrays was investigated. SAHA is the first drug of its type to receive FDA approval for clinical use and represents a class of agents of increasing therapeutic importance [20, 21]. Unlike many conventional cytotoxic chemotherapy agents which target DNA to kill cancer cells, SAHA inhibits a family of enzymes referred to as "histone deacetylases" (HDAC). The HDAC enzymes are known to increase levels of acetylation of many proteins, and in particular, HDAC6 targets beta-actin, alpha- and beta-tubulin and additional actin-binding proteins comprising the cytoskeleton [22-24] . Our work is the first to address the use of microdevices to study this emerging class of anti-cancer agents.

5.2 Materials and methods

5.2.1 Silicon device fabrication

The fabrication process of 3-D microstructures is similar to our previous work [3, 6] which relies on the applicability of RIE lag and its dependence on geometrical patterns of the photomask layout to etch silicon to different depths [3, 7]. Briefly, the etching process starts by depositing of plasma enhanced chemical vapor deposition (PECVD) oxide layer on a silicon wafer. After patterning with S1813 photoresist, the oxide layer is etched using deep reactive ion etching (DRIE) process. After oxide etching, silicon is etched using DRIE SF_6 plasma to form

arrays composed of star- and circular-shaped microchambers. After removal of photoresist and oxide layer, the wafer is diced into 1 cm^2 chips. Figure 5-1 shows the photo image of the fabricated devices and the SEM images of the resulting microstructures. The dimensions of the etched cavities vary between 60-70 µm in depth and between 150-170 µm in diameter. These cavities contain internal microstructures consisting of either 1) circular-shaped microchambers with smooth side walls and concentric circular rings deep within the cavity or 2) star-shaped microchambers having scalloped edges that process into the depth of the cavity as shallow tracts the chips were sterilized in 95% ethanol then air-dried prior to use in cell culture.

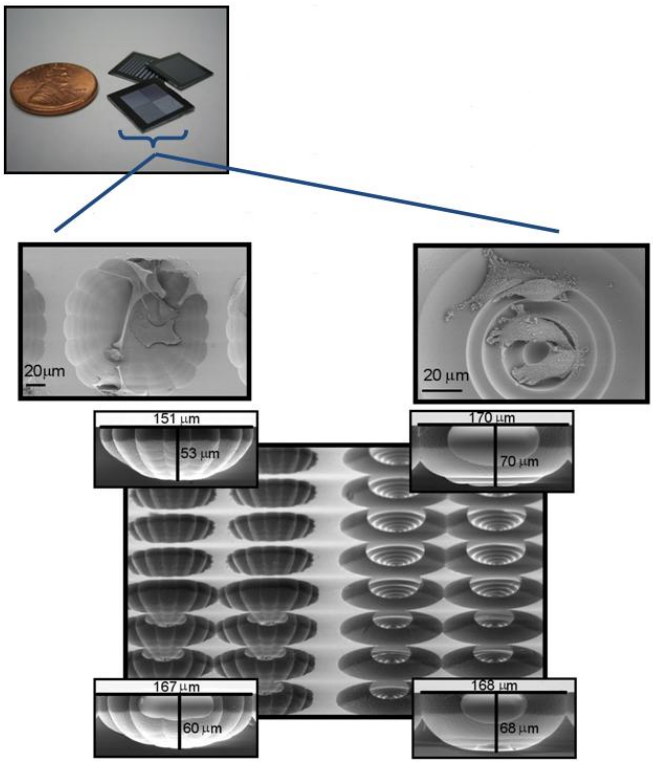

Figure 5-1 Photo image of the fabricated devices in silicon and SEM images of the three dimensional (3-D) silicon substrates as cell culture Substrates comprising star and circular-shaped microchambers with the corresponding top view images.

5.2.2 Cell culture

The well-established cell culture model of invasive human breast cancer, MDA-MB-231 [25], originally isolated from the pleural effusion of a patient with metastatic disease was purchased from the American Type Culture Collection (Manassas, Virginia). Cells were maintained in plastic T-75 cm^2 culture flasks in a humidified incubator at 37^oC. MDA-MB-231 cells were

propagated in RPMI culture medium containing 5% fetal bovine serum (FBS, Atlanta Biologicals,Atlanta, Georgia), 4 mM glutamine, 1 mM sodium pyruvate, and penicillin-streptomycin (100 Units/ml). For adhesion analysis the cells were grown on silicon chips for 48 h at 37°C in humidified 7% CO_2-93% air atmosphere after plating at a density of 1.1×10^4cells/mm^2.

For experiments involving SAHA, 5 x 10^4 MDA-MB-231 cells were plated into 12-well multi-well dishes containing 3 mL of culture medium supplemented with 10% FBS and a single 1 cm^2 silicon chip. Cells were incubated for 24 h after plating to allow cells to attach to the substrate and adapt to the fresh medium;then SAHA (1.5 µl) was added directly into the culture medium to a final concentration of 3 µM SAHA in 0.05% DMSO using a 2000x stock solution of SAHA dissolved in 100% DMSO. After exposing cells to SAHA for 24 h, cells were processed for imaging.

5.2.3 Immunohistochemistry

Cells grown on silicon were washed in Hank's balanced salt solution (HBSS), then fixed with 3% paraformaldehyde (PF) in 250mM Tris, pH 7.2 for 10 minutes followed by 6% PF- 0.25% Triton X-100 in PBS for 10 minutes. Cells were washed free of the PF, then vinculin, filamentous (F-) actin, and cell nuclei were stained at room temperature as follows. Cells were incubated for 30 minutes with mouse monoclonal anti-vinculin (1:100 in 2% chicken serum albumin-PBS, Abcam, Cambridge, MA), then with rhodamine-tagged goat anti-mouse IgG (1:300 in 2% chicken serum albumin-PBS, Invitrogen, Carlsbad, CA) for 30 minutes. Next, cells were incubated for 15 minutes with AlexaFluor488-phalloidin (10U/ml in 140 mM NaCl-6% bovine serum albumin in 40 mM Tris, pH 7.2, Invitrogen), and Hoeschst33342 (Invitrogen,30 µg/ml) was added for 5 minutes. Cells were washed with three exchanges of PBS between each step. The silicon chips were mounted on glass coverslips using ProLong Gold antifade (Invitrogen) and air-dried overnight prior to imaging using confocal microscopy (ZEISS-LSM-510 META) in the reflection mode.

To stain microtubules, the procedures were as described above except a 20 minute incubation with mouse monoclonal anti-β-Tubulin I+II antibody (1:1000 in 2% chicken serum albumin in PBS, Sigma) followed by a 20 minute incubation with the rhodamine-tagged goat anti-mouse

IgG were used. Images of the microtubules were obtained using fluorescence microcopy with a Nikon Eclipse 80i instrument.

5.2.4 Scanning electron microscopy (SEM)

The cells were fixed in 3.7% formaldehyde in PBS for 10 minutes 48 h after plating, critical-point-dried and sputter-coated with a thin layer of gold palladium. SEM images were obtained using a Leo ZEISS 1550 instrument.

5.2.5 Atomic force microscopy (AFM)

Cells (3×10/ml) were grown on type IV Collagen-coated 25 mm round glass coverslips in 35 mm^2 dishes in RPMI culture medium supplemented with 10% FBS for 24-48 h. Immediately prior to the experiments, 20 mM HEPES buffer was added to the culture medium to maintain pH 7.2. Atomic force microscopy instrumentation MFP-3D-Bio (Asylum Research Corporation, Santa Barbara, CA) was used for the force measurement. The AFM was combined with an inverted optical and fluorescence microscope for precise positioning of the AFM cantilever tip over the center of the cell nucleus and cell visualization while force was applied. Soft V-shaped silicon nitride cantilevers, TR400PSA (Olympus), with the nominal length of 200µm and a spring constant of 0.02 N/m was used for force measurement at the tip velocity of 0.5µm/s. A ~10µm glass bead (Duke Scientific) was attached to the cantilever tip to reduce any nonlinearity in deforming stress and to minimize cell damage. All measurements were carried out using a standard fluid cell (Asylum Research) at room temperature.

The Young's modulus of individual cells was computed as detailed previously [7] by using the Hertz's model where, the relationship between the applied force, F, and the indentation depth, δ, can be expressed as:

$$F = \frac{4\sqrt{R}}{3(1-\nu^2)} E\delta^{3/2} \qquad (5\text{-}1)$$

R is the radius of the tip, and E and ν are the Young's modulus and Poisson's ratio of the indented cell, respectively. The Poisson's ratio, ν, is assumed to be 0.5 in accordance with the incompressibility assumption usually employed for cells and soft tissues. We used the linear

version in δ of the Hertz's model to define the elasticity and initial contact point with the cell. This model leads to equation (5-2).

$$F^{2/3} = \left[\frac{4\sqrt{R}}{3(1-\nu^2)}E\right]^{2/3}(z-d) - \left[\frac{4\sqrt{R}}{3(1-\nu^2)}E\right]^{2/3}(z_0 - d_0) \qquad (5\text{-}2)$$

Equation (5-2) can be evaluated as the equation of a line in the plane $(F^{2/3}, z-d)$. The Young's modulus and initial contact point can be calculated from the linear slope of $F^{2/3}$ and the intercept of equation (5-2) [7]. All the data analysis and curve fitting of the Hertz's model to the collected force-indentation data were performed using MATLAB 7.0 software (MathWorks).

5.2.6 Data analysis

Cell and nuclear areas were measured using the National Institutes of Health (NIH) ImageJ (v. 1.41) software. Statistical analyses (two-tailed t-test or analysis of variance and appropriate post-hoc t-tests) were performed using GraphPad Prism 5.02 software (La Jolla,CA).

5.3 Results

For the first set of experiments, we analyzed the morphology and cytoskeletal organization of the cells attached on flat silicon surfaces in both control conditions and after treatment with SAHA using fluorescent microscopy. The morphology and cytoskeleton in control and SAHA-treated MDA-MB-231 cells attached to flat silicon is compared in Figure 5-2. Control MDA-MB-231 cells (Figure 5-2(a)) were well-separated. F-actin filament structures (green color) and focal adhesions marked by discrete dots of vinculin (red color) or co-localized actin and vinculin dots (yellow color) were seen along the outer cell margins. Vinculin links the actin cytoskeleton to integrins through focal adhesion complexes [26], and vinculin-staining is useful in identifying focal adhesion sites. The orientation of the focal adhesions within these cells as well as the presence of prominent actin-rich lamellipodia including many with clearly defined leading edge morphology were indicative of cell motility on silicon. Vinculin staining was also evident throughout the cytoplasm where is known to play a role in cell spreading through its actin contacts [27]. Negative controls for vinculin staining using the rhodamine-conjugated secondary antibody alone were performed and confirmed the specificity of this staining (data not shown).

The microtubule structures (red color) in control MDA-MB-231 cells are illustrated in Figure 5-2(d).

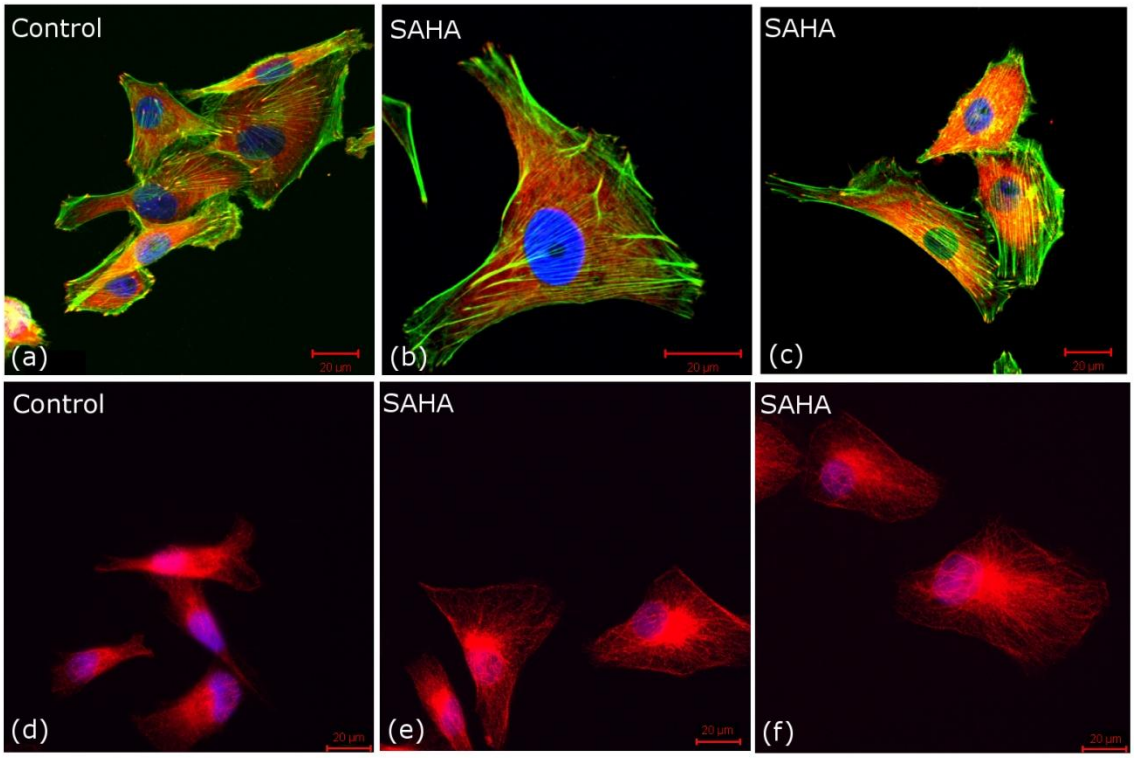

Figure 5-2 Cytoarchitecture of cells attached to silicon. Confocal microscope images of MDA-MB-231 cells showing F-actin (green color), vinculin (red) and cell nuclei (blue) (a,b,c) or fluorescent microscope images of MDA-MB-231 cells showing microtubules (red) and cell nuclei (blue) (d,e,f). Control cells no additions, 24 h) appear in a and d; SAHA (3μM, 24 h) treated cells appear in b,c,e,f.

The functional consequences of SAHA's actions with respect to cytoskeleton remodeling have not been intensively investigated previously. In MDA-MB-231 cells, SAHA appeared to increase cell spreading on silicon (Figure 5-2(b-f)). MDA-MB-231 cells adopted a more angular shape and exhibited thicker actin filaments along the cell periphery (Figure 5-2(b)); both of these morphologies have been associated with decreased motility and stronger cell-substrate attachment in this cell line [28]. SAHA-treated cells exhibited striking alterations in the microtubules. These cells exhibited very prominent microtubule organizing centers adjacent to the cell nuclei and an elaborate extension of the microtubule networks from this site (Figure 5-2(e,f)). A number of morphometric analyses were performed to quantify SAHA's effects upon the cytoskeleton of MDA-MB-231 cells attached to flat silicon chips.

As summarized in Table 5-1, SAHA-treated cells displayed a significant increase in cell area, length, and nuclear area. The mean cell area of MDA-MB-231 cells after 24 h in SAHA was 1.8-fold greater ($p<0.001$) than the control MDA-MB-231 cells. The corresponding increased in cell length and nuclear area were determined to be 1.3-fold (Table 5-1). From these measurements, the ratio of the nuclear/cytoplasmic area (N/C) in control and SAHA-treated cells was calculated to be 0.16 and 0.11, respectively. Thus, SAHA decreased N/C by 1.5-fold in MDA-MB-231 cells adherent to silicon. The significance of this result is that a high N/C is a widely accepted pathological marker of highly aggressive breast tumors [29]. We next evaluated the role of cytoskeletal proteins, F-actin and microtubules, in the cellular response to SAHA. The F-actin profile over the nucleus in MDA-MB-231 cells was quantified where the fluorescent signals were not saturated. Based upon the average intensity of the AlexaFluor488-phalloidin signal measured in the nuclear area and by the number of F-actin fibers that traversed the nuclei, SAHA had no significant effect on nuclear F-actin levels or F-actin fiber density (Table 5-2). A frequency distribution analysis of F-actin staining intensity confirmed there was no difference in nuclear F-actin content between control and SAHA-treated cell populations (Figure 5-3). In contrast, SAHA had a significant impact upon the expansion of the microtubule network which was quantified by measuring the area enclosed by the outer margins of the microtubule staining (Table 5-2, Figure 5-2(d-f)). Our results are consistent with the model of cell spreading proposed by Maurin et al. [30] and suggest that elongation of the microtubule filaments in response to SAHA exerts a significant influence upon cell area and attachment to silicon.

Table 5-1 Morphometric Analyses of MDA-MB-231 Cells on Flat Silicon

	Cell area (μm^2)	Nuclear area (μm^2)	Cytoplasm area (μm^2)	Nuclear to Cytoplasmic area (μm^2)	Cell length (μm)
Control n = 49	1066 ± 589	147 ± 72	919	0.16	65 ± 20
SAHA n = 25	1920 ± 795***	189 ± 57*	1731	0.11	83 ± 20***

Data shown are the mean ± S.D. of n number of fluorescent confocal cell images collected in three independent experiments. Statistically significant effects of SAHA are indicated: * $p<0.01$; ***$p<0.0001$.

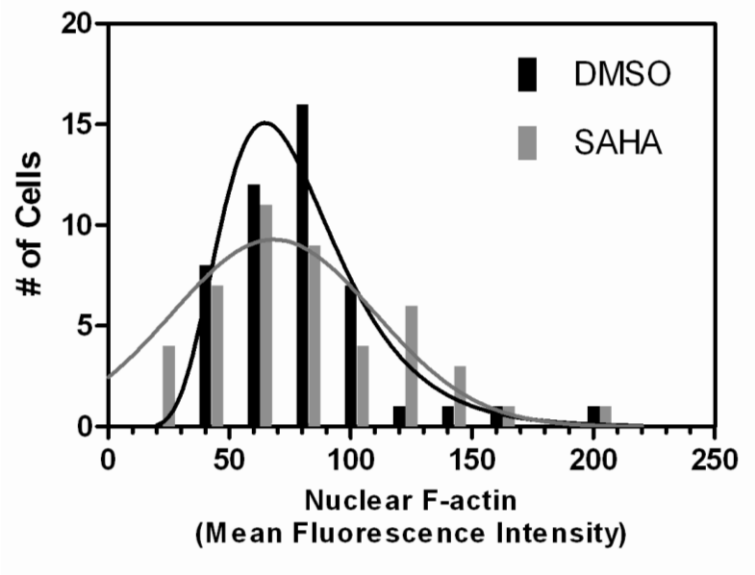

Figure 5-3 F-Actin response to SAHA in MDA-MB-231 cells. Frequency distribution of the mean fluorescent intensity of the F-actin-AlexaFluor488-phalloidin signal over the nuclear area determined using ImageJ Software in n= 47 control and n= 47 SAHA -treated cells. Data shown are mean ± S.E. determined in two independent experiments.

Table 5-2 F-Actin and Tubulin Analyses

	F-Actin Fluorescence Intensity (nuclear)	#F-Actin Fiber/Nucleus	Nuclear area (μm^2)	#F-Actin Fiber Density (nuclear)	Microtubule Network Area (μm)
Control	78 ± 31, n=47	9 ± 4, n=31	147	6.0×10^{-2} / μm^2	536 ± 44 n=40
SAHA	78 ± 40, n=47	11 ± 5, n=33	189	5.7×10^{-2} / μm^2	1047 ± 103*** n=41

Data shown are the mean ± S.D. in n number of fluorescent cells imaged by confocal microscopy (F-actin) or standard fluorescent microscopy (tubulin). Statistically significant effects of SAHA are indicated: ***$p<0.001$.

To investigate whether the cytoskeletal stiffness was affected by SAHA treatment, the Young's modulus of the cells was measured using AFM and Hertz's model (Figure 5-4(a)). The population elasticity (Young's modulus, E) of the cells in both control condition as well as after treatment with SAHA were not normally distributed according to Shapiro-Wilks test and was

best described by log-normal distributions (Figure 5-4(b)). The peak modulus of the cells in control condition was located at 0.2 kPa whereas the peak modulus after treatment with SAHA slightly increased to 0.24 kPa. The collected AFM data yielded an average E value (mean±S.D.) of 0.51±0.35 (kPa) (n=47) for the cells in control condition and 0.49±0.34 (kPa) (n=170) for the cells after treatment with SAHA. The AFM data suggested that the alteration in the Young's modulus of the cells after treatment with SAHA was not statistically significant compared to the control condition.

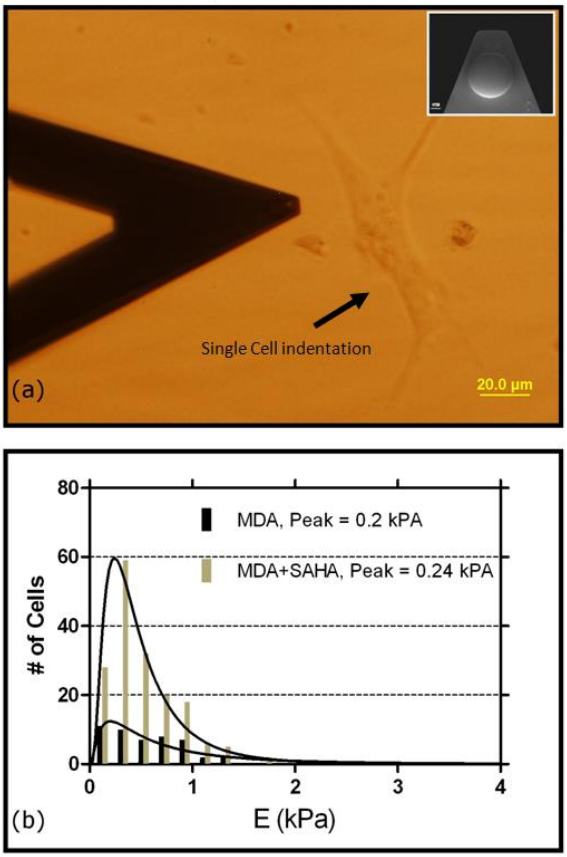

Figure 5-4 (a) Single cell indentation using AFM. Top right inset shows the SEM image of a glass sphere with a diameter of ~ 10 µm attached to the cantilever tip. (b) Young's modulus distribution of the MDA-MB-231 in control condition and after treatment with SAHA. Population elasticity of the cells in both conditions was best fit by log-normal distributions.

After investigating the cytoskeletal organization of the cells attached on flat silicon surfaces, we assessed the adhesion behavior and cytoskeletal organization of the cells attached inside the 3-D etched cavities. The 3-D silicon microstructures (Figure 5-1) present a variety of topological domains to challenge cell attachment and were used to experimentally probe whether SAHA-

mediated changes in the cytoskeleton would affect the mode of MDA-MB-231 cell attachment within such microstructures. Cells were cultured for 24h in standard culture medium, then test agents were added for the final 24 h. Scanning electron micrographs of cell attachment are shown in Figure 5-5.

Control MDA-MB-231 cells in the circular-shaped microchambers attached to the smooth side-walls or adopted their shapes to mold within the concentric ring structures (Figure 5-5(a)). SAHA altered the way cells attached within these microstructures (Figure 5-5(c)). Now, the cell extensions stretched the cells beyond the interior dimensions of the rings, and cell attachments to the side-walls raised the cells above the substrate.

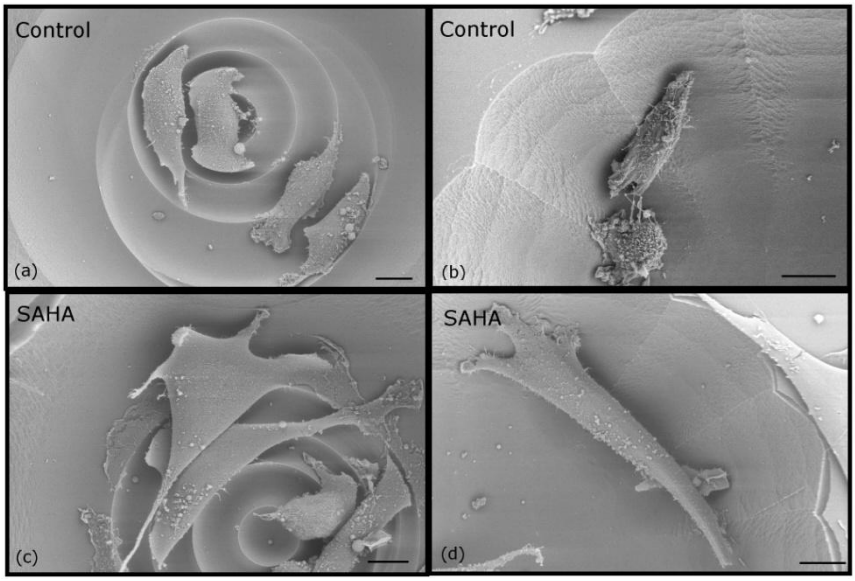

Figure 5-5 Cell adhesion response to SAHA in 3-D Silicon Microarrays. SEM images of MDA-MB-231 grown on the microarrays: Control cells (a,b), SAHA (3 µM, 24 h (c,d) Circular microstructures (a,c); star microstructures (b,d). Scale bars represent 10 µm.

Figure 5-5(b) shows that control cells adhered to the side-walls of the star microstructures without obvious orientation to the trace edges, and displayed a relaxed cell morphology. The attachment of cells exposed to SAHA was similar to that seen in the circular microstructures where cell extensions and cell spreading raised the cells above the surface of the microstructures such that cells became suspended within the microcavities (Figure 5-5(d)). The significance of this response to SAHA is the ability to incorporate biosensors within the microstructures to monitor reorganization of cell surface attachments in real-time and eliminate the requirement for cell imaging analyses.

Table 5-3 Morphometric Analyses of MDA-MB-231 Cells in Silicon Microstructures

	Circular Microstructures		Star Microstructures	
	Cell length (μm)	Cell area (μm^2)	Cell length (μm)	Cell area (μm^2)
Control	39 ± 10 (31)	292 ±107 (31)	29 ± 7 (10)	279 ± 111 (17)
SAHA	69 ± 27 (23) ***	770 ± 255 (23) ***	69 ± 13 (4) ***	890 ± 164 (4) ***

Data shown are the mean ± S.D. The number of cells analyzed for each determination is shown in parentheses. Statistically significant effects of SAHA are indicated: *** $p<0.0001$.

The adhesion of MDA-MB-231 in the microstructures contrasts with that of non-invasive MCF10A human breast cells which maintain a planar cell shape and tend to form cell sheets without regard to the microstructures [7]. The contrasting morphology of these two cell lines representing invasive and non-invasive cells within etched microstructures might reflect underlying differences in cytoarchitecture that exist in differing states of breast pathology.

Table 5-3 summarizes the morphometric analyses of the MDA-MB-231 cells attached within the circular and star microstructures performed using SEM cell images. In these experiments SAHA significantly increased both the length and the area of cells adherent within the microstructures. For example, analysis of SEM images showed the mean cell area of control cells attached to flat silicon was 474 μm^2 (S.D. = 169, n=20 cells) as compared with 292 μm^2 and 279 μm^2 in the circular and star microstructures, respectively (Table 5-3). Similarly, the mean area of cells on flat silicon after SAHA was increased to 1631 μm^2 (S.D. = 757, n=21 cells) as compared to 770 μm^2 and 890 μm^2, respectively, in the circular and star microstructures (Table 5-3). The smaller cell area of cells adhered to silicon within the microstructures is evidence that the configuration of the microstructures poses a challenge to cell spreading. The actions of SAHA serve to enhance cell spreading and overcome the obstacles posed by the microstructures.

A comparison of the results in Table 5-2 and Table 5-3 also indicates that cell measurements as expressed as μm or μm^2 differ. A likely explanation for this is that the fixation processes affect cell size as reported by others [31]. The cell measurements from the SEM images in Table 5-3 are in good agreement with our previously data of cell lengths from SEM [3] and from

confocal images [7]. In addition, by comparing the cell area of identical cells in silicon microstructures after SEM processing or confocal image processing, we confirmed that cell areas are approximately 1.5-fold larger after the confocal processing (data not shown).

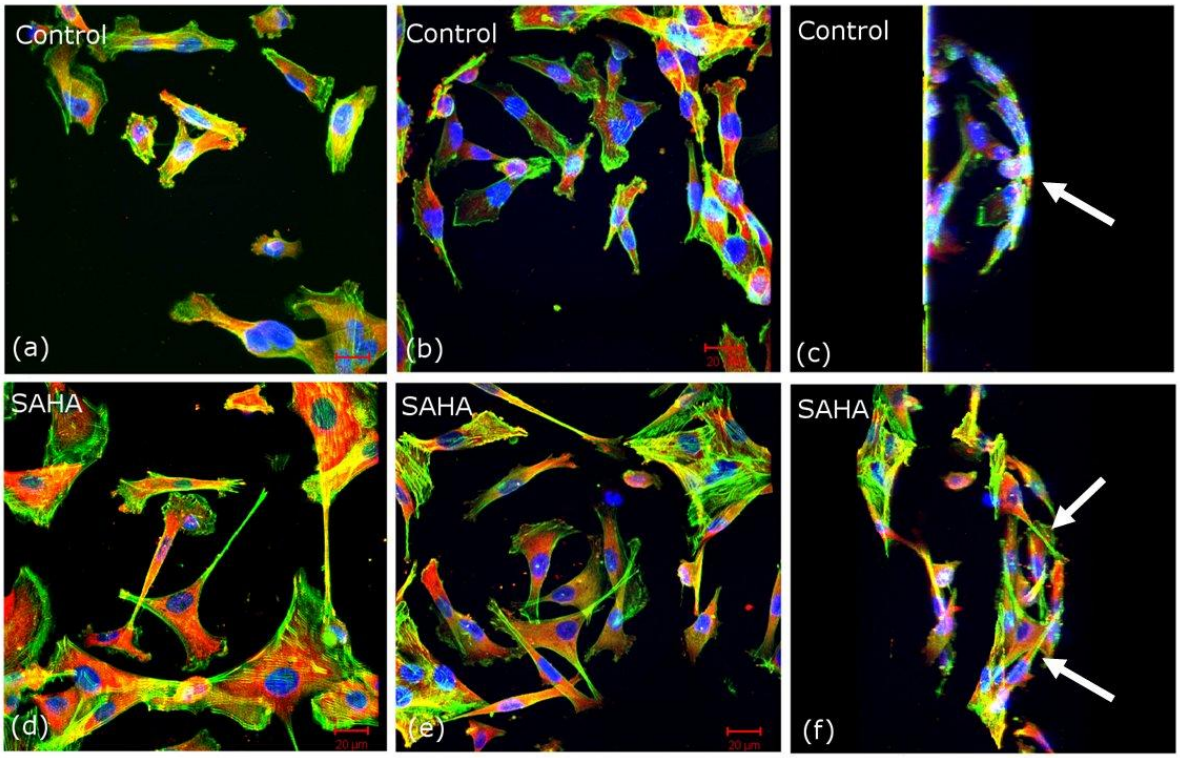

Figure 5-6 Confocal images actin and vinculin cytoarchitecture inside the 3-D silicon microarrays. Actin cytoskeleton is stained in green and vinculin is stained in red. Images (a,b,c) show the control cell in star microstructures; (c) is the rotated image of (b).Images (d,e,f) show the cells after treatment with SAHA (3 µM); (d) is the star microstructure, (e) is the circular microstructure, and (f) is the rotated image of (e). Scale bars represent 20 µm.

Cell adherence to the 3-D silicon microstructures was also examined using confocal microscopy to visualize fluorescently stained nuclei, actin, and vinculin (Figure 5-6). (a,b) show top views of control cells in the microstructures, and Figure 5-6(c) is a side-view of control cells in the microstructures. In comparison, Figure 5-6(d) and 6e are top views of SAHA-treated cells and Figure 5-6(f) is a side-view of SAHA-treated cells. The side-views in Figure 5-6(c,f) are shown in 3-D rotation videos. The SAHA-treated cells retained their larger cell area and reduced N/C within the microstructures. In contrast with control cells, F-actin is prominent in the cytoplasm and frequently appeared as green fibers traversing the cell or alternatively, as yellow fibers indicative of co-localized actin and vinculin in the SAHA-treated cells. F-actin-rich

extensions were typical of SAHA treated cells and the white arrows in Figure 5-6(f) indicate how these actin-rich extensions were able to lift the cells above the etched features within the microstructures. This behavior was absent in control cells where cells can be seen adhering smoothly to the surface of the microstructure (Figure 5-6(c), white arrow). These results show that reorganization of the actin cytoskeleton in response to SAHA alters the attachment of MDA-MB-231 cells in 3-D silicon microstructures[†].

5.4 Discussion

Early diagnosis and interventions are successful for many women with breast cancer but when metastatic disease develops it is usually fatal [19, 32, 33]. Metastatic cancer cells acquire sets of capabilities that confer motility and invasiveness including specialized invadopodia structures and matrix degrading proteins, as well as abilities to survive and proliferate in non-breast settings including successful angiogenesis [34, 35]. Finding new treatments for metastatic breast cancer remains a major research challenge.

The MDA-MB-231 human breast cancer cell line is a well-studied model of human metastatic breast cancer. MDA-MB-231 cells show motility in cell migration assays in cell culture; these cells are invasive in matrigel assays and produce proteins involved in matrix degradation [18]. Work in many laboratories has shown how MDA-MB-231 cells colonize and propagate in non-mammary tissues in rodent models [36]. MDA-MB-231 cells show gene expression signatures characteristic of cells after an epithelial-mesenchymal transition, and cells typically lose E-cadherin and cell-cell junctions, up-regulate intermediate filaments such as vimentin, and become more invasive [37].

Cell motility is one hallmark of metastatic cancer cells involving the coordinated actions of actin and other cytoskeleton proteins, and investigation of the relationships between cytoarchitecture and cell migration has moved to the forefront of research in the pathobiology of cancer metastasis [34, 35, 38].

[†] Supplementary movies associated with this chapter can be found at [1] J. S. Strobl, *et al.*, "Actions of the anti-cancer drug suberoylanilide hydroxamic acid (SAHA) on human breast cancer cytoarchitecture in silicon microstructures," *Biomaterials*, vol. 31, pp. 7043-7050, Sep 2010.

SAHA is the first clinically-approved anti-cancer drug of an increasingly important group of compounds which were first identified as histone deacetylase inhibitors [20, 21]. Although histone proteins are clearly an important drug target, SAHA was also shown to increase acetylation of the cytoskeletal proteins beta-actin, cortactin, alpha-4-actinin, and alpha- and beta-tubulin in MDA-MB-231 cells [23]. The ways protein acetylation regulates cytoskeleton reorganization in breast cancer are just beginning to be understood. The F-actin binding protein, cortactin, is involved in cell adhesion, migration, and invasion [39]. Cortactin acts by tethering F-actin to membrane sites and facilitating the formation of actin-rich lamellipodia and invadapodia. However upon acetylation, cortactin disengages F-actin and cells lose their ability to stabilize these structures. Impaired invasiveness is one important consequence of cortactin acetylation in MDA-MB-231 cells [40]. The role of acetylation of tubulin proteins is another active area of investigation. Polymeric heterodimers of the alpha- and beta-tubulin proteins are the main structural components of highly dynamic microtubule networks within cells that play important roles in chromosome segregation, cell migration, and vesicular transport [41]. Microtubules also contribute to the biomechanical properties of cells by laterally reinforcing the cytoskeleton [42]. While others have documented that inhibition of HDAC6 results in alpha-tubulin protein acetylation [43], we showed that the microtubule network in MDA-MB-231 cells is subject to regulation by SAHA resulting in a highly developed web of fibers emanating from the microtubule organizing center (Figure 5-2). Azuma et al. [44] showed an inverse correlation between acetylated alpha-tubulin and invasiveness in the MCF-7 human breast cancer cell line. Thus, the published work predicts that cytoskeleton protein acetylation changes produced by SAHA will blunt the invasiveness of MDA-MB-231 cells. In fact, using an *in vivo* animal model, SAHA was found to inhibit the metastatic spread of a brain-seeking sub-line of MDA-MB-231 cells [45]. Therefore, although the underlying biochemical pathways responsible for SAHA's changes in the adhesion behavior of cells in the 3-D silicon microstructures are not yet defined, we suggest that the change in adhesion of MDA-MB-231 cells within the microstructures might reflect this decrease in cell invasion potential.

In support of this idea, we highlight lines of evidence from our own work indicating SAHA reduced the degree of malignancy of MDA-MB-231 cells. The N/C is a widely accepted clinical prognostic indicator used along with nuclear size and mitotic index to assess the tumor nuclear

grade [29, 46]. Nuclear grade shows a direct correlation with patient 5-year survival rates; the most favorable patient outcomes occur when tumors show small nuclear size and high N/C [47]. Our results showed that SAHA shifted the MDA-MB-231 cells towards a more favorable nuclear grade evidenced by an increase in the N/C and a decrease in nuclear size.

The biomechanical mechanisms which are responsible for stretching behavior of the MDA-MB-231 cells inside 3-D silicon microstructures after addition of SAHA are also of considerable importance. The cytoskeletal structure of the cell is composed of three major biopolymers namely actin filaments, intermediate filaments and microtubules. Our primary findings indicated that SAHA causes striking alterations in the microtubules of MDA–MB-231 cells resulting in the extension of a prominent microtubule network that originates from the microtubule organizing center adjacent to cell nuclei and expands through the cell body (Figure 5-2(e-f)). The tensegrity theory has been very successful in describing the complex mechanical behavior of adherent cells. Based on this theory, the cell can be viewed as a tensional structure in which actin filaments bear tensile loads and microtubules bear compression loads [48]. The prestress, defined as the tensile stress in the cytoskeleton prior to application of an external load, is determined by actin filaments and balanced by microtubules and attachments to substrates or other cells [49]. The internal traction forces within the cytoskeletal structure accompanied with the adhesion to the substrate ensure the shape stability of the cells and ultimately results in a mechanically equilibrated structure [30]. The contractile forces within the cytoskeleton are also dependent on the cell morphology such that the cytoskeletal tension increases as the cell area increases [50]. This cited work predicts that, after treatment with SAHA which extends the microtubule network and increases cell area, the tension within the actin cytoskeletal structure of the cells increases. We propose that it is this increase in cytoskeletal tension that is responsible for the cell stretching behavior

On the other hand, the tensegrity theory also predicts that the prestress within the cell cytoskeleton is proportional to cell stiffness [49]. Although, our AFM analysis performed on the center of the cell nucleus did not show a significant increase in the cells' stiffness (Young's modulus) after SAHA treatment, it is important to note that AFM analysis throughout the cell body showed that cells' Young's modulus significantly increases from the nucleus region toward

the edges of the cell [51]. Furthermore, simulation analysis on cytoskeletal structure of the cell indicated that as cells adhere to the substrate and microtubules expand toward adhesion sites in the cell periphery, the resulting tension generated within the actin cytoskeleton is generated primarily in the basal regions and edges of the cell; less tensioned elements are mostly located on the apical regions of the cells [30] which in MDA-MB-231 cells is centered upon the cell nucleus.. We (Figure 5-2(b)) and others [28] have experimentally confirmed the formation of stress fibers on the basal regions as well as on the edges of cells [52]. In fact, the fluorescence intensity of actin filaments (as the major determinant of the cellular elasticity [53]) over the MDA-MB-231 cell nucleus did not significantly increase in response to SAHA. Therefore, after treatment with SAHA, the generated tensioned elements are mainly located on the edges of the cells. The actin filament extensions which serve to partially suspend metastatic breast cells within the microstructures are a novel response to SAHA treatment. A future aim of this laboratory is to clarify the relationship between the conformation of cells within these microstructures and a map of cellular elasticity. Such work might reveal patterns of stretching behavior that would mark changes in cellular elasticity without the need for extensive elasticity measurements through AFM indentations. A significant advantage of our isotropic 3-D microstructures is the detection of cytoskeletal reorganization and adhesion alterations (i.e. stretching behavior) which shift the distribution of tensional elements in the cytoarchitecture of diseased cells. Our isotropic 3-D microstructures can be potentially used for assessing the metastatic potential of breast cancer cells and for drug screening to identify anti-cancer agents able to curb breast cancer metastasis.

5.5 Conclusion

We analyzed the cytoskeletal reorganization and morphological responses of MDA-MB-231 human metastatic mammary tumor cells to an experimental anti-breast cancer drug, SAHA, using a novel cell culture substrate comprised of 3-D isotropic silicon microstructures. The results of this work demonstrate the feasibility of using isotropically etched silicon microdevices to screen chemotherapeutic agents for actions upon the cytoskeleton. The conclusion from these studies is that the mode of cell attachment in isotropically etched 3-D silicon microarrays might serve as a surrogate marker of cytoarchitectural features in breast cancer cells that reflect their

responses to drugs and ability to metastasize. Thus, 3-D silicon microstructures might find applicability in the identification of the metastatic potential of breast cancer cells as well as compounds to impair cancer cell metastasis. It also revealed that AFM analysis on the cell center alone is insufficient to detect all cytoskeletal rearrangements in cancer cells.

5.6 References

[1] J. S. Strobl, *et al.*, "Actions of the anti-cancer drug suberoylanilide hydroxamic acid (SAHA) on human breast cancer cytoarchitecture in silicon microstructures," *Biomaterials,* vol. 31, pp. 7043-7050, Sep 2010.

[2] K. K. Jain, "Recent advances in nanooncology," *Technology in Cancer Research and Treatment,* vol. 7, pp. 1-13, Feb 2008.

[3] M. Nikkhah, *et al.*, "Cytoskeletal role in differential adhesion patterns of normal fibroblasts and breast cancer cells inside silicon microenvironments," *Biomedical Microdevices,* vol. 11, pp. 585-595, Jun 2009.

[4] W. Saadi, *et al.*, "A parallel-gradient microfluidic chamber for quantitative analysis of breast cancer cell chemotaxis," *Biomed Microdevices,* vol. 8, pp. 109-18, Jun 2006.

[5] K. W. Kwon, *et al.*, "Label-free, microfluidic separation and enrichment of human breast cancer cells by adhesion difference," *Lab on a Chip,* vol. 7, pp. 1461-8, Nov 2007.

[6] M. Nikkhah, *et al.*, "Attachment and response of human fibroblast and breast cancer cells to three dimensional silicon microstructures of different geometries," *Biomedical Microdevices,* vol. 11, pp. 429-441, Apr 2009.

[7] M. Nikkhah, *et al.*, "The cytoskeletal organization of breast carcinoma and fibroblast cells inside three dimensional (3-D) isotropic silicon microstructures," *Biomaterials,* vol. 31, pp. 4552-4561, Jun 2010.

[8] Y. S. Torisawa, *et al.*, "Multi-channel 3-D cell culture device integrated on a silicon chip for anticancer drug sensitivity test," *Biomaterials,* vol. 26, pp. 2165-72, May 2005.

[9] J. Aggeler, *et al.*, "Cytodifferentiation of mouse mammary epithelial cells cultured on a reconstituted basement membrane reveals striking similarities to development in vivo," *Journal of Cell Science,* vol. 99 (Pt 2), pp. 407-17, Jun 1991.

[10] M. J. Bissell, "Modelling molecular mechanisms of breast cancer and invasion: lessons from the normal gland," *Biochemical Society Transactions,* vol. 35, pp. 18-22, Feb 2007.

[11] G. Y. Lee, *et al.*, "Three-dimensional culture models of normal and malignant breast epithelial cells," *Nature Methods,* vol. 4, pp. 359-65, Apr 2007.

[12] P. Keely, "Cell matrix adhesions in three dimensions," in *Cell Junctions. Adhesion, Development, and Disease,* ed Weinheim: Wiley-VCH, 2008, pp. 135-152.

[13] O. W. Petersen, *et al.*, "Interaction with basement membrane serves to rapidly distinguish growth and differentiation pattern of normal and malignant human breast epithelial cells," *Proceedings of the National Academy of Sciences of the United States of America,* vol. 89, pp. 9064-8, Oct 1 1992.

[14] M. Thery and M. Piel, "Adhesive micropatterns for cells: a microcontact printing protocol," *Cold Spring Harbor Protocols,* Jul 2009.

[15] E. S. Park, *et al.*, "Continuously perfused, non-cross-contaminating microfluidic chamber array for studying cellular responses to orthogonal combinations of matrix and soluble signals," *Lab on a Chip,* vol. 10, pp. 571-80, Mar 2010.

[16] E. T. den Braber, *et al.*, "Quantitative analysis of fibroblast morphology on microgrooved surfaces with various groove and ridge dimensions," *Biomaterials,* vol. 17, pp. 2037-44, Nov 1996.

[17] A. M. P. Turner, *et al.*, "Attachment of astroglial cells to microfabricated pillar arrays of different geometries," *Journal of Biomedical Materials Research,* vol. 51, pp. 430-41, Sep 2000.

[18] L. Hughes, *et al.*, "Characterisation of breast cancer cell lines and establishment of a novel isogenic subclone to study migration, invasion and tumourigenicity," *Clinical & Experimental Metastasis,* vol. 25, pp. 549-557, Sep 2008.

[19] S. Dawood, *et al.*, "Triple receptor-negative breast cancer: the effect of race on response to primary systemic treatment and survival outcomes," *Journal of Clinical Oncology,* vol. 27, pp. 220-6, Jan 2009.

[20] A. A. Lane and B. A. Chabner, "Histone deacetylase inhibitors in cancer therapy," *Journal of Clinical Oncology,* vol. 27, pp. 5459-68, Nov 2009.

[21] V. M. Richon, *et al.*, "Development of vorinostat: current applications and future perspectives for cancer therapy," *Cancer Letters,* vol. 280, pp. 201-10, Aug 2009.

[22] C. Boyault, *et al.*, "HDAC6, at the crossroads between cytoskeleton and cell signaling by acetylation and ubiquitination," *Oncogene,* vol. 26, pp. 5468-76, Aug 2007.

[23] Q. Zhou, *et al.*, "Screening for therapeutic targets of vorinostat by SILAC-based proteomic analysis in human breast cancer cells," *Proteomics,* Jan 2010.

[24] A. Valenzuela-Fernandez, *et al.*, "HDAC6: a key regulator of cytoskeleton, cell migration and cell-cell interactions," *Trends in Cell Biology,* vol. 18, pp. 291-7, Jun 2008.

[25] R. Cailleau, *et al.*, "Breast tumor cell lines from pleural effusions," *Journal of the National Cancer Institute,* vol. 53, pp. 661-74, Sep 1974.

[26] C. T. Mierke, "The role of vinculin in the regulation of the mechanical properties of cells," *Cell Biochemistry and Biophysics,* vol. 53, pp. 115-26, 2009.

[27] R. M. Ezzell, *et al.*, "Vinculin promotes cell spreading by mechanically coupling integrins to the cytoskeleton," *Experimental Cell Research,* vol. 231, pp. 14-26, Feb 1997.

[28] C. T. Brew, *et al.*, "Indole-3-carbinol inhibits MDA-MB-231 breast cancer cell motility and induces stress fibers and focal adhesion formation by activation of Rho kinase activity," *International Journal of Cancer*, vol. 124, pp. 2294-2302, May 2009.

[29] P. P. Rosen, *Rosen's breast pathology*, Third ed.: Lippincott Williams & Wilkins, 2008.

[30] B. Maurin, *et al.*, "Mechanical model of cytoskeleton structuration during cell adhesion and spreading," *Journal of Biomechanics*, vol. 41, pp. 2036-2041, 2008.

[31] M. J. Doughty, *et al.*, "Shrinkage and distortion of the rabbit corneal endothelial cell mosaic caused by a high osmolality glutaraldehyde-formaldehyde fixative compared to glutaraldehyde," *Tissue and Cell*, vol. 29, pp. 533-47, Oct 1997.

[32] B. Cox, "The effect of service screening on breast cancer mortality rates," *European Journal of Cancer Prevention* vol. 17, pp. 306-11, Aug 2008.

[33] L. Tabar, *et al.*, "The natural history of breast carcinoma: what have we learned from screening?," *Cancer*, vol. 86, pp. 449-62, Aug 1999.

[34] D. Vignjevic and G. Montagnac, "Reorganisation of the dendritic actin network during cancer cell migration and invasion," *Seminars in Cancer Biology*, vol. 18, pp. 12-22, Feb 2008.

[35] H. Yamaguchi and J. Condeelis, "Regulation of the actin cytoskeleton in cancer cell migration and invasion," *Biochimica et Biophysica Acta* vol. 1773, pp. 642-52, May 2007.

[36] T. Bauerle, *et al.*, "Characterization of a rat model with site-specific bone metastasis induced by MDA-MB-231 breast cancer cells and its application to the effects of an antibody against bone sialoprotein," *International Journal of Cancer*, vol. 115, pp. 177-86, Jun 2005.

[37] M. Guarino, "Epithelial-mesenchymal transition and tumour invasion," *International Journal of Biochemistry & Cell Biology* vol. 39, pp. 2153-60, 2007.

[38] K. Wolf and P. Friedl, "Mapping proteolytic cancer cell-extracellular matrix interfaces," *Clinical & Experimental Metastasis*, vol. 26, pp. 289-298, Apr 2009.

[39] W. S. Ammer AG "Cortactin branches out: Roles in regulating protrusive actin dynamics," *Cell Motility and the Cytoskeleton*, vol. 65, pp. 687-707, Sept 2008.

[40] Y. Zhang, *et al.*, "Deacetylation of cortactin by SIRT1 promotes cell migration," *Oncogene*, vol. 28, pp. 445-60, Jan 2009.

[41] S. Etienne-Manneville, "From signaling pathways to microtubule dynamics: the key players," *Current Opinion in Cell Biology*, vol. 22, pp. 104-111, Feb 2010.

[42] C. P. Brangwynne, *et al.*, "Microtubules can bear enhanced compressive loads in living cells because of lateral reinforcement," *J Cell Biol*, vol. 173, pp. 733-41, Jun 5 2006.

[43] C. Hubbert, *et al.*, "HDAC6 is a microtubule-associated deacetylase," *Nature*, vol. 417, pp. 455-8, May 2002.

[44] K. Azuma, *et al.*, "Association of estrogen receptor {alpha} and histone deacetylase 6 causes rapid deacetylation of tubulin in breast cancer cells," *Cancer Research*, vol. 69, pp. 2935-2940, April 2009.

[45] D. Palmieri, *et al.*, "Vorinostat inhibits brain metastatic colonization in a model of triple-negative breast cancer and induces DNA double-strand breaks," *Clinical Cancer Research*, vol. 15, pp. 6148-57, Oct 2009.

[46] K. W. Gilchrist, *et al.*, "Interobserver reproducibility of histopathological features in stage II breast cancer. An ECOG study," *Breast Cancer Research and Treatment*, vol. 5, pp. 3-10, 1985.

[47] P. Kronqvist, *et al.*, "Morphometric grading of invasive ductal breast cancer. I. Thresholds for nuclear grade," *British Journal of Cancer*, vol. 78, pp. 800-5, Sep 1998.

[48] M. R. King, *Principles of cellular engineering: understanding the biomolecular interface*. Burlington: Elsevier Academic Press, 2005.

[49] N. Wang, *et al.*, "Cell prestress. I. Stiffness and prestress are closely associated in adherent contractile cells," *American Journal of Physiology. Cell Physiology*, vol. 282, pp. C606-C616, Mar 2002.

[50] J. L. Tan, *et al.*, "Cells lying on a bed of microneedles: An approach to isolate mechanical force," *Proceedings of the National Academy of Sciences of the United States of America*, vol. 100, pp. 1484-1489, Feb 2003.

[51] H. Haga, *et al.*, "Elasticity mapping of living fibroblasts by AFM and immunofluorescence observation of the cytoskeleton," *Ultramicroscopy*, vol. 82, pp. 253-8, Feb 2000.

[52] V. M. Laurent, *et al.*, "Partitioning of cortical and deep cytoskeleton responses from transient magnetic bead twisting," *Annals of Biomedical Engineering*, vol. 31, pp. 1263-1278, Nov 2003.

[53] R. Ananthakrishnan, *et al.*, "Quantifying the contribution of actin networks to the elastic strength of fibroblasts," *Journal of Theoretical Biology*, vol. 242, pp. 502-516, Sep 2006.

6 Chapter Six: Co-cultivation of Non-malignant (MCF10A) and Malignant (MDA-MB-231) Human Breast Basal Epithelial Cells in Three Dimensional Silicon Micro-Arrays: Anti-cancer Drug Responsiveness

6.1 Introduction

Cells are exquisitely sensitive to chemical, electrical, mechanical and physical stimuli inherent in and imposed upon their microenvironment [1, 2]. In recent years, there has been a growing appreciation for cellular adaptations that occur in response to topography features and stiffness of their substrate and surrounding matrix, and in this domain, precision micro-engineering approaches to the design of desired substrates have provided powerful investigative tools [3]. An excellent example of this type of cell-substrate interaction is "contact guidance," an induced reorganization of the cytoskeleton resulting in cell alignment along etched micro-grooves within the substrate [4-8]. Advanced micro- and nano-technologies have created substrates bearing precise topographical patterns able to successfully direct the processes of cell differentiation [9, 10], migration [11-14], adhesion [15-18] and proliferation [19]. Microstructures comprised of anisotropic geometries fabricated in PDMS [10, 11, 20, 21], silicon [17, 18], polymeric fibrous networks [22], nano-scaffold [23, 24], and polyacrylamide sheets [25, 26] are commonly used in this work. In addition, there is considerable application of substrate in 3-D collagen gels and synthetic extracellular matrix created through microfabrication technology for the *ex vivo* simulation of *in vivo* microenvironments [27-29]. The applications of these research endeavors span the fields of tissue engineering [4, 5], developmental and stem cell biology [8, 10, 21], and cancer research [28, 29].

Our group has developed three dimensional (3-D) isotropic silicon microstructures which are comprised of precisely defined curved surfaces to characterize the growth and adhesion of three cell types representative of the human breast microenvironment: normal fibroblasts, normal fibrocystic mammary epithelial cells and metastatic breast cancer epithelial cells [30-33] (Chapters 2-5). Silicon is a stiff material which has been previously used to study several cell functions such as cell growth, adhesion [16-18, 34-36] and migration [14]. One of the major advantages of using silicon as a substrate for cellular analysis is the control and flexibility in

designing the substrate geometry and surface roughness by varying the etching process [34, 37-39].

The focus of our laboratory is the role of physical and mechanical inputs from the microenvironment on cell adhesion to the substrate. Our hypothesis is that metastatic and non-metastatic breast cells have non-identical responses to mechanical and chemical stimuli in their microenvironment. This hypothesis is based upon documented differences in the biomechanical properties of metastatic and non-metastatic breast cancer cells [40] and the underlying differences in the cytoskeletal composition and organization in these cells [32]. We have used precisely defined curved surfaces (isotropic) in our work to show that such imposed mechanical constraints to the cell cytoarchitecture differentially modulate the adhesion pattern of metastatic MDA-MB-231 and non-malignant MCF10A cells. We previously demonstrated that the cytoarchitectural response of breast tumor cells within 3-D microstructures is selectively altered in the presence of the anti-cancer histone deacetylase inhibitor drug, suberoylanilide hydroxamic acid (SAHA) [33]. Here, we analyze a co-culture system containing malignant MDA-MB-231 cells interspersed among non-malignant MCF10A human breast epithelial cells in a micro-engineered silicon microarray. The two cell types display a continuous and dynamic interaction in co-culture, yet maintain their distinct cytoarchitectural behaviors, including SAHA responsiveness. We conclude that the imposition of physical and mechanical constraints using isotropic 3-D silicon microstructures as cellular substrates combined with chemical stimuli is a significant micro-engineering contribution to the detection of malignant cells in a cell mixture.

6.2 Materials and methods

6.2.1 Silicon device fabrication

Figure 6-1 shows a photo image of the 0.5 cm square device and the corresponding scanning electron microcopy (SEM) images. The fabrication process is a single-mask single-etch-step process which utilizes reactive ion etching (RIE) lag as described in detail in previous chapters. The fabrication process starts by cleaning the wafers using standard procedures. The silicon wafers are then vapor-primed with hexamethyldisylazane (HMDS) and then spun coated with S1827 photoresist. After patterning the photoresist, silicon is etched using DRIE SF_6 plasma to

achieve final 3-D microstructures. After removing photoresist, the wafer is cleaned using DRIE oxygen plasma for 15 minutes and finally diced into 0.5cm square chips. The etched features are comprised of array of ellipsoidal-shaped microchambers (16 × 16) (Figure 6-1(b)). Table 6-1summarizes the geometrical parameters and dimensions of the proposed microstructures etched for 10 minutes. The cross sectional view of the etched cavity has been approximated with an elliptical shape in order to calculate the ratio of the etched surfaces to total surfaces available for cell adhesion within the fabricated chip. The SEM images of the etched cavities have been demonstrated in Figure 6-1(b,c). Figure 6-1(d) shows a high magnification image of the etched cavities sidewall.

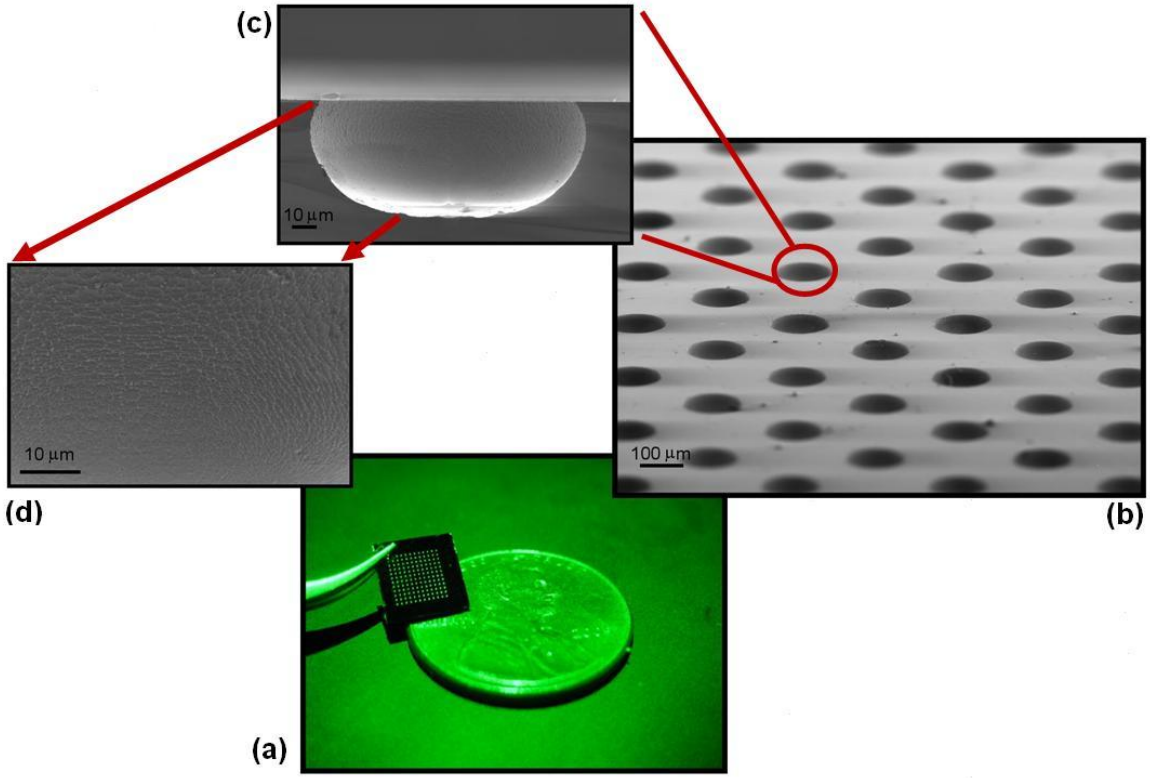

Figure 6-1(a) Photo image of the fabricated devices in silicon and (b) the corresponding SEM images of the substrate and (c) cross sectional view of the etched cavity. Image (d) shows a high magnification of the surfaces inside the etched cavity.

Table 6-1 Summary of the geometrical parameters for the etched silicon substrate

Depth (µm)	Diameter (µm)	Spacing (µm)	Surface Ratio Etched/Total
60	140	130	0.43

6.2.2 Cell culture preparation

Non-invasive MCF10A and highly invasive MDA-MB-231 breast cells were used in this work. The cells were purchased from the American Type Culture Collections (ATCC). MDA-MB-231 cells were maintained in plastic T-75 cm^2 culture flasks in F12:DMEM (50:50) culture medium (Mediatech) which contained 10% fetal bovine serum (FBS) (Atlanta Biologicals), 4 mM glutamine (Mediatech) and penicillin-streptomycin (100 Units/ml) (Mediatech). MCF10A cells were grown in plastic T-75 cm^2 culture flasks using Hams F12:DMEM (50:50), 2.5 mM L-glutamine, 20 ng/ml epidermal growth factor (EGF) (Sigma), 0.1 µg/ml cholera toxin (CT) (Sigma), 10 µg/ml insulin (Sigma), 500 ng/ml hydrocortisone (Sigma) and 5% horse serum (Atlanta Biologicals). Cells were grown at 37 °C in humidified 5% CO2-95% air atmosphere.

MDA-MB-231 cells were transfected with plasmid pEGFP-IRESpuro (Clontech) using Lipofectamine2000 as recommended by the manufacturer (Invitrogen). Stable transfectants constitutively expressing EGFP were selected by growth in the presence of 3 µg/ml puromycin. MCF10A cells expressing mCherry were obtained using ready-made mCherry Lentifect purified lentiviral particles (GeneCopoeia). Cells were transduced at a multiplicity of infection of 10 in the presence of 5 µg/ml of polybrene. Stably transduced cells expressing mCherry were selected by growth in the presence of 3 µg/ml puromycin followed by flow cytometric sorting of positive mCherry cells. Cells were maintained in selection media during passaging.

To investigate the cell trapping mechanism within the etched cavities, MCF10A and MDA-MB-231 were randomly mixed with the densities of 1×10^5 and 1×10^4, respectively (1/10 ratio) and plated on the silicon chips placed in 12-well multi-well plate containing 1.5 mL of F12:DMEM (50:50) supplemented with 10% FBS. Immediately after seeding the cells, the multi-well plate was placed on the microscope stage for time-laps and real-time imaging.

For anti-cancer drug responsiveness of the co-culture experiments, MCF10A and MDA-MB-231 were randomly mixed with the same above mentioned densities (1/10 ratio) and then plated on the silicon chips placed in 12-well multi-well plate containing 1.5 mL of F12:DMEM (50:50) culture medium supplemented with 10% FBS. Cells were incubated for 12 h after plating to allow cells to attach to the substrate, then SAHA drug (Suberoylanilide hydroxamic acid) (0.75 µl) was added directly into the culture medium to a final concentration of 2.75 µM in 0.05% DMSO using a 2000× stock solution of SAHA dissolved in 100% DMSO . After exposure of the cells to SAHA for 18 h, the cells were fixed and processed for cytoskeletal organization staining. For real-time imaging, the chips were placed and fixed inside a 35 mm round cell culture dish on the microscope stage and imaging started immediately after adding SAHA to the medium.

6.2.3 Immunofluorescence for cytoskeletal organization and focal adhesions

We assessed the formation of focal adhesion complexes, actin cytoskeleton and microtubules in cells attached on the silicon substrates using confocal (ZEISS-LSM-510 META) and fluorescence microscopy (ZEISS Axiovison). 3% paraformaldehyde (PF) solution (Electron Microscopy Sciences) in 250mM HEPES (Sigma), pH 7.2 was used to fix the cells on the silicon substrates for 10 minutes. Then, the cells were exposed to 6% PF solution with 0.25% Triton X-100 in PBS for another 10 minutes to permeabilize the cell membrane. The samples were washed free of PF in 50 mM of glycine (Fischer) in PBS for 10 min and then blocked in 2% chicken serum albumin (Sigma) in PBS for 30 minutes at room temperature. For vinculin staining, a monoclonal mouse anti-vinculin antibody (Abcam) was diluted 1/100 in 2% chicken serum albumin in PBS and added to the samples for 30 minutes. Next, Alexa Fluor-350 conjugated goat anti-mouse secondary antibody (Invitrogen) was diluted 1/300 in 2% chicken serum albumin in PBS and added to the samples for 1 hour. Actin cytoskeleton staining was performed using 1/5 dilution of Alexa Fluor-350 phalloidin (Invitrogen) in 2% chicken serum albumin in PBS for 2 hours. Finally, for microtubules staining, a mouse monoclonal anti-β-Tubulin I+II antibody (Sigma) was diluted 1/750 in 2% chicken serum albumin in PBS and added to the samples for 1 hour. After washing the cells, Alexa Fluor-350 conjugated goat anti-mouse secondary antibody (Invitrogen) was diluted 1/150 in 2% chicken serum albumin in PBS and added to the samples for 3 hours. Following vinculin, actin cytoskeleton and microtubules staining, the samples were

rinsed three times in PBS and mounted on ProLong Gold antifade reagent (Invitrogen) for final imaging.

6.2.4 Viability assay

The live/dead viability/cytotoxicity kit for mammalian cells (Invitrogen) was used to test the viability of the cells attached on the silicon substrates in control condition as well as after treatment with SAHA drug. Non-transfected MDA-MB-231 and MCF10A cells were used for viability testing experiment. After the desired culture time, cells were washed three times in warm PBS (37 °C), and then incubated for 30 minutes in the presence of 0.5 µl of Calcein-AM and 1 µl of Ethidium homodimer-1 (EthD-1) in 1 ml of PBS. The fluorescence images were obtained at four different random locations of the silicon substrates using ZEISS Axiovison D1 upright microscope with 10X immersion objective. Finally, the number of the live cells (stained in green) and the number of the dead cells (stained in red) were quantified using the obtained fluorescence images.

6.2.5 MTS assay

The MTS assay is a frequently used method to enumerate functional, viable cells [41]. 3-(4,5-Dimethylthiazol-2-yl)-5-(3-carboxymethoxyphenyl)-2-(4-sulfophenyl)-2H-tetrazolium (MTS) (Promega) is metabolized by mitochondria in living cells to a colored formazan product with an absorbance maximum at 490 nm. Numbers of functional cells are directly correlated with the magnitude of light absorbance at 490 nm measured spectrophotometrically. Cells were seeded onto 7 mm square silicon chips in 24-well plates and incubated for 12 h, then serial dilutions of SAHA were added in duplicate, and cells were incubated for an additional 18 or 48 hours. Chips were transferred to fresh plates containing the MTS substrate diluted 1:5 in serum-free medium and incubated 1 h at 37 C. Levels of viable cells on control and drug-treated chips were assessed using the absorbance (490 nm) in 100 µL aliquots of the culture medium. Background absorbance of wells containing no cells was subtracted from the raw absorbances and the data were expressed as the percent of drug-free controls.

6.2.6 Time laps imaging

Real-time fluorescence microscopy was performed using ZEISS Axiovison D1 upright microscope which is fitted with an environmental chamber and equipped with a temperature and CO_2 control unit. The temperature was set to 37 ºC and CO_2 was set to 5% during the experiments. For trapping cell experiments, images were acquired using a 10X immersion objective every minute for duration of 3 hours.

6.2.7 Quantification of cell morphology

Cell area measurements were performed on the flat surfaces surrounding the etched cavities on each silicon chip using fluorescence images obtained by ZEISS Axiovison D1 and the National Institutes of Health (NIH) ImageJ (v. 1.41) software. For MCF10A cells, the area of a cluster of cells was measured and divided by the number of the cells within the cluster to obtain the average area of a single cell.

For quantification of cell stretching density, two different morphologies of spread and stretched were assumed. The spread cells were those in which the cell body has a uniform contact with the sidewalls of the microchamber while the stretched ones possessed extensions, anchored to different location of the microchambers and suspended over the curved sidewalls of isotropic microstructures. The number of the stretched cells within each etched cavity was quantified through obtaining fluorescence images using ZEISS Axiovison D1.

6.2.8 Statistical analysis

A two-sample independent t-test was performed using Graph Pad Prism 5.0 statistical software to compare the cell morphological analysis and cell viability data.

6.3 Results

In our previous study [42], we demonstrated that for the etched microenvironments with close spacing (25-50 µm), cells accumulate mainly inside the pits. In fact, about 90% of the cells fall into the cavities. In contrast, for intermediate spacing (100-300 µm), cells are evenly distributed on flat surfaces and inside the cavities while for large pitch sizes (300-700 µm), cells are mostly seen on flat surfaces. For the geometries proposed in the current work, we chose the intermediate spacing between the etched cavities in order to have flexibility to perform cellular analysis on

both flat surfaces (surrounding the cavities) and inside the etched features. The cell trapping efficiency was quantified after 4 hours following seeding the cells on the silicon chips. During this time, the cells settled on flat surfaces surrounding the cavities or were trapped inside the etched features. In order to define the cell occupancy and capture efficiency of the substrate, fluorescence images were obtained at nine different fields within the chip using 10X magnification objective. The selected fields almost covered the entire fabricated substrate. The quantitative data indicated the cell occupancy was 99% on the substrate following seeding MDA-MB-231 cells with density of 1×10^4 and MCF10A cells with density of 1×10^5 cells per chip. The capture efficiency was defined as the ratio of the number of cells trapped inside the etched cavities to the total number of cells within each field. The number of the cells was manually counted from the fluorescence images to define the capture efficiency. The capture efficiency was calculated to be 51±4% for the above mentioned seeding density. 32% of the cavities on the silicon chip were occupied by both MCF10A and MDA-MB-231 cells which was suitable for adhesion analysis and performing anti-cancer drug sensitivity testing in the co-culture experiment. The average ratio of MDA-MB-231 cells to MCF10A cells within each cavity on the silicon chip was 27%.

In order to investigate the mechanism of cell trapping inside the microstructures, we performed real-time fluorescence microscopy on the co-culture of MCF10A and MDA-MB-231 cells (1/10 ratio) immediately after seeding the cells on the silicon substrates. Typical time-lapse images have been shown in Figure 6-2, indicating that the cells are captured and accumulated inside the etched features as early as 30 minutes after introducing the cells to the substrate. These images suggest that trapping of the cells inside the etched features were mainly due to the gravitational force and flow effects immediately after the cell seeding on the chips (Passive capturing). In addition, the real-time imaging, confirmed rapid capture and subsequent formation of colonies of both cell types inside the etched cavities suggesting that the proposed substrates are suitable for the study of cell-cell interactions in a colony of normal and cancerous cells as well as anti-cancer drug sensitivity testing in a 3-D architecture.

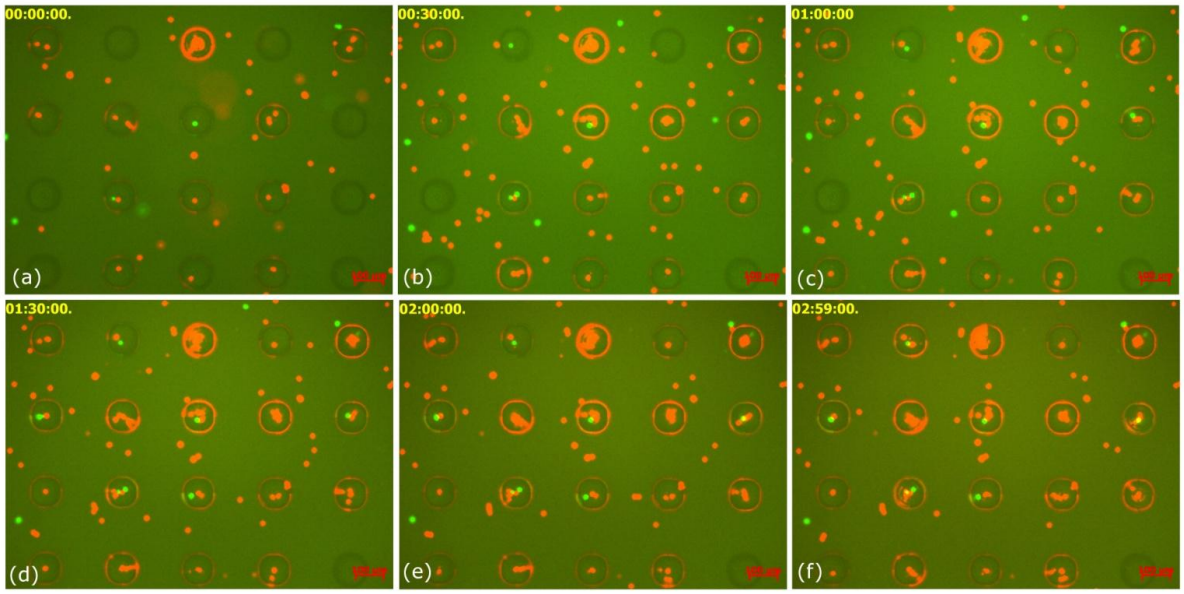

Figure 6-2 Time-lapse video microscopy showing the capturing process in co-cultures of MDA-MB-231 and MCF10A cells in silicon substrate ((a) 0 min ,(b) 30 min, (c) 1 hr , (d) 1 hr 30 min (e) 2 hr (f) 3 hr). MDA-MB-231 cells stained in green dye and MCF10A cells stained in the red dye. Scale bars represent 100µm.

For the first set of anti-cancer drug sensitivity experiments (SAHA drug), we performed MTS assay to quantify functional and viable cells as a function of SAHA concentration and time. MTS assay demonstrated that the reductions in the number of viable cells in response to SAHA were more pronounced in the MDA-MB-231 cancer cells than in MCF10A cells, and were both concentration and time-dependent. The number of functional MDA-MB-231 cells attached to the silicon chips was reduced by ~20% and ~60% by 2.75 µM SAHA after 18 and 48 hours respectively. The results show 2.75 µM is a pharmacologically relevant concentration of SAHA which produces modest cell loss during the initial 18 h of treatment and exerts substantial cell toxicity upon more prolonged exposure consistent with SAHA's known anti-cancer activity. The non-tumorigenic MCF10A cells were less sensitive to SAHA (2.75 µM), with cell losses half of that measured in the MDA-MB-231 cells: ~11% and ~33% at 18 and 48 hours respectively (Figure 6-3).

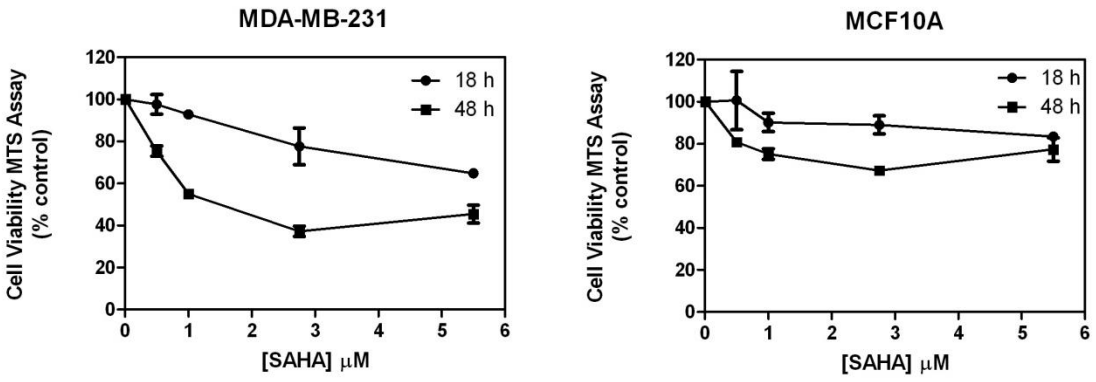

Figure 6-3 MTS assay results showing the in the number of viable cells as a unction of SAHA concentration and time.

Based on the MTS assay analysis, we selected 18 h time point and 2.75 µM SAHA concentration for the remaining experiments. Cells were cultured for 12 hours, then SAHA (2.75 µM final concentration) was added for an additional 18 hours to the samples. Viability analysis indicated that 94% of MDA-MB-231 and 88% of MCF10A cells were live after adding SAHA to the samples in separate culture, confirming that treatment of the cells with SAHA for the selected time point did not significantly alter the percentage of the live cells on silicon surfaces (In comparison to control condition: 97% viability for MDA-MB-231 and 95% viability for MCF10A). We then assessed the viability of the co-culture of MCF10A and MDA-MB-231 cells in response to SAHA on the 3-D silicon substrates comprised of etched cavities. As shown in Figure 6-4, the data indicated that the percentage of the live cells after addition of SAHA (94±1%) did not significantly decrease compared to the control condition (95±4%).

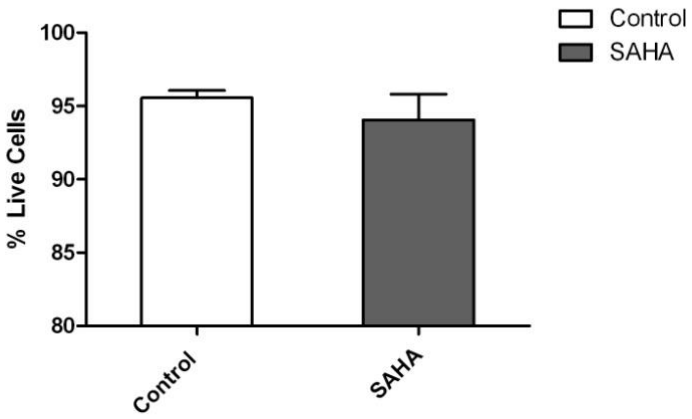

Figure 6-4 Percent of live cells in co-cultures experiment on the etched silicon substrates in control condition and after exposure to 3 µM final concentration SAHA.

The morphological parameters of MCF10A and MDA-MB-231 cells in both control and SAHA treated conditions are compared in Figure 6-5. Control MCF10A and MDA-MB-231 cells grown on flat silicon are very similar in length and area, however, the MDA-MB-231 responded to SAHA treatment with a highly significant increase ($p<0.0001$) in both cell length and cell area (Figure 6-5) consistent with our previous observations [33]. The mean cell area and cell length of MDA-MB-231 cells was measured to be 55.9 ± 12.5 µm (n=63) and 1107 ± 343 μm^2 (n=61) in control condition which were significantly increased ($p<0.0001$) to 76.3 ± 16.1 (n=76) and 1807 ± 601 μm^2 (n=73) after treatment of the cells with SAHA.

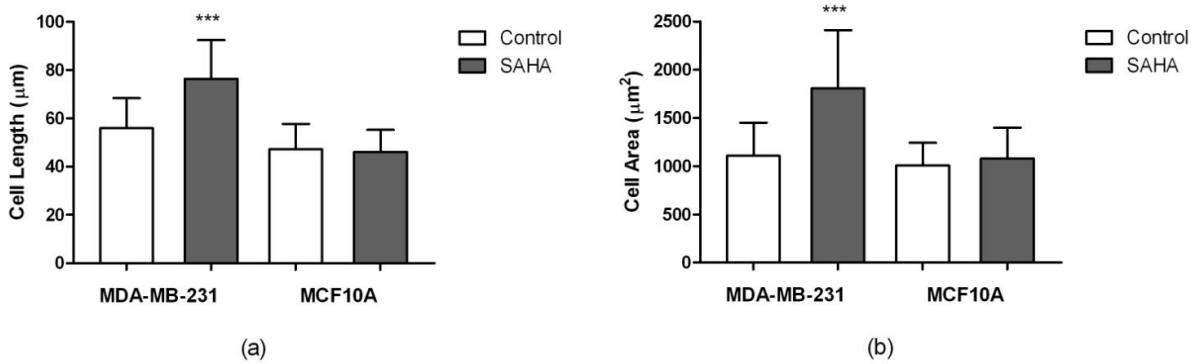

Figure 6-5 Comparison of cell length (left Panel) and cell area (right Panel) in MDA-MB-231 and MCF10A cells grown on flat silicon surfaces. Data are presented in mean ± S.D. and represent 55-111 cells in n= 3 independent experiments. Statistical significant (*p <0.0001) differences between control and SAHA were determined by an unpaired t-test.**

Figure 6-6 shows the actin cytoskeleton, microtubules organization and vinculin formation of MCF10A and MDA-MB-231 cells (blue color) attached on flat silicon surfaces in both control and SAHA treated conditions. MDA-MB-231 cells (stained in green) were usually seen as isolated cells while MCF10A cells (stained in red) formed clusters and maintained their cell-cell junctions in both conditions. The actin cytoskeleton of MCF10A cells was distributed in a more dense mesh compared to the MDA-MB-231 cells (Figure 6-6(a-d)). Formations of actin–rich extensions were evident in MDA-MB-231 cells after treatment of the cells with SAHA. SAHA caused striking alterations in microtubule network of the MDA-MB-231 cells, while the changes in MCF10A cells were not significant (Figure 6-6(e-h)). Expansion of microtubules from microtubule organizing center to the cell extensions in MDA-MB-231 cells after treatment with SAHA is clearly seen in Figure 6-6(g,h). The microtubule reorganization of the MDA-MB-231 after adding SAHA in co-culture was consistent with our previous findings on MDA-MB-231 in

separate culture [33]. Vinculin were seen in the form of discrete dots on the periphery of MDA-MB-231 cells and on outer regions of the cells body in both conditions. For MCF10A cells, in addition to the periphery, vinculin were also localized on the cell-cell junction regions (Figure 6-6(i-l)).

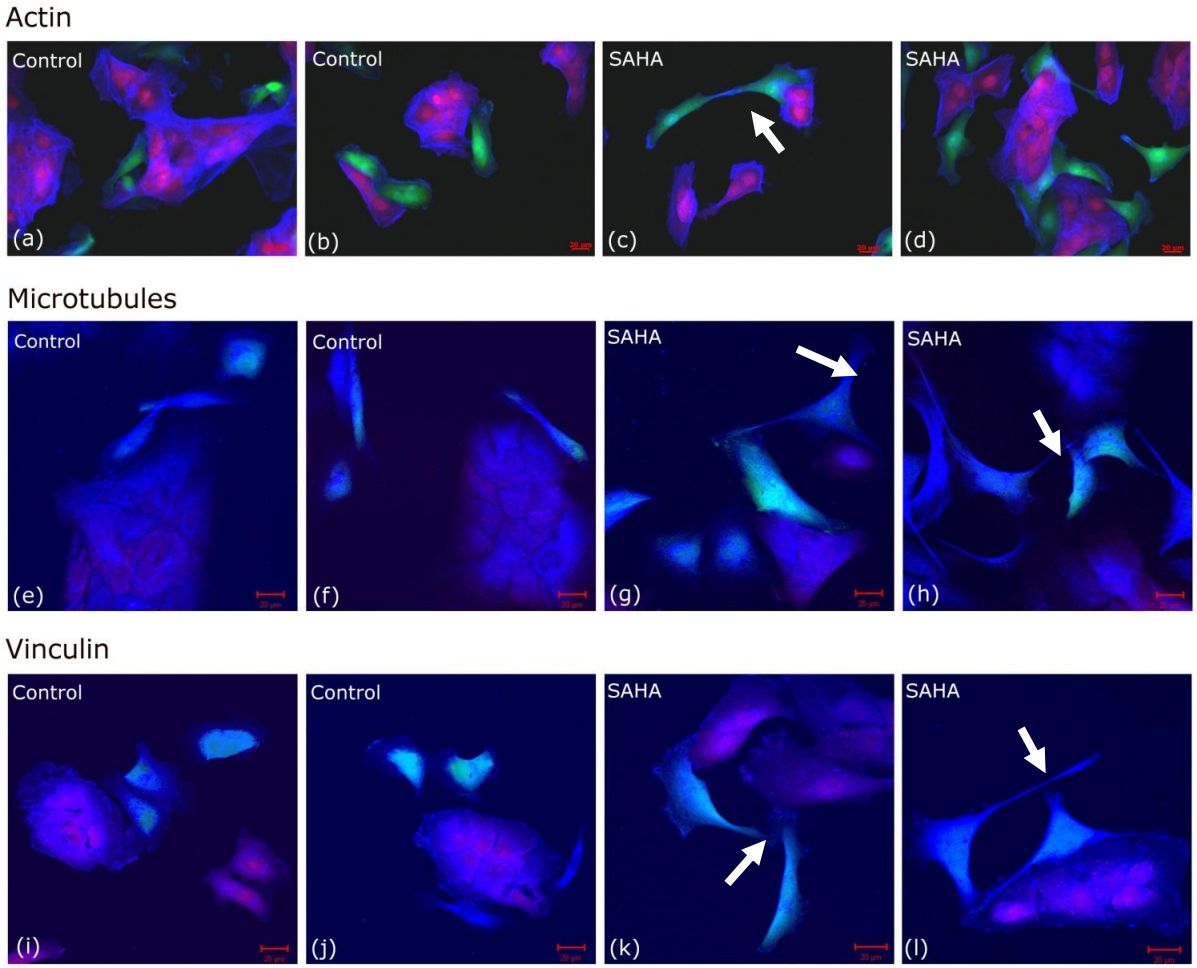

Figure 6-6 Confocal and fluorescence images of MDA-MB-231 and MCF10A cells in a random co-culture experiment attached on flat silicon surfaces. MDA-MB-231 cells are stained in green and MCF10A cells are stained in red. Actin cytoskeleton, microtubules and vinculin are stained in blue in separate experiments. Images (a-d) show the actin cytoskeleton, images (e-h) show the microtubuels and (i-l) shows the vinculin. Arrow shows the extension of the cells after adding SAHA. Scale bars represent 20 µm.

Following the investigation of the cytoskeletal organization of the cells on flat surfaces, we assessed the adhesion pattern of the cells attached inside the etched cavities using confocal imaging. The confocal images were obtained at different depth of focus to construct 3-D images.

In control condition, both MCF10A (stained in red) and MDA-MB-231 (stained in green) cells adopted their shape to the curvature of the etched cavities (Figure 6-7). After treatment of the cells with SAHA, the adhesion pattern of the MCF10A cells remained unaltered; these cells formed sheets and maintained their cell-cell junction on curved surfaces within the etched cavities. However, MDA-MB-231 responded to the SAHA treatment and stretched inside the cavities (Figure 6-7(d-f)). Formation of cell extensions in MDA-MB-231 cells in response to SAHA, lifted the cells above the substrate and the cells became suspended within the cavities. Figure 6-7(f) shows a single MDA-MB-231 cell stretched over a colony of MCF10A cells.

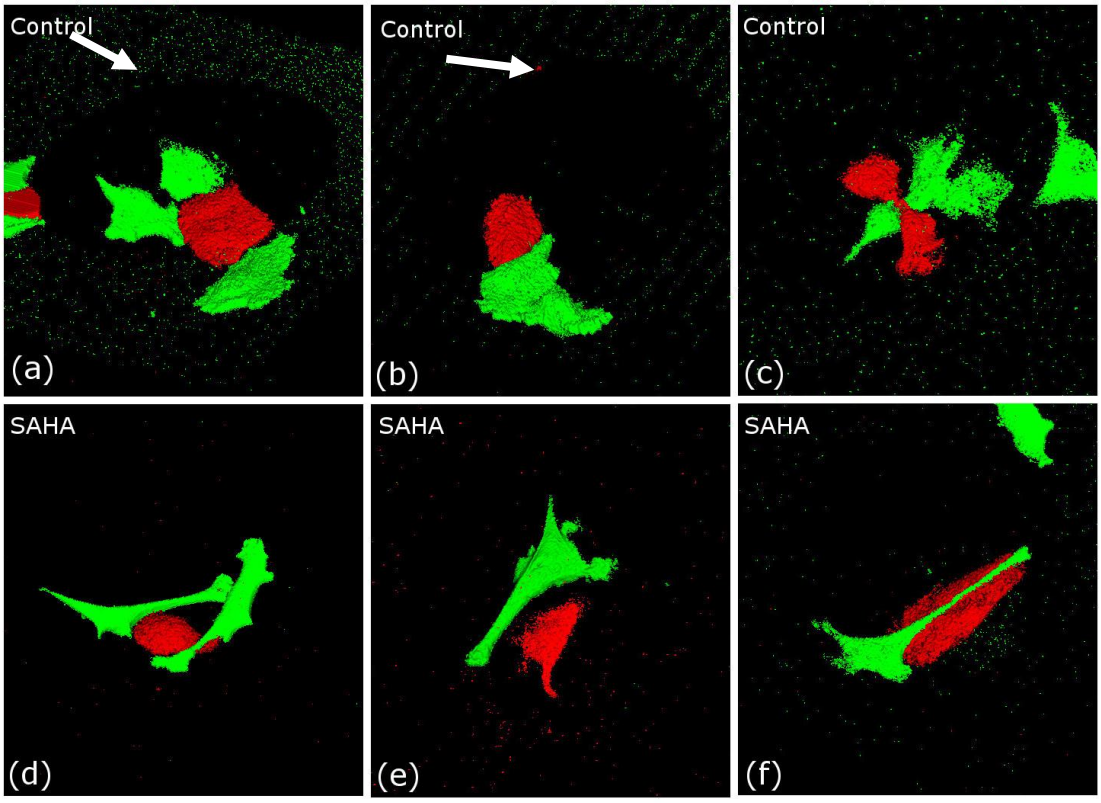

Figure 6-7 3-D confocal images of the MDA-MB-231 and MCF10A cells attached inside the etched cavities in a random co-culture experiment in control condition and after adding SAHA. MDA-MB-231 cells are stained in green and MCF10A cells are stained in red. In control condition both cells adapted to the curved surfaces of the etched geometries whereas after adding SAHA MDA-MB-231 cell adhesion altered and the cells stretched over MCF10A cells within the cavities. Arrows in (a-c) show the flat surfaces top of the etched cavities.

Quantitative data shown in Figure 6-8 indicated that, on average 54.3% of MDA-MB-231 cells stretch inside the 3-D etched microstructures within each silicon chip after exposure to SAHA

for 18 h (n=356 cells). This number was significantly (p<0.002) higher compared to the control condition (average 9.8% stretched cells within each chip, n=553 cells). However, with respect to MCF10A cells, only 1.25 % of the cells (n=1446 cells) stretched inside the etched cavities after adding of SAHA which was not statistically different compared to the control condition (average 0.45 % stretched cells within each chip, n=1190 cells).

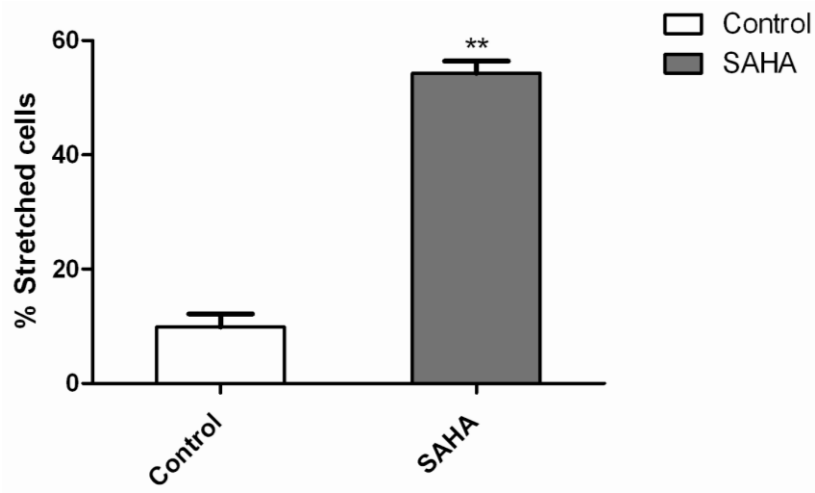

Figure 6-8 Quantitative data showing the percent of the stretched MDA-MB-231 cells after adding SAHA. The stretched cells after adding SAHA significantly increases compared to the control condition. Data is presented in mean± S.D. (p<0.002).**

6.4 Discussion

Cells do not only adhere to their underlying substrate, but they also respond to stimuli such as chemical, mechanical and topographical features within their microenvironment. Benefiting from well-established micro/nano technology, numerous substrates have been developed to modulate the cell function and study the cell adaptation to the topographical features of the substrate. In this work, we focused on integrating the effect of mechanical and chemical stimuli (isotropic silicon microstructures and SAHA anti-cancer drug) to investigate the behavior of normal and cancerous breast cells in a co-culture system within a 3-D architecture. Silicon is a stiff and biocompatible material that is a suitable substrate for creating precise topographical patterns for cellular analysis due to the flexibility in the etching process [37, 38]. SAHA is one of an emerging class of clinically-approved anti-cancer drugs of an increasingly important group of compounds which were first identified as histone deacetylase inhibitors [43, 44]. SAHA was also shown to increase acetylation of the cytoskeletal proteins beta-actin, cortactin, alpha-4-actinin,

and alpha- and beta-tubulin in MDA-MB-231 cells [45] which provides a mechanistic basis for the cytoskeletal changes we observed in these cells. In contrast to other works [46], our intent in this study was not to test for drug-sensitivity but rather to exploit SAHA's ability to selectively alter cytoarchitecture and cytoskeleton proteins such as actins and tubulins only in cancer cells and modulate their adhesion characteristics to 3-D isotropic silicon microstructures. The results presented herein defined a cancer-specific response to SAHA drug within the 3-D isotropic microstructures which can have ultimate applications in identification of a few invasive tumor cells in an abnormal breast lesion.

Analysis on the cytoskeletal organization of the cells demonstrated that actin fibers in the cytoskeleton of MCF10A cells were distributed in a much more dense mesh network compared to MDA-MB-231 cells. Previous studies have reported that the changes in the cytoskeletal organization of the cells is associated with tumorigenesis [47, 48] and there is a progressive dysregulation of actin fiber in cancerous cells compared to their normal counterparts [49]. Therefore, it is predictable that the actin mesh in MCF10A cells should be significantly denser compared to cancerous cells under similar growth condition. On the other hand, it is well established that the actin cytoskeleton is a major determinant of cellular elasticity [50]. Studies on cells elasticity and deformation measurements using atomic force microscopy (AFM) and optical stretched methods have also confirmed that the MCF10A cells are significantly stiffer than MDA-MB-231 cells [40, 51]. Within the co-culture system, only MDA-MB-231 cells significantly responded to SAHA in terms of morphological alterations. These changes were associated with a marked expansion in the microtubule network emanated from the microtubule organizing center and localization of dense actin fibers on the periphery of the cells (Figure 6-6). In fact, this was consistent with our previous study performed only on MDA-MB-231 cells on a different set of topographical patterns [33]. Hence, the interactions among MDA-MB-231 and MCF10A cells in a co-culture system did not markedly affect the behavior of the cells in terms morphological alteration and cytoskeletal reorganization in response to SAHA.

A considerable change in the behavior of the cells was the stretching pattern of MDA-MB-231 cells within the etched cavities. This observation along with the cytoskeletal reorganization of the cells can be explained by referring to the tensegrity theory. Within the context of this theory,

the cell can be viewed as a tensional structure in which actin filaments bear tensile loads and microtubules bear compression loads [52]. According to this theory, the prestress within the cell cytoskeletal structure is mainly balanced by microtubules and attachments to substrates or neighboring cells. Therefore, following the expansion in microtubule network in MDA-MB-231 cells after treatment with SAHA, the level of tension within the cytoskeletal structure of the cells which is carried by actin filaments will increase. Previous studies have shown that that the most tensioned elements are mainly located on the edges, periphery and basal regions of the cells [53-55]. This, in fact was observable in Figure 6-6 indicating the formation of actin rich extension in MDA-MB-231 cells in response to SAHA. The increase in the level of cytoskeletal tension in MDA-MB-231 was associated with a significant increase in both cell length and cell area. On flat surfaces the cells have enough space to extend beyond their original location and expand beyond their original morphology. Within the etched cavities, the isotropic microstructures having a variable cross sectional circular shape, pose a mechanical constraint which challenges the cell expansion and spreading. Therefore, after treatment of the cells with SAHA, MDA-MB-231 cells probe the substrate topographical pattern and stretch inside the etched cavities to reach shape stability and mechanical equilibrium. Others have also discussed that the traction forces within the cell cytoskeletal structure accompanied with the adhesion to the substrate ensure the shape stability of the cells and ultimately results in a mechanically equilibrated structure [56].

With respect to MCF10A cells, the microtubules network of the cells was not considerably altered after adding SAHA. In addition, the cells maintained their cell-cell junctions in both control and SAHA treated condition. Therefore, one can argue that the cell-cell junctions in these cells pose a key constraint which limits the expansion of the cells beyond their original morphology in response to a chemical stimuli (SAHA). Even after disruption of the microtubule network of the cells using nocodazole, the cells maintain their cell-cell junction and their adhesion pattern remained unaltered on curved surfaces [32].

The contrasting morphology and adhesion pattern of MDA-MB-231 cells compared to MCF10A cells in a co-culture system indicates that SAHA significantly modifies the cytoarchitectural response of MDA-MB-231 metastatic breast cancer cells within 3-D isotropic silicon microstructures. This reflects a cancer-specific response which can be ultimately used to

determine the pathological grade of the cells and identify biomechanical signatures in normal and diseased cells for cell separation purposes.

6.5 Conclusion

This work was focused on development of arrays of istotropically etched silicon microstructures to investigate morphological, cytoskeletal, and adhesion pattern alterations in MDA-MB-231 and MCF10A cells in a random co-culture system in response to SAHA anti-breast cancer drug. The primary findings of this work demonstrated efficient trapping and formation of colonies of both cell types inside the etched cavities. SAHA selectively alerted the chytoarchitecture in MDA-MB-231 cells which was observed through reorganization of major cytoskeletal components; actin filament and microtubules. The analysis on the morphological parameters of the cells demonstrated a significant increase in both cell area and cell length of only MDA-MB-231 cells. MDA-MB-231 cells stretched on the curved surfaces of etched cavities, while the adhesion pattern of MCF10A cells remained unaltered. The conclusion from this study is that the mode of chemically-induced attachment of the cells to the isotropic microstructures can be used as a potential marker to distinguish metastatic breast cancer cells in a background of normal breast cell types.

6.6 References

[1] R. G. Flemming, *et al.*, "Effects of synthetic micro- and nano-structured surfaces on cell behavior," *Biomaterials*, vol. 20, pp. 573-588, Mar 1999.

[2] D. E. Discher, *et al.*, "Tissue cells feel and respond to the stiffness of their substrate," *Science*, vol. 310, pp. 1139-1143, Nov 2005.

[3] C. J. Bettinger, *et al.*, "Engineering Substrate Topography at the Micro- and Nanoscale to Control Cell Function," *Angewandte Chemie-International Edition*, vol. 48, pp. 5406-5415, 2009.

[4] C. J. Bettinger, *et al.*, "Micro fabrication of poly (glycerol-sebacate) for contact guidance applications," *Biomaterials*, vol. 27, pp. 2558-2565, Apr 2006.

[5] M. D. Guillemette, *et al.*, "Surface topography induces 3D self-orientation of cells and extracellular matrix resulting in improved tissue function," *Integrative Biology*, vol. 1, pp. 196-204, Feb 2009.

[6] X. F. Walboomers, *et al.*, "Contact guidance of rat fibroblasts on various implant materials," *Journal of Biomedical Materials Research*, vol. 47, pp. 204-212, Nov 1999.

[7] X. F. Walboomers, *et al.*, "Attachment of fibroblasts on smooth and microgrooved polystyrene," *Journal of Biomedical Materials Research,* vol. 46, pp. 212-220, Aug 1999.

[8] D. Zahor, *et al.*, "Organization of mesenchymal stem cells is controlled by micropatterned silicon substrates," *Materials Science & Engineering C-Biomimetic and Supramolecular Systems,* vol. 27, pp. 117-121, Jan 2007.

[9] J. L. Charest, *et al.*, "Myoblast alignment and differentiation on cell culture substrates with microscale topography and model chemistries," *Biomaterials,* vol. 28, pp. 2202-2210, Apr 2007.

[10] E. K. F. Yim, *et al.*, "Synthetic nanostructures inducing differentiation of human mesenchymal stem cells into neuronal lineage," *Experimental Cell Research,* vol. 313, pp. 1820-1829, May 2007.

[11] J. Y. Mai, *et al.*, "A microfabricated platform probing cytoskeleton dynamics using multidirectional topographical cues," *Biomedical Microdevices,* vol. 9, pp. 523-531, Aug 2007.

[12] E. K. F. Yim, *et al.*, "Nanopattern-induced changes in morphology and motility of smooth muscle cells," *Biomaterials,* vol. 26, pp. 5405-5413, Sep 2005.

[13] T. Tzvetkova-Chevolleau, *et al.*, "The motility of normal and cancer cells in response to the combined influence of the substrate rigidity and anisotropic microstructure," *Biomaterials,* vol. 29, pp. 1541-1551, Apr 2008.

[14] H. Miyoshi, *et al.*, "Control of highly migratory cells by microstructured surface based on transient change in cell behavior," *Biomaterials,* vol. 31, pp. 8539-8545, Nov 2010.

[15] J. Lu, *et al.*, "Improved endothelial cell adhesion and proliferation on patterned titanium surfaces with rationally designed, micrometer to nanometer features," *Acta Biomaterialia,* vol. 4, pp. 192-201, Jan 2008.

[16] A. I. Teixeira, *et al.*, "Epithelial contact guidance on well-defined micro- and nanostructured substrates," *Journal of Cell Science,* vol. 116, pp. 1881-1892, May 2003.

[17] N. W. Karuri, *et al.*, "Biological length scale topography enhances cell-substratum adhesion of human corneal epithelial cells," *Journal of Cell Science,* vol. 117, pp. 3153-3164, Jul 2004.

[18] A. M. P. Turner, *et al.*, "Attachment of astroglial cells to microfabricated pillar arrays of different geometries," *Journal of Biomedical Materials Research,* vol. 51, pp. 430-441, Sep 2000.

[19] E. Rebollar, *et al.*, "Proliferation of aligned mammalian cells on laser-nanostructured polystyrene," *Biomaterials,* vol. 29, pp. 1796-1806, Apr 2008.

[20] L. Wang, *et al.*, "Influence of micro-well biomimetic topography on intestinal epithelial Caco-2 cell phenotype," *Biomaterials,* vol. 30, pp. 6825-6834, Dec 2009.

[21] S. Gerecht, *et al.*, "The effect of actin disrupting agents on contact guidance of human embryonic stem cells," *Biomaterials,* vol. 28, pp. 4068-4077, Oct 2007.

[22] C. M. Hwang, *et al.*, "Controlled cellular orientation on PLGA microfibers with defined diameters," *Biomedical Microdevices*, vol. 11, pp. 739-746, Aug 2009.

[23] P. Rajagopalan, *et al.*, "Polyelectrolyte nano-scaffolds for the design of layered cellular Architectures," *Tissue Engineering*, vol. 12, pp. 1553-1563, Jun 2006.

[24] C. S. Hajicharalambous, *et al.*, "Nano- and sub-micron porous polyelectrolyte multilayer assemblies: Biomimetic surfaces for human corneal epithelial cells," *Biomaterials*, vol. 30, pp. 4029-4036, Aug 2009.

[25] D. S. Gray, *et al.*, "Repositioning of cells by mechanotaxis on surfaces with micropatterned Young's modulus," *Journal of Biomedical Materials Research Part A*, vol. 66A, pp. 605-614, Sep 2003.

[26] C. M. Lo, *et al.*, "Cell movement is guided by the rigidity of the substrate," *Biophysical Journal*, vol. 79, pp. 144-152, Jul 2000.

[27] B. Weigelt and M. J. Bissell, "Unraveling the microenvironmental influences on the normal mammary gland and breast cancer," *Seminars in Cancer Biology*, vol. 18, pp. 311-321, Oct 2008.

[28] N. Gjorevski and C. M. Nelson, "Endogenous patterns of mechanical stress are required for branching morphogenesis," *Integrative Biology*, vol. 2, pp. 424-434, 2010.

[29] C. M. Nelson, *et al.*, "Three-dimensional lithographically defined organotypic tissue arrays for quantitative analysis of morphogenesis and neoplastic progression," *Nature Protocols*, vol. 3, pp. 674-678, 2008.

[30] M. Nikkhah, *et al.*, "Attachment and response of human fibroblast and breast cancer cells to three dimensional silicon microstructures of different geometries," *Biomedical Microdevices*, vol. 11, pp. 429-441, Apr 2009.

[31] M. Nikkhah, *et al.*, "Cytoskeletal role in differential adhesion patterns of normal fibroblasts and breast cancer cells inside silicon microenvironments," *Biomedical Microdevices*, vol. 11, pp. 585-595, Jun 2009.

[32] M. Nikkhah, *et al.*, "The cytoskeletal organization of breast carcinoma and fibroblast cells inside three dimensional (3-D) isotropic silicon microstructures," *Biomaterials*, vol. 31, pp. 4552-4561, Jun 2010.

[33] J. S. Strobl, *et al.*, "Actions of the anti-cancer drug suberoylanilide hydroxamic acid (SAHA) on human breast cancer cytoarchitecture in silicon microstructures," *Biomaterials*, vol. 31, pp. 7043-7050, Sep 2010.

[34] F. Gentile, *et al.*, "Cells preferentially grow on rough substrates," *Biomaterials*, vol. 31, pp. 7205-7212, Oct 2010.

[35] C. H. Choi, *et al.*, "Cell growth as a sheet on three-dimensional sharp-tip nanostructures," *Journal of Biomedical Materials Research Part A*, vol. 89A, pp. 804-817, Jun 2009.

[36] A. Ranella, *et al.*, "Tuning cell adhesion by controlling the roughness and wettability of 3D micro/nano silicon structures," *Acta Biomaterialia*, vol. 6, pp. 2711-2720, Jul 2010.

[37] K. Gantz, *et al.*, "Development of a comprehensive model for RIE-lag-based three-dimensional microchannel fabrication," *Journal of Micromechanics and Microengineering,* vol. 18, Feb 2008.

[38] P. Zellner, *et al.*, "A fabrication technology for three-dimensional micro total analysis systems," *Journal of Micromechanics and Microengineering,* vol. 20, Apr 2010.

[39] C. H. Choi, *et al.*, "Cell interaction with three-dimensional sharp-tip nanotopography," *Biomaterials,* vol. 28, pp. 1672-1679, Mar 2007.

[40] M. Nikkhah, *et al.*, "Evaluation of the Influence of Growth Medium Composition on Cell Elasticity," *Journal of Biomechanics,* vol. In Press, 2010.

[41] A. R. Martirosyan, *et al.*, "Differentiation-inducing quinolines as experimental breast cancer agents in the MCF-7 human breast cancer cell model," *Biochemical Pharmacology,* vol. 68, pp. 1729-1738, Nov 2004.

[42] M. Nikkhah, *et al.*, "Development of a Three Dimensional (3-D) Silicon Micro-Array for Cell Capturing," presented at the 9th IEEE Conference on Sensors (Sensors '10), Waikoloa, HI, 2010.

[43] A. A. Lane and B. A. Chabner, "Histone deacetylase inhibitors in cancer therapy," *Journal of Clinical Oncology,* vol. 27, pp. 5459-68, Nov 2009.

[44] V. M. Richon, *et al.*, "Development of vorinostat: current applications and future perspectives for cancer therapy," *Cancer Letters,* vol. 280, pp. 201-10, Aug 2009.

[45] Q. Zhou, *et al.*, "Screening for therapeutic targets of vorinostat by SILAC-based proteomic analysis in human breast cancer cells," *Proteomics,* Jan 2010.

[46] Y. S. Torisawa, *et al.*, "Multi-channel 3-D cell culture device integrated on a silicon chip for anticancer drug sensitivity test," *Biomaterials,* vol. 26, pp. 2165-72, May 2005.

[47] A. Buda and M. Pignatelli, "Cytoskeletal network in colon cancer: from genes to clinical application," *International Journal of Biochemistry & Cell Biology,* vol. 36, pp. 759-765, May 2004.

[48] U. Lindberg, *et al.*, "The microfilament system and malignancy," *Seminars in Cancer Biology,* vol. 18, pp. 2-11, Feb 2008.

[49] Q. S. Li, *et al.*, "AFM indentation study of breast cancer cells," *Biochemical and Biophysical Research Communications,* vol. 374, pp. 609-613, Oct 2008.

[50] C. Rotsch and M. Radmacher, "Drug-induced changes of cytoskeletal structure and mechanics in fibroblasts: An atomic force microscopy study," *Biophysical Journal,* vol. 78, pp. 520-535, Jan 2000.

[51] J. Guck, *et al.*, "Optical deformability as an inherent cell marker for testing malignant transformation and metastatic competence," *Biophysical Journal,* vol. 88, pp. 3689-3698, May 2005.

[52] D. E. Ingber, "Cellular tensegrity: defining new rules of biological design that govern the cytoskeleton," *Journal of Cell Science,* vol. 104, pp. 613-627, Mar 1993.

[53] B. Maurin, *et al.*, "Mechanical model of cytoskeleton structuration during cell adhesion and spreading," *Journal of Biomechanics*, vol. 41, pp. 2036-2041, 2008.

[54] V. M. Laurent, *et al.*, "Partitioning of cortical and deep cytoskeleton responses from transient magnetic bead twisting," *Annals of Biomedical Engineering*, vol. 31, pp. 1263-1278, Nov 2003.

[55] S. Wendling, *et al.*, "Stiffening response of a cellular tensegrity model," *Journal of Theoretical Biology*, vol. 196, pp. 309-325, Feb 1999.

[56] N. Wang, *et al.*, "Cell prestress. I. Stiffness and prestress are closely associated in adherent contractile cells," *American Journal of Physiology. Cell Physiology*, vol. 282, pp. C606-C616, Mar 2002.

7 Chapter Seven: Evaluation of the Influence of Growth Medium Composition on Cell Elasticity

This chapter is produced from [1] with permission from Elsevier.

M. Nikkhah, et al., "Evaluation of the Influence of Growth Medium Composition on Cell Elasticity" Journal of Biomechanical, In Press.

7.1 Introduction

With the advances in micro and nanofabrication technologies, it has been possible to probe mechanical properties of a single cell. To date, several techniques such as optical stretchers [2], scanning force microscopy (SFM) [3, 4], micropipette aspiration [5], and atomic force microscopy (AFM) [6-13] have been used to measure deformation characteristics of normal and malignant cells.

Among different types of cancer, breast cancer remains the second leading cause of cancer death in American women. A number of studies have focused on exploring the biomechanical properties of non-malignant and malignant breast cells using techniques such as AFM [10], optical stretcher [2], and microfluidic systems [14, 15] and have established that cancer cells are generally softer than their normal counterparts. While providing valuable data, all of the previous studies have compared the biomechanical properties of malignant and non-malignant cells grown in different media because typically these cells are propagated in media which differ in composition with respect to serum and growth factors. None of the previous work has addressed the influence of growth medium composition on cell mechanics.

The focus of this work is to establish whether the biomechanical properties of the cells (i.e. cellular elasticity) are responsive to the composition of the growth medium. We utilized AFM method to address the variation in the elasticity of non-malignant, non-metastatic MCF10A and highly metastatic MDA-MB-231 breast cells grown in different growth media. We performed controlled studies to test the effect of the serum percentage, EGF, and culture medium base (DMEM:F12 or RPMI) on the elasticity of the cells.

7.2 Materials and methods

7.2.1 Cell culture preparation

Both MCF10A and MDA-MB-231 were purchased from American Type Culture Collection (ATCC, Manassas, VA). MDA-MB-231 cells were maintained in plastic T-75 cm^2 culture flasks in RPMI (Mediatech, Manassas, VA) culture medium which contained 10% fetal bovine serum (FBS) (Atlanta Biologicals, Lawrenceville, GA), penicillin-streptomycin (100 Units/ml) (Mediatech) and 2.5 mM L-glutamine (Mediatech). MCF10A were grown in plastic T-75 cm^2 culture flasks using DMEM:HamsF12 (50:50) (DMEM:F12) (Mediatech), 5% horse serum (HS) (Atlanta Biologicals), 20 ng/ml Epidermal Growth Factor (EGF) (Sigma, St. Louis, MO), 100 ng/ml Cholera Toxin (CT) (Sigma), 10 ug/ml Insulin (INS) (Sigma), 500 ng/ml hydrocortisone(HC) (Sigma), and 2.5 mM L-glutamine (Mediatech). Cells were grown at 37 °C in humidified 5% CO_2.

For AFM experiments, cells were seeded with a density of 3×10^4 cells/ml on 25 mm round glass coverslips (VWR, West Chester, PA) coated with 100 µg/ml collagen type IV (Sigma). Cells were grown for 24 h and in one of the five different growth media detailed in Table 7-1. The cells' passage number was maintained between 3 and 20.

Table 7-1 Specifications of the growth media used to perform AFM experimentations.

Growth Medium #	Components
Medium No. 1 (M1)	RPMI, 10% FBS
Medium No. 2 (M2)	RPMI, 5% FBS
Medium No. 3 (M3)	DMEM:F12, 5% FBS
Medium No. 4 (M4)	RPMI, 5% FBS, 20 ng/ml EGF
Medium No. 5 (M5)	DMEM:F12, 5% HS, 20 ng/ml EGF, 100 ng/ml CT, 0.01 mg/ml INS, 500 ng/ml HC

Abbreviations: FBS: Fetal Bovine Serum, HS: Horse Serum EGF: Epidermal Growth Factor, CT: Cholera Toxin, INS: Insulin, HC: hydrocortisone. Note: Glutamine and Penicillin/Streptomycin was added to all the media.

7.2.2 Atomic force microscopy

All the AFM measurements were carried out using MFP-3D-Bio (Asylum Research, Santa Barbara CA) combined with an optical and an inverted fluorescence microscope (Olympus IX71, Tokyo, Japan). Soft V-shaped silicon nitride cantilevers, TR400PSA (Olympus**,** Tokyo, Japan), with a nominal length of 200 µm and a spring constant of 0.02 N/m were used in this study. The spring constant was experimentally measured using thermal noise fluctuations. A glass sphere (Duke Scientific, Palo Alto, California) with a nominal diameter of ~10 µm was attached to the cantilever tip to reduce any nonlinearity in deforming stress and to avoid damaging the sample (Figure 7-1, top right inset). Two-part epoxy (Miller Stephenson, Sylmar, CA) was used to attach the glass sphere to the cantilever tip. The epoxy was cured overnight at room temperature followed by cleaning the cantilever for 20 minutes using UV light. Optical microscopy (HIROX KH-7700, Hackensack, NJ) was used to measure the exact diameter of the glass sphere attached to the tip. All the AFM measurements were carried out using standard fluid cell (Asylum Research) in room temperature. After plating the cells, 20 mM HEPES (Sigma) was added to the cell culture medium to maintain a physiological pH of 7.2 during the experimentation. The AFM measurements were performed at the center of the cell nucleus with a tip velocity of 0.5 µm/s.

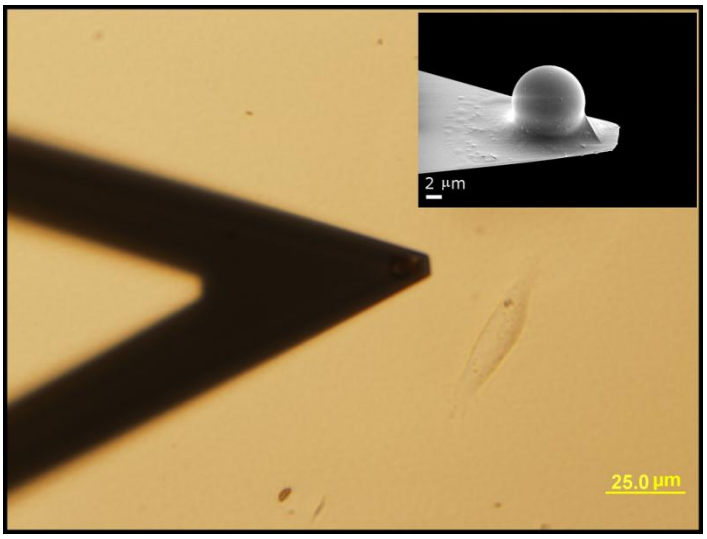

Figure 7-1 Single cell indentation experiment using AFM. Soft V-shaped silicon nitride cantilevers, TR400PSA (Olympus) used for force measurements. Top right inset shows the SEM image of a spherical glass bead with a diameter of ~ 10 µm attached to the cantilever tip.

7.2.3 Data analysis

In order to define the deformability of cells, their Young's modulus was defined using the Hertz's model [16, 17]. For a cantilever with a spherical tip:

$$F = \frac{4\sqrt{R}}{3(1-\nu^2)} E\delta^{3/2} \tag{7-1}$$

where F is the applied force, δ is the indentation depth, R is the radius of the spherical glass bead attached on the tip (Figure 7-1(a)), and E is the Young's modulus. We used the linear version in δ of the Hertz's model to define the elasticity and initial contact point with the cell as explained before [8, 12, 18]:

$$F^{2/3} = \left[\frac{4\sqrt{R}}{3\left(1-\nu^2\right)}E\right]^{2/3}\left(z-d\right) - \left[\frac{4\sqrt{R}}{3\left(1-\nu^2\right)}E\right]^{2/3}\left(z_0-d_0\right) \tag{7-2}$$

The Young's modulus can be directly calculated from the linear slope and the contact point $\left(z_0 - d_0\right)$ can be calculated from the intercept of equation (7-2). In elasticity calculations, ν is assumed to be 0.5. The Young's moduli of the cells were determined within an indentation range of 196±7 nm.

All data analysis was performed using MATLAB 7.0 software (MathWorks, Natick, MA). Two sample independent t-tests were performed using Graph Pad Prism 5.0 statistical software (GraphPad Software Inc., La Jolla, CA) to compare the cells' Young's modulus in different growth media.

7.3 Results

The Hertz's model fitted well to the experimental data for both cell types to obtain their Young's modulus ($0.90 \leq R^2 \leq 0.99$). Population elasticity (Young's modulus, E) of MDA-MB-231 was not normally distributed in any of the growth media (Table 7-1) according to the Shapiro-Wilks test, and was best described by log-normal distributions. MDA-MB-231 cells displayed a narrow peak modulus close to 0.2 kPa which was not significantly altered by a change in growth medium composition (Figure 7-2). However, the average Young's modulus of the cells in RPMI + 5% FBS growth medium decreased by 18% (0.41±0.22 kPa) as compared with cells in RPMI +

10% FBS. Interestingly, the addition of EGF to RPMI + 5% FBS growth medium (Table 7-1, M4) further reduced the average Young's modulus of the MDA-MB-231 cells by 12% to the value of 0.36±0.20 kPa. When grown in medium typically used for MCF10A cells containing additional supplements of CT, INS and HC, (Table 7-1, M5), the average Young's modulus of the cells was measured to be 0.37±0.25 kPa. Substitution of the RPMI culture medium base with DMEM:F12 had no effect on the elasticity of MDA-MB-231 cells (Figure 7-2 and Table 7-2). Statistical analysis performed on log-transformed elasticity data showed that the variation in the Young's modulus of MDA-MB-231 cells among these five media was not significant.

MCF10A cells exhibited a broad peak modulus compared to the MDA-MB-231 cells in all different growth media. Except in DMEM + 5% FBS medium, the population elasticity of MCF10A cells was best described by log-normal distribution (Figure 7-3). The variation and dependence of the Young's modulus of the MCF10A cells in response to different growth media was similar to MDA-MB-231 cells; MCF10A cells became softer (10% reduction in average Young's modulus) in RPMI + 5% FBS growth medium which contained less serum (5%) as compared to RPMI + 10% FBS medium. Adding EGF to RPMI + 5% FBS medium (M4) further reduced the average Young's modulus of the cells by 12% to 0.88±0.57 kPa. The average Young's modulus of the MCF10A cells in M5 (ATCC recommended formulation for MCF10A cells) was measured to be 0.72±0.54 kPa. This reveals that the elasticity of these cells is more responsive to the supplements present in M5, EGF, CT, HC and INS, when compared to MDA-MB-231 cells (Figure 7-3 and Table 7-2). Statistical analysis showed that among the five media, the Young's modulus of MCF10A cells significantly reduced ($p<0.002$) when grown in medium M5 compared to medium M1. Pair-wise comparisons of MDA-MB-231 elasticity with that of MCF10A cells in identical medium compositions confirmed that in every case, the MDA-MB-231 cells were significantly softer ($p<0.0001$) than the MCF10A cells (Figure 7-4). In addition, the elasticity of MDA-MB-231 cells cultured in standard MDA-MB-231 culture medium (M1), was significantly lower ($p<0.004$) than MCF10A cells cultured in standard MCF10A culture medium (M5). Table 7-2 shows the summary of the elasticity measurements of MDA-MB-231 and MCF10A cells in different growth media.

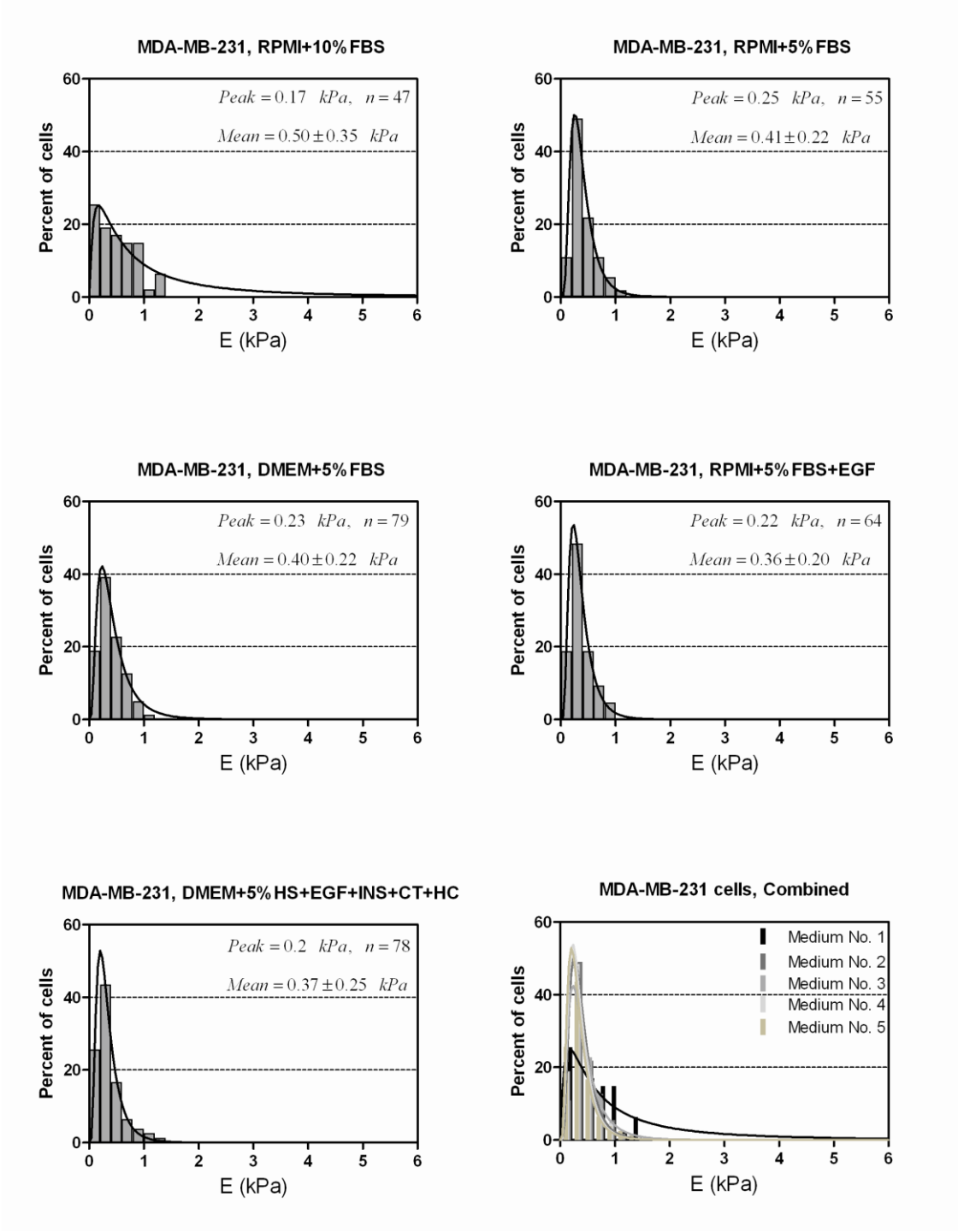

Figure 7-2 Young's modulus distribution of the MDA-MB-231 cells seeded in different growth media. Population elasticity of MDA-MB-231 at all the growth media were best fit by log-normal distributions. E: Young's modulus, n: number of the cells analyzed. ± Values denote the standard deviation.

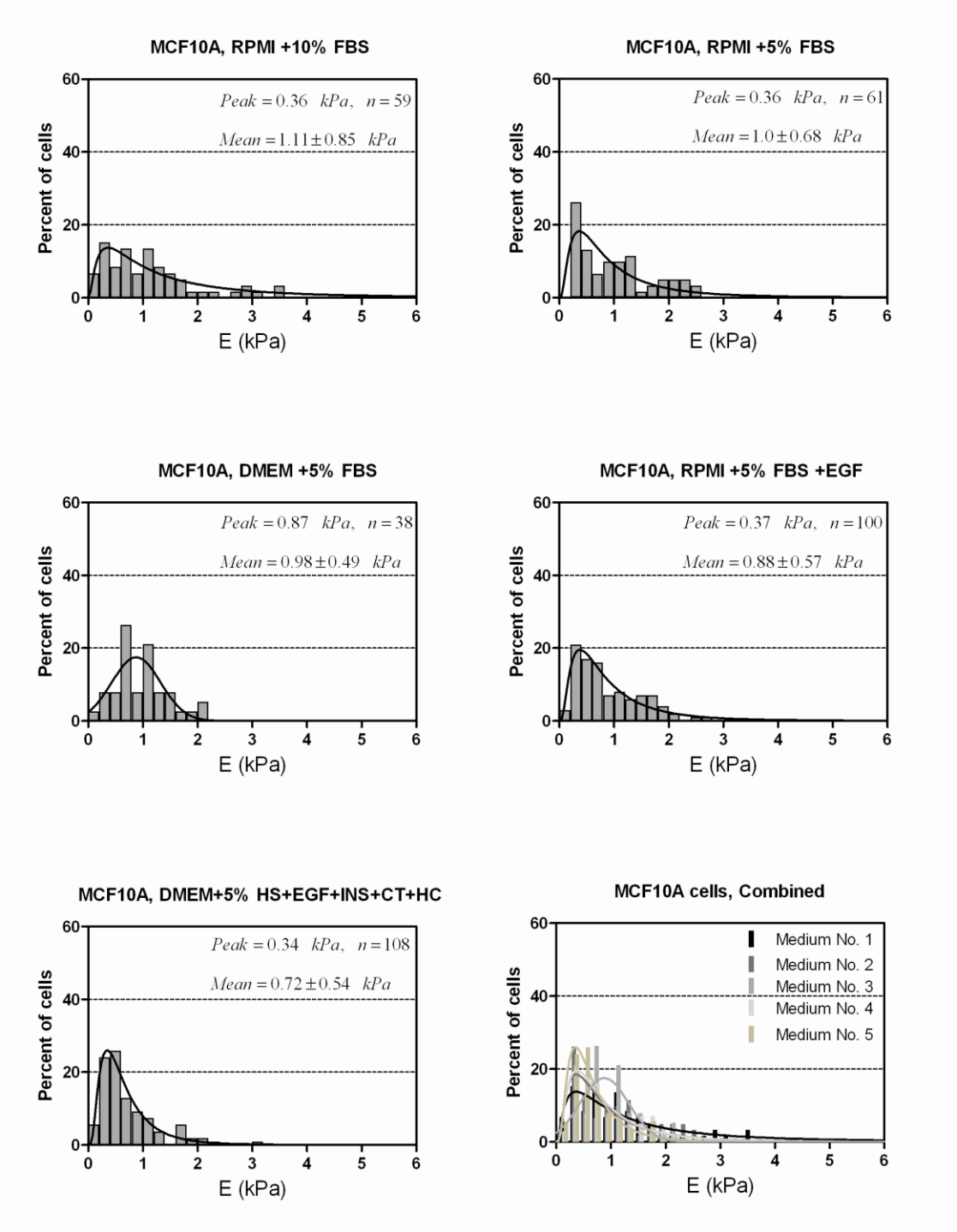

Figure 7-3 Young's modulus distribution of the MCF10A cells seeded in the 5 proposed growth media. Except in DMEM+5%FBS medium, population elasticity of MCF10A cells were best fit by log-normal distributions. MCF10A cells exhibited a broad peak modulus compared to the MDA-MB-231 cells in all the growth media. E: Young's modulus, n: number of the cells analyzed. ± Values denote the standard deviation.

Table 7-2 Elastic parameters for non-malignant, non-metastatic MCF10A and highly metastatic MDA-MB-231 breast cells in different growth media.

	n	E (kPa)		Indentation range (nm)
MDA-MB-231				
M1: RPMI+10%FBS	47	0.50±0.35		200±3
M2: RPMI+5%FBS	55	0.41±0.22		200±1
M3: DMEM+5%FBS	79	0.40±0.22		200±0.2
M4: RPMI+5%FBS+EGF	64	0.36±0.20		200±0.1
M5: DMEM+5%HS+EGF+CT+INS+HC	78	0.37±0.25		200±1
MCF10A				
M1: RPMI+10%FBS	59	1.11±0.85		182±34
M2: RPMI+5%FBS	61	1.0±0.68		196±20
M3: DMEM+5%FBS	38	0.98±0.49	**	199±0.2
M4: RPMI+5%FBS+EGF	100	0.88±0.57		187±26
M5: DMEM+5%HS+EGF+CT+INS+HC	108	0.72±0.54		196±17

E: Elastic Modulus, n: number of the cells analyzed. Data are presented in mean ± standard deviation (**p<0.002, comparing M1 to M5).

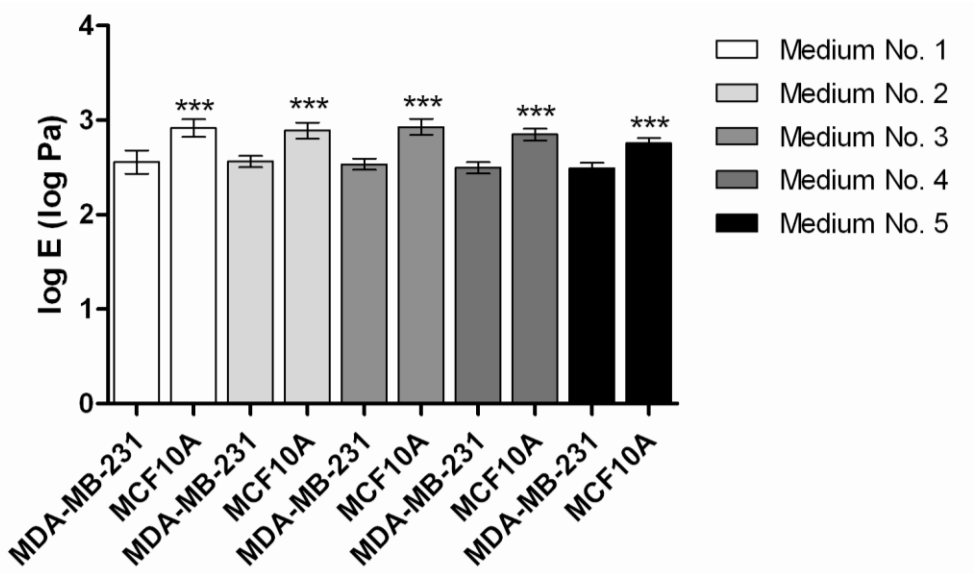

Figure 7-4 The log-transformed average Young's modulus of the MCF10A and MDA-MB-231 cells. MDA-MB-231 cells are significantly (*p<0.0001) softer than non-malignant MCF10A cells under all the culture medium conditions tested. E: Young's modulus. Errors bars represent the 95% confidence interval.**

7.4 Discussion

In this work, we presented the effect of the composition of the growth medium on elasticity measurement of non-malignant MCF10A and malignant MDA-MB-231 human breast cells. Previous studies typically compared the biomechanical properties of non-malignant and malignant breast cells grown in the medium usually used for cell propagation [2, 10, 14, 15], without considering any possible influence of the growth medium composition on cellular biomechanics. We found that reducing the serum percentage from 10% to 5% as well as supplementation of the culture medium with EGF reduced the elasticity of both MDA-MB-231 and MCF10A cells. Though these responses did not reach statistical significance, they were of a magnitude that could be of biological significance. MCF10A cells cultured in medium M5, the ATCC recommended medium composition, were significantly softer than identical cells cultured in the more generic medium M1. It is important to note that our results support what others have reported previously, that malignant MDA-MB-231 cells are significantly softer ($p<0.0001$) than non-malignant MCF10A cells under all the culture medium conditions tested.

It is well established that serum components such as lysophosphatidic acid (LPA) activate the small GTP-binding protein Rho which subsequently promote focal adhesions and actin stress fiber formation [19, 20] that impact the overall cellular elasticity [21, 22]. Hence LPA is one of perhaps multiple serum components that impact the biomechanical properties of the cells. We were unable to compare elasticity of the cells in HS vs. FBS because the MDA-MB-231 cells failed to attach to the substrate when HS was substituted for FBS in RPMI. This behavior suggests biologically significant differences exist between FBS and HS, consistent with the documented enrichment of FBS with growth factors (Atlanta Biologicals product data sheets).

With respect to EGF, its ability to stimulate MDA-MB-231 cell chemotaxis and cell migration is well documented before [23, 24]. The associated biochemical changes such as integrin beta-1 clustering in the cell membrane and protein phosphorylation events, which promote actin polymerization and cell adhesion to the substrate [25], reflect EGF-induced cytoskeletal reorganization within migratory cells. Hence it is logical to find that cellular elasticity is altered when cells are cultured in the presence of added EGF. It is surprising that this aspect of cellular biomechanics has not been more thoroughly investigated.

Overall, our work is consistent with previous studies showing the malignant cells are significantly softer than non-malignant ones [2, 10, 14]. However the current study establishes the need to consider the possible impact of the composition of the cell growth medium on elasticity measurements of the cells while evaluating and comparing the biomechanical properties of different cell lines.

7.5 References

[1] M. Nikkhah, *et al.*, "Evaluation of the Influence of Growth Medium Composition on Cell Elasticity," *Journal of Biomechanics*, vol. In Press, 2010.

[2] J. Guck, *et al.*, "Optical deformability as an inherent cell marker for testing malignant transformation and metastatic competence," *Biophysical Journal*, vol. 88, pp. 3689-3698, May 2005.

[3] M. Lekka, *et al.*, "Elasticity of normal and cancerous human bladder cells studied by scanning force microscopy," *European Biophysics Journal*, vol. 28, pp. 312-316, 1999.

[4] S. Leporatti, *et al.*, "Cytomechanical and topological investigation of MCF-7 cells by scanning force microscopy," *Nanotechnology*, vol. 20, Feb 2009.

[5] K. A. Ward, *et al.*, "Viscoelastic properties of transformed cells: role in tumor cell progression and metastasis formation," *Biorheology*, vol. 28, pp. 301-13, 1991.

[6] S. E. Cross, *et al.*, "Nanomechanical analysis of cells from cancer patients," *Nature Nanotechnology*, vol. 2, pp. 780-783, Dec 2007.

[7] S. E. Cross, *et al.*, "AFM-based analysis of human metastatic cancer cells," *Nanotechnology*, vol. 19, Sep 2008.

[8] E. M. Darling, *et al.*, "Viscoelastic properties of human mesenchymally-derived stem cells and primary osteoblasts, chondrocytes, and adipocytes," *Journal of Biomechanics*, vol. 41, pp. 454-464, 2008.

[9] E. C. Faria, *et al.*, "Measurement of elastic properties of prostate cancer cells using AFM," *Analyst*, vol. 133, pp. 1498-1500, 2008.

[10] Q. S. Li, *et al.*, "AFM indentation study of breast cancer cells," *Biochemical and Biophysical Research Communications*, vol. 374, pp. 609-613, Oct 2008.

[11] S. Iyer, *et al.*, "Atomic force microscopy detects differences in the surface brush of normal and cancerous cells," *Nature Nanotechnology*, vol. 4, pp. 389-393, Jun 2009.

[12] M. Nikkhah, *et al.*, "The cytoskeletal organization of breast carcinoma and fibroblast cells inside three dimensional (3-D) isotropic silicon microstructures," *Biomaterials*, vol. 31, pp. 4552-4561, Jun 2010.

[13] J. S. Strobl, *et al.*, "Actions of the anti-cancer drug suberoylanilide hydroxamic acid (SAHA) on human breast cancer cytoarchitecture in silicon microstructures," *Biomaterials,* vol. 31, pp. 7043-7050, Sep 2010.

[14] Y. C. Kim, *et al.*, "Biomechanical analysis of cancerous and normal cells based on bulge generation in a microfluidic device," *Analyst,* vol. 133, pp. 1432-1439, 2008.

[15] H. W. Hou, *et al.*, "Deformability study of breast cancer cells using microfluidics," *Biomedical Microdevices,* vol. 11, pp. 557-564, Jun 2009.

[16] H. Hertz, "On the elastic contact of elastic solids," *J. Reine Angew. Math,* vol. 92, pp. 156–171, 1881.

[17] S. P. Timoshenko and J. N. Goodier, *Theory of Elasticity,* 3 rd ed. New York: McGraw-Hill Companies, 1970.

[18] S. L. Guo and B. B. Akhremitchev, "Packing density and structural heterogeneity of insulin amyloid fibrils measured by AFM nanoindentation," *Biomacromolecules,* vol. 7, pp. 1630-1636, May 2006.

[19] X. D. Ren, *et al.*, "Regulation of the small GTP-binding protein Rho by cell adhesion and the cytoskeleton," *Embo Journal,* vol. 18, pp. 578-585, Feb 1999.

[20] M. ChrzanowskaWodnicka and K. Burridge, "Rho-stimulated contractility drives the formation of stress fibers and focal adhesions," *Journal of Cell Biology,* vol. 133, pp. 1403-1415, Jun 1996.

[21] R. Ananthakrishnan, *et al.*, "Quantifying the contribution of actin networks to the elastic strength of fibroblasts," *Journal of Theoretical Biology,* vol. 242, pp. 502-516, Sep 2006.

[22] C. Rotsch and M. Radmacher, "Drug-induced changes of cytoskeletal structure and mechanics in fibroblasts: An atomic force microscopy study," *Biophysical Journal,* vol. 78, pp. 520-535, Jan 2000.

[23] J. T. Price, *et al.*, "Epidermal growth factor promotes MDA-MB-231 breast cancer cell migration through a phosphatidylinositol 3 '-kinase and phospholipase C-dependent mechanism," *Cancer Research,* vol. 59, pp. 5475-5478, Nov 1999.

[24] S. J. Wang, *et al.*, "Differential effects of EGF gradient profiles on MDA-MB-231 breast cancer cell chemotaxis," *Experimental Cell Research,* vol. 300, pp. 180-189, Oct 2004.

[25] J. N. Wang, *et al.*, "Reduction of Akt2 expression inhibits chemotaxis signal transduction in human breast cancer cells," *Cellular Signalling,* vol. 20, pp. 1025-1034, Jun 2008.

8 Chapter Eight: Summary and Outlook

8.1 Summary

The focus of this dissertation was to engineer, control, and investigate cell-substrate interaction using well-established micro and nanotechnology techniques. The goal was to conduct comprehensive analysis on the behavior of the key cellular components in human breast tumor microenvironment (fibroblast cells, normal epithelial and highly metastatic breast cells) on precisely designed microstructures to identify cell biomechanical signatures which discriminate between normal and cancerous cells. The outcome of this research can be used to create substrates and cell-based biosensors for cell segregation and diagnostics purposes. Three different generations of isotropic microstructures comprised of curved surfaces were developed using a single-mask, single-etch-step fabrication process. In addition, atomic force microscopy (AFM) was employed to measure cell elasticity and to correlate the cell adhesion characteristics on the isotropic microstructures to their biomechanical properties. This dissertation was divided into four major sections:

The first section (Chapter 2) was focused on development of the first generation of the isotropic silicon microstructures to study the adhesion, growth and trapping behavior of HS68 and MDA-MB-231 cells. The substrates consisted of arrays of isotropic microchambers connected with micro-channels. Our findings demonstrated that breast cancer cells (MDA-MB-231) and fibroblasts had distinct attachment and adhesion properties on the developed microstructures. The breast cancer cells deformed on the curved sidewalls; however, fibroblasts stretched and elongated their cytoskeleton and actin filaments inside the microchambers. Statistical analysis revealed that fibroblast cells grew on both flat silicon surfaces and inside the microchambers regardless of microchambers depth. However, the localization of breast cancer cells on the same substrates was dependent on their depth. After 72 hours in culture, the ratio of the number of MDA-MB-231 cells on flat surfaces compared to the cells inside the etched features was significantly decreased as a function of microchambers' depth; for microchambers having depth of 88 µm, less than 5% of the breast cancer cells grew on the flat surfaces. This behavior was sustained for 120 hours, the longest time point examined.

The second section (Chapters 3 and 4) of this dissertation was devoted to development of the second generation of isotropic microstructures comprised of star and circular-shape microchambers for detailed analysis on adhesion pattern and cytoskeletal organization of HS68, MDA-MB-231 and MCF10A cells. We specifically looked into the role of major cytoskeletal components namely actin filaments and microtubules as well as focal adhesion proteins (vinculin) and cell biomechanical properties in adhesion behavior of the cells inside the 3-D microstructures. Similar to the previous generation, HS68 fibroblasts typically stretched and formed vinculin-rich focal adhesions at anchoring sites inside the etched cavities. In contrast, MCF10A and MDA-MB-231 cells adopted the curved surfaces of isotropic microstructures and exhibited more diffuse vinculin cytoplasmic staining in addition to vinculin localized in focal adhesions. Our primary findings demonstrated that treatment of the fibroblast cell with cytochalasin D significantly altered their morphology and adhesion inside the etched features. The adhesion of cancer cells to the curved microstructures was not significantly altered after disrupting of their cytoskeleton using cytochalasin D. The measurement of cells' elasticity using AFM revealed that HS68 cells are significantly stiffer than MCF10A and MDA-MB-231 cells. Furthermore, upon microtubule disruption with nocodazole, fibroblasts no longer stretched, but adhesion of MCF10A and MDA-MB-231 remained unaltered within the etched features. Within this section we demonstrated that cytoskeletal tension (prestress) and microtubules in HS68 cells, cell-cell junctions and adhesion strength to the substrate in MCF10A cells, and deformability and soft cytoskeletal structure in MDA-MB-231 cells, are the dominant factors defining their behavior inside the isotropic microstructure. The result of the first two sections confirmed that the 3-D microstructures have the potential to probe cytoskeletal-based differences between healthy and diseased cells.

In the third section (Chapter 5), we reported the effects of an experimental anti-breast cancer drug, SAHA, on the cytoarchitecture and adherence of MDA-MB-231 cells on flat silicon surfaces and inside 3-D isotropic microstructures. The results of this section indicated that there was a marked expansion of the microtubule network of the cells in response to SAHA which was associated with a significant increase in both cell area and cell length. SAHA also decreased the cells nuclear-to-cytoplasmic area (N/C) ratio. AFM analysis showed that there was no significant change in cellular elasticity over the nuclear region in response to SAHA. The alteration in

cytoarchitecture produced by SAHA was associated with changes in the mode of adhesion of the cells in silicon microstructures. In contrast to control cells which conformed to the microstructures, SAHA caused cells to stretch and attach to the microstructures through actin-rich cell extensions.

The fourth section (Chapter 6) of this dissertation was focused on development of the third generation of isotropic geometries for comprehensive analysis on cell trapping and drug responsiveness (SAHA) of MDA-MB-231 in a random co-culture with normal MCF10A cells. The result of this section demonstrated efficient trapping and formation of colonies of both cell types inside the etched cavities after seeding the cells on the substrates. SAHA caused cytoskeletal reorganization only in MDA-MB-231 metastatic cells which was associated with a significant increase in cell length and cell area. Metastatic cells suspended and produced actin filaments that raised them above the substrate and enabled them to span the 3-D microstructures. Taken together, the studies performed in the third and fourth sections, led us to the point that the mode of cell attachment within the 3-D isotropic silicon microarrays might serve as a surrogate marker of cytoarchitectural features in breast cancer cells that reflect their responses to drugs and ability to metastasize. The highly innovative 3-D silicon microstructures might have applicability in identifying the presence of metastatic cancer cells in a mixture of normal cells based upon SAHA-induced alterations which occur selectively in the metastatic cells.

In addition to the four major sections of this dissertation, in chapter 7 we investigated the variation in the Young's modulus of MCF10A and MDA-MB-231 breast cells seeded in five different growth media under controlled experimental conditions. Our findings demonstrated that the average Young's modulus of MDA-MB-231 cells was significantly lower than the mean Young's modulus of MCF10A cells when compared in identical medium compositions. However, we found that growth medium composition affected the elasticity of MCF10A and MDA-MB-231 cells. The average Young's modulus of both cell lines decreased by 10-18% upon reducing the serum percentage and adding epidermal growth factor to the medium. However, the elasticity of MCF10A was significantly more responsive than MDA-MB-231 cells to the medium composition supplemented with epidermal growth factor, cholera toxin, insulin, and hydrocortisone, which is recommended for routine cultivation of MCF10A cells. The results of

this chapter highlighted the need to take the effect of cell culture medium composition into consideration when interpreting elasticity measurements in cells grown in different media.

8.2 Significance and contributions

Most of the previous studies on cell-substrate interactions have been mainly focused on tissue engineering applications or development of implantable devices. A number of studies have also used the principle of cell-substrate interactions for fundamental biological studies. Previously reported substrates fabricated in PDMS or silicon, were mostly anisotropic having microstructures with vertical sidewalls. To the best of our knowledge, this is the first attempt in development of 3-D isotropic microstructures with curved surfaces to perform in-depth cell-substrate interaction studies on normal and cancerous cells. We conducted our studies in static culture condition on the 3-D substrates without the presence of any chemical gradient, flow shear stress or external fields (electrical, magnetic, etc.) Our major contributions can be summarized in: development of highly innovative 3-D MEMS-based isotropic microstructures, studying the cytoskeletal organization, adhesion pattern, morphology, growth and trapping mechanism of normal and diseased cells in a 3-D architecture, investigation of anti-cancer drug responsiveness of cancerous cells on the 3-D substrates separately and in co-culture with normal cells, and finally exploring the effect of the growth medium composition on cell elasticity using AFM technique. The research efforts and extensive studies reported in this dissertation built a foundation for evaluating the applicability of the 3-D microstructures for cell separation and development of cell-based biosensors for early cancer diagnosis purposes. Figure 8-1 shows a diagram which maps the major contribution of this work.

This interdisciplinary research has been performed through collaboration with Virginia College of Osteopathic Medicine (VCOM) (2006-2009) and the Department of Human Nutrition, Food and Exercise at Virginia Tech. The scientific production of this work includes five published peer-reviewed original research journal articles, one journal article in submission, and eight papers in peer-reviewed conference proceedings. Table 8-1 summarizes the major outcomes of this research during the course of completion of the dissertation.

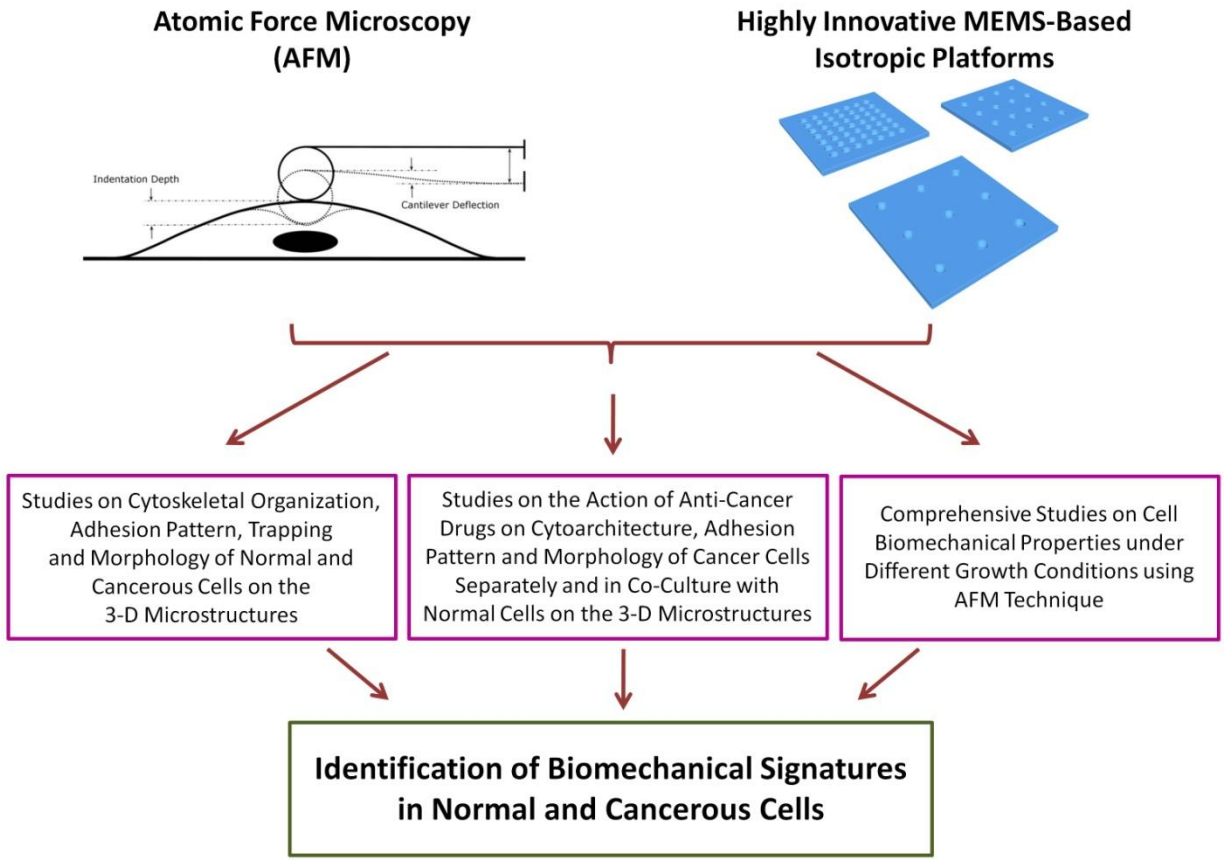

Figure 8-1 An illustrative image showing the major contributions of this dissertation

Table 8-1 Overview of the major publications and outcome of this research effort

Type of Production	Name	Metric	Publisher
Journal Article (2 papers)*	Biomaterials	7.3 Impact Factor	Elsevier
Journal Article (2 papers)	Biomedical Microdevices	3.3 Impact Factor	Springer
Journal Article	Journal of Biomechanics	2.6 Impact Factor	Elsevier
Conference Paper (4 papers)	µTAS Conference	35% Acceptance	The Chemical and Biological Microsystems Society
Conference Paper	IEEE Sensors Conference	35% Acceptance	IEEE
Conference Paper	ASME IMECE	65% Acceptance	ASME
Conference Paper (2 papers)	ASME NEMB	65% Acceptance	ASME

*One paper featured on the 2010 Biomaterials Journal leading page.

8.3 Project challenges

This interdisciplinary project was completed in collaboration with several researchers and departments including: the Bradley Department of Electrical and Computer Engineering, Department of Chemical Engineering, Department of Human Nutrition, Food and Exercise, and Edward Via Virginia College of Osteopathic Medicine (VCOM). One of my major challenges in the beginning of this research was to learn cell biology methodology and terminology in order to conduct biological experiments and communicate with an interdisciplinary team of researchers. After taking courses in the Departments of Biological Sciences and Chemical Engineering and receiving numerous trainings, I was able to independently design and conduct cell biological experiments and successfully collaborate with other researchers.

During January 2006- June 2009, all the silicon chips were fabricated in MICRON clean room facilities in Electrical and Computer Engineering Department (Whittemore Hall) and all the biological experiments were performed in VCOM lab located in Corporate Research Center (CRC). In summer 2009, we established VT MEMS Bio Lab in Electrical and Computer Engineering Department (Whittemore Hall). I was responsible for purchasing, characterization and setting up key equipments in the lab. The process to establish a fully functional biology lab in the College of Engineering was completed in September 2009.

There were several technical challenges through the course of completion of this research. One of the major difficulties was to perform real time experiments to study the cell behavior on the silicon substrates. Since silicon is not a transparent material, we have to stain the cells with fluorescent dyes/proteins and use an upright fluorescent microscope to perform real time experimentations. Most of the fluorescent microscopes available on Virginia Tech campus are inverted to accommodate biologists' needs who conduct their experiments on transparent materials such as glass slides or standard plastic cell culture assays. Due to such limitations, in 2008 we submitted a proposal to SCHEV (State Council of Higher Education for Virginia) Research Trust Fund to purchase an upright fluorescent microscope for VT MEMS lab. The proposal was successfully funded and the microscope was purchased in 2008. In 2009, a separate proposal was submitted to the same council to buy the necessary accessories for the microscope. With the help of two undergraduate students, an environmental chamber was designed and built

for the microscope to control the temperature and CO_2 during the real time experimentations. The total cost to build the environmental chamber setup was about $3500 (Compare to an external quote for $14000). The process to purchase the microscope and complete all its necessary accessories took about one year.

The other technical difficulty was to perform AFM analysis to measure cell biomechanical properties. It took me about 6 month to successfully set up and define the experimental procedures through the online help of Asylum Research company technical support. I also had to make a one day trip to Asylum Research office in North Carolina State University for additional trainings. It also took some time to properly learn how to attach a glass bead to an AFM cantilever tip for force analysis. One of the current limitations of the AFM equipments located in Nanoscale Characterization and Fabrication Laboratory (NCFL) is the lack of environmental chambers to precisely control the temperature and CO_2 during the experimentations.

8.4 Outlook

Looking at the outcomes of this dissertation, it can be seen that a significant effort and progress has been made in the course of the completion of this research during the past four years. However, there are still many interesting questions and novel ideas which need to be answered and explored. The followings are some of the future research directions which are related to the framework of this dissertation.

8.4.1 Exploring the behavior of other cell types within the breast tumor tissue on the 3-D microstructures

Within the framework of this dissertation, our experimental model included three major cell lines which are embedded within the human breast tumor microenvironment; normal fibroblast cells, normal mammary epithelial cells and highly metastatic breast cancer cells. However, other cell types such as immune cells, myoepithelial cells, vascular endothelial cells are present in breast tumor tissue. One possible direction is to study the adhesion, cytoskeletal organization and growth characteristics of the aforementioned cell types on the 3-D microstructures. The outcome of such efforts can lead to analysis of tumor tissue biopsy on the silicon substrates for possible clinical applications.

8.4.2 Gene expression analysis

We demonstrated that non-invasive and invasive breast epithelial cells differ in their mode of attachment, cell shape and cytoskeletal organization when grown on curved surfaces of 3-D isotropic microstructures. One possible hypothesis is that underlying gene expression changes in invasive breast cells are responsible for distinct responses of the cells to 3-D structure. On the other hand, the 3-D microstructure modulates the cell function which can also lead to expression of different genes in normal and diseased cells. Therefore, the 3-D microstructure can be used as an assay to monitor the genetic events in normal and diseased cells as potential biomarkers for early breast cancer risk assessment.

8.4.3 Cell signal transduction pathways on the 3-D microstructures

Considering that most of the previous works in the field of cell signal transduction pathways have been performed on standard 2-D substrates, the presented 3-D microstructures provide a unique way to conduct cell signal transduction pathways analysis during several biological processes such as differentiation and metastasis inside a 3-D architecture. As an example, it is possible to look into the level of activation of RhoA or ROCK in fibroblast cells while they are stretched inside the cavities and compare it to 2-D flat surfaces.

8.4.4 Integration of microfluidic components with the 3-D microstructures

All the experiments in this research were performed under static culture condition (passive mode). One interesting avenue is to integrate the 3-D silicon substrates with microfluidic components (i.e. pumps, valves, etc.) to induce shear stress on the cells and study the cell adhesion pattern and cytoskeletal reorganization under flow shear stress condition (active mode).

A. Appendix

A-I. Development of a Three Dimensional (3-D) Silicon Micro-Array for Cell Capturing

This section was reproduced from [1] with permission from IEEE

M. Nikkhah, et al., "Development of a Three Dimensional (3-D) Silicon Micro-Array for Cell Capturing," presented at the 9th IEEE Conference on Sensors (Sensors '10), Waikoloa, HI, 2010.

a. Introduction

With the recent advances in the field of biology, large amounts of data are required for protein identification and single cell analysis. Many experiments are performed semi-automatically or manually which limits the amount of information that can be gathered by scientists [2]. With respect to therapeutic strategies, there has been an unprecedented challenge to expand the pool of molecular targets, novel compounds, and bioassays to foster new drug discoveries [3]. Scale and flexibility are the certain demand of pharmaceutical industries in a move towards cell-based assays with parallel processing capabilities for different cell lines derived from various tissue origins [4, 5]. Therefore, there is a significant motivation to design higher throughput systems in order to perform experiments in order to acquire larger amount of data [6-12].

Using microelectromechanical systems (MEMS) technology is a promising approach to address the need for creating high throughput systems. MEMS technology is an extension of microelectronic industries and MEMS devices can be fabricated using standard circuit technology and photolithographic techniques with features at the length scale in the range of millimeters to micrometers and less. Recently microtechnology has been extensively used in biomedical and biological applications. Integration of MEMS technology and biology (BioMEMS) offers high throughput systems and also enables tight control over the cellular microenvironments established by varying cell-cell, cell-substrate (including extra cellular matrix (ECM)) and cell-medium interactions [13]. The other advantages of microminiaturized systems include small sample size and reagent consumption, small power consumption, and fast analysis of due to small length scale [3, 14, 15].

We previously reported the development of the first generation of three dimensional (3-D) silicon microstructures to study and address growth and adhesion behavior of normal fibroblast

and breast carcinoma cells in response to substrate topography [16-19]. This paper presents the second generation of 3-D microstructures consisting of a wide range of isotropically-etched cavities and a model based upon their corresponding shape to efficiently capture and trap normal and cancerous breast cells separately and in a co-culture system.

b. Materials and methods

i. Silicon device fabrications

Figure A. 1 shows a photo image of the 0.5cm square chips. The fabrication process is a single-mask single-etch-step process which utilizes reactive ion etching (RIE) lag as described in detail in our previous work [18, 20, 21].

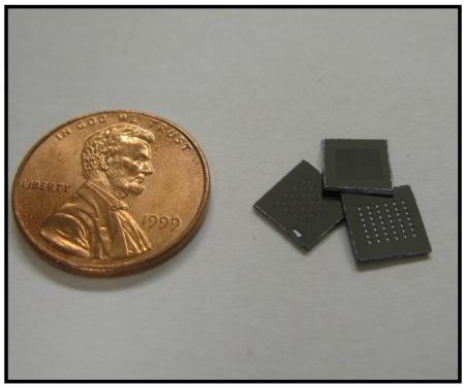

Figure A. 1 Photo image of the fabricated devices.

The silicon wafers are first vapor-primed with hexamethyldisylazane (HMDS) and then spun coated with S1827 photoresist. After patterning the photoresist, silicon is etched using DRIE SF_6 plasma to achieve final 3-D microstructures. After removing photoresist, the wafer is cleaned using DRIE oxygen plasma for 15 minutes and finally diced into 0.5cm square chips.

The etched features are comprised of spherical/ellipsoidal-shaped microchambers with variable width and depth. As the microchamber depth increases, its cross sectional shape merges toward an ellipse and its etched surface area increases (Figure A. 2). In addition to variable depth and width, the spacing between the microchambers (pitch size) has been varied in order to provide different ratios of the etched surface area to total surface area within each fabricated chip (Table A. 1).

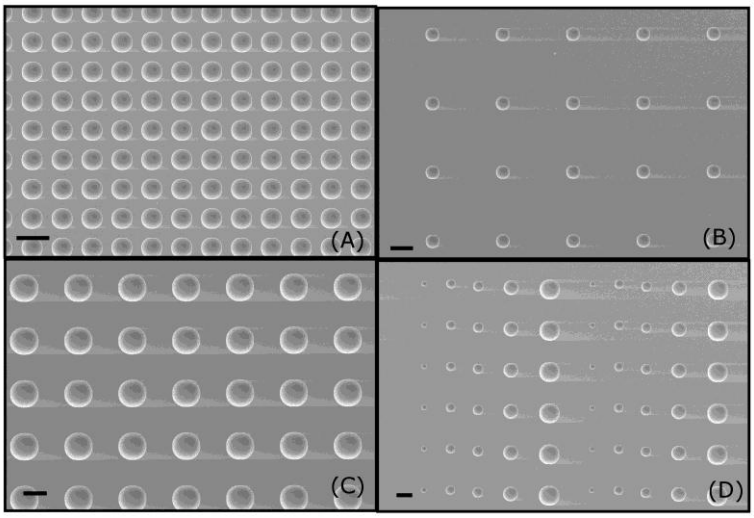

Figure A. 2 SEM images of the fabricated chips including spherical/ellipsoidal- shape etched features with variable geometries. Scale bars represent 100µm.

Table A. 1 summarizes the dimension of the substrates etched for 10 minutes. The novelty of the presented approach lies in the fact that the fabrication process allows the creation of 3-D etched features with variable depth and spacing. This provides flexibility in the design in all three dimensions and leads to the formation of comprehensive screening substrates to investigate fundamental cellular behaviors.

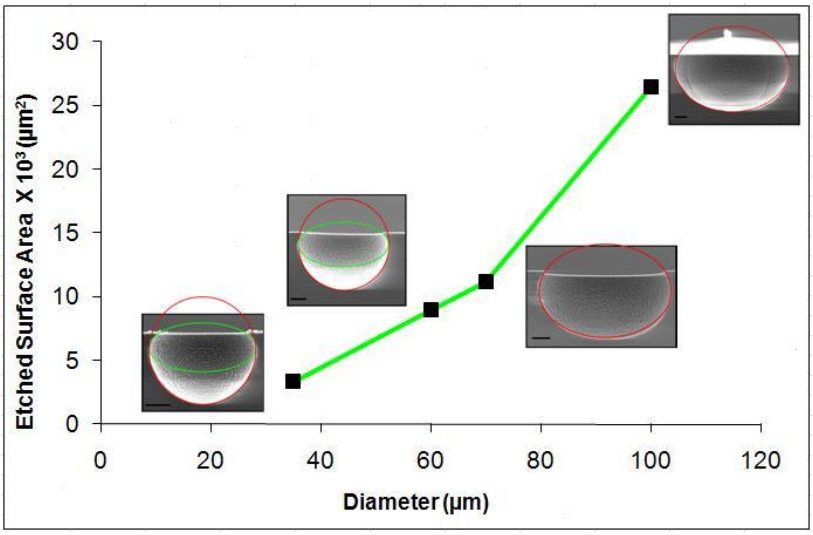

Figure A. 3 Variation of the etched surface area within each cavity as a function of the depth. Scale bars represent 10µm.

Table A. 1 Summary of the dimension of the proposed design for each silicon chip.

Substrate Number	Depth (µm)	Diameter (µm)	Spacing (µm)	Surface Ratio Etched/Total
D11	28	35	30	0.47
D12	28	35	120	0.12
D13	28	35	265	0.04
D21	42	60	25	0.63
D22	42	60	245	0.09
D23	42	60	550	0.02
D31	39	70	40	0.53
D32	39	70	305	0.09
D33	39	70	660	0.03
D41	54	100	50	0.68
D42	54	100	311	0.19
D43	54	100	625	0.07

ii. Cell culture and staining

Non-invasive MCF10A and highly invasive MDA-MB-231 were used in this work. The cells were purchased from the American type culture collections (ATCC). Cells were maintained in plastic T-75 cm^2 culture flasks in DMEM culture medium which contained 5% fetal bovine serum (FBS), 1 mM sodium pyruvate, and penicillin-streptomycin (100 Units/ml). Cells were grown at 37 °C in humidified 7% CO2-93% air atmosphere.

For real-time fluorescence microscopy, MDA-MB-231 cells were labeled with membrane permeable fluorescent vital dye Cell Tracker Orange (Invitrogen). Briefly, 1 µl/ml of Cell Tracker Orange dye was added to the T-75 cm^2 culture flask for 25 minutes. Then, the cells were rinsed twice with HBSS, suspended in DMEM medium containing 10% fetal bovine serum, and plated with a density of 1×10^5 on the silicon chips. For the co-culture experiment MCF10A cells were labeled with Cell Tracker Orange and MDA-MB-231 nuclei were labeled with Hoechst 33342 dye (6.6 µg/ml final concentration) using the same protocol mentioned earlier.

Sample preparation for SEM imagining and quantification of cell number inside the microchambers

SEM images were obtained to quantify the percentage of the cells inside the microchambers for each design. After fixation of the cells with 3.7% formaldehyde in phosphate buffered saline (PBS) for 10 minutes, samples were critical point dried and sputter-coated with a thin layer of gold palladium prior to SEM imaging. SEM images were obtained for nine different fields within each chip. The dimension of each field was 950 µm × 1450 µm which included the etched microchambers and their surrounding flat surfaces. The selected fields almost covered the entire fabricated substrate in order to count the number of cells inside the etched features as well as on the flat surfaces.

iii. Imaging

All photographic images were taken using a CALTEXVZM-2000 digital-video optical microscope with a maximum magnification of 2000. Real-time fluorescence microscopy was performed using ZEISS Axiovison D1 upright microscope which is fitted with an environmental chamber and equipped with a temperature and CO_2 control unit. The temperature was set to 37 ºC and CO_2 was set to 5% during the experiments. Cells were imaged using a 10X immersion objective. Images were acquired every 1 min for 4 hours.

c. Results

Figure A. 4 shows the quantitative representation of the percentage of cancerous cells (MDA-MB-231) trapped inside the etched features after 72 hours obtained from SEM images. It is clearly seen that in the etched microenvironments with close spacing, there was significant cell accumulation inside the cavities. In contrast, in chips comprised of intermediate and large pitch sizes, cells are mostly seen on the flat surfaces. This behavior is consistent for all the proposed designs (D11…D43). Therefore, as the spacing between the etched features decreases, cells accumulated inside the cavities; we found there is a direct correlation between the etched surface ratio and the capture capacity of each chip (Figure A. 3).

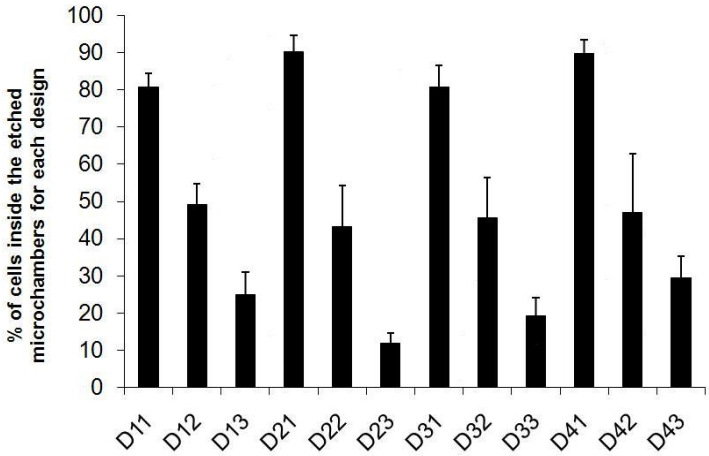

Figure A. 4 Quantitative data showing the percentage of MDA-MB-231cells trapped inside the cavities for each design.

In order to investigate the mechanism of cell trapping inside the microstructures, we performed real-time fluorescence microscopy on MDA-MB-231 cells separately as well as in co-culture with MCF10A cells on D41 substrates. Time lapse images obtained through real-time fluorescence microscopy on MDA-MB-231 cells shown in Figure A. 5 indicated the cells are captured and accumulated inside the etched features as early as 20 minutes after cell seeding on the chips. These images suggest that the mechanism of trapping of the cells inside the features might be mainly due to the gravitational force and flow effects immediately after the cell seeding on the chips before the cells spread on the surfaces.

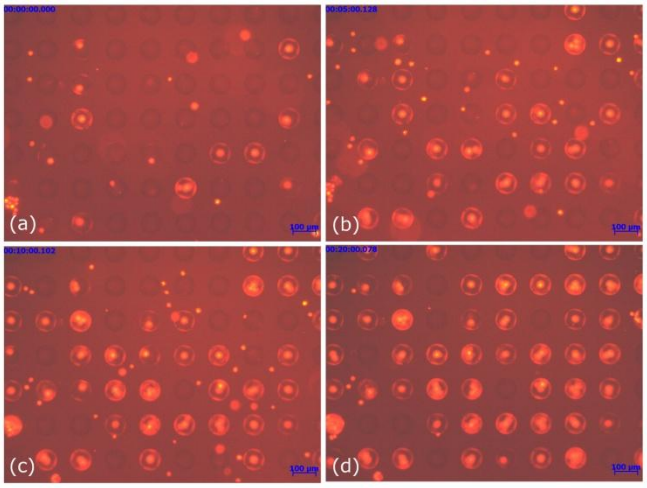

Figure A. 5 Time-lapse video microscopy showing the capturing process for MDA-MB-231 cells in D41 substrates ((a) 0 min ,(b) 5 min, (c) 10min , (d) 20 min). Scale bars represent 100µm.

Figure A. 6 shows the time lapse images of the co-cultures of MDA-MB-231 and MCF10A cells on D41 substrates. The co-culture experiments confirmed the rapid capture and subsequent formation of colonies of both cell types inside the etched cavities (Figure A. 6). Therefore, in addition to cell capturing, the substrates are suitable for the study of cell-cell interactions between normal and cancerous cells as well as anti-cancer drug sensitivity testing in a co-culture system which may better mimic in-*vivo* microenvironments.

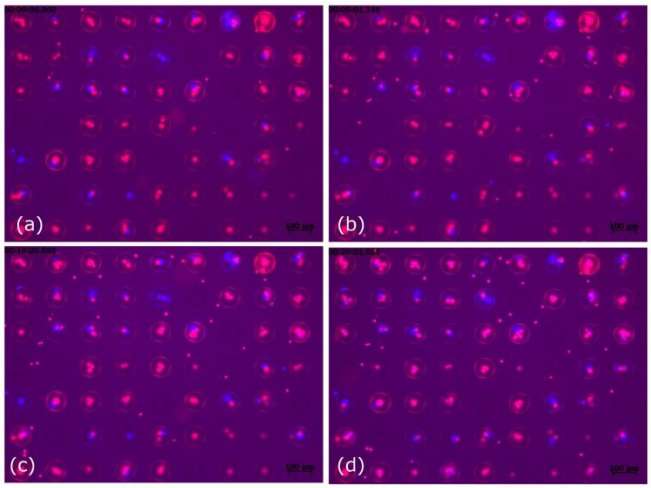

Figure A. 6 Time-lapse video microscopy showing the capturing process in co-cultures of MDA-MB-231 and MCF10A cells in D41 substrates ((a) 0 min ,(b) 5 min, (c) 10min , (d) 20 min). MDA-MB-231 cells stained in blue dye and MCF10A cells stained in the red dye. Scale bars represent 100µm.

d. Conclusion

In this paper, we reported the design, fabrication and characterization of 3-D silicon microarrays consisting of a wide range of isotropically etched microstructures. The results of the current work indicate that with the proposed microstructures, it is possible to efficiently capture cancerous and normal cells separately and in a co-culture system. The presented platforms can find various applications for cell trapping, cell sorting, cell-based- sensing as well as fundamental biological studies.

e. References

[1] M. Nikkhah, *et al.*, "Development of a Three Dimensional (3-D) Silicon Micro-Array for Cell Capturing," presented at the 9th IEEE Conference on Sensors (Sensors '10), Waikoloa, HI, 2010.

[2] H. Lodish, *et al.*, *Molecular cell biology*. New York: W. H. Freeman, 2000.

[3] A. Prokop, *et al.*, "NanoLiterBioReactor: Long-term mammalian cell culture at nanofabricated scale," *Biomedical Microdevices*, vol. 6, pp. 325-339, Dec 2004.

[4] K. Slater, "Cytotoxicity tests for high-throughput drug discovery," *Current Opinion in Biotechnology*, vol. 12, pp. 70-74, Feb 2001.

[5] P. G. Wang, *High-Throughput Analysis in the Pharmaceutical Industry*: CRC, 2008.

[6] G. Z. Weng, *et al.*, "Complexity in biological signaling systems," *Science*, vol. 284, pp. 92-96, Apr 1999.

[7] J. Drews, "Drug discovery: A historical perspective," *Science*, vol. 287, pp. 1960-1964, Mar 2000.

[8] C. Sander, "Genomic medicine and the future of health care," *Science*, vol. 287, pp. 1977-1978, Mar 2000.

[9] S. A. Sundberg, "High-throughput and ultra-high-throughput screening: solution- and cell-based approaches," *Current Opinion in Biotechnology*, vol. 11, pp. 47-53, Feb 2000.

[10] E. H. Davidson, *et al.*, "A genomic regulatory network for development," *Science*, vol. 295, pp. 1669-1678, Mar 2002.

[11] H. Kitano, "Systems biology: A brief overview," *Science*, vol. 295, pp. 1662-1664, Mar 2002.

[12] E. C. Butcher, *et al.*, "Systems biology in drug discovery," *Nature Biotechnology*, vol. 22, pp. 1253-1259, Oct 2004.

[13] T. H. Park and M. L. Shuler, "Integration of cell culture and microfabrication technology," *Biotechnology Progress*, vol. 19, pp. 243-253, Mar-Apr 2003.

[14] S. D. Senturia, *Microsystem Design*: Kluwer Academic Publishers, 2001.

[15] K. F. Jensen, "Microreaction engineering—is small better?," *Chemical Engineering Science*, vol. 56, pp. 293-303, Jan 2001.

[16] M. Nikkhah, *et al.*, "Attachment and response of human fibroblast and breast cancer cells to three dimensional silicon microstructures of different geometries," *Biomedical Microdevices*, vol. 11, pp. 429-441, Apr 2009.

[17] M. Nikkhah, *et al.*, "Cytoskeletal role in differential adhesion patterns of normal fibroblasts and breast cancer cells inside silicon microenvironments," *Biomedical Microdevices*, vol. 11, pp. 585-595, Jun 2009.

[18] M. Nikkhah, *et al.*, "The cytoskeletal organization of breast carcinoma and fibroblast cells inside three dimensional (3-D) isotropic silicon microstructures," *Biomaterials*, vol. 31, pp. 4552-4561, Jun 2010.

[19] J. S. Strobl, *et al.*, "Actions of the anti-cancer drug suberoylanilide hydroxamic acid (SAHA) on human breast cancer cytoarchitecture in silicon microstructures," *Biomaterials*, vol. 31, pp. 7043-7050, Sep 2010.

[20] K. Gantz, *et al.*, "Development of a comprehensive model for RIE-lag-based three-dimensional microchannel fabrication," *Journal of Micromechanics and Microengineering*, vol. 18, Feb 2008.

[21] P. Zellner, *et al.*, "A fabrication technology for three-dimensional micro total analysis systems," *Journal of Micromechanics and Microengineering*, vol. 20, Apr 2010.